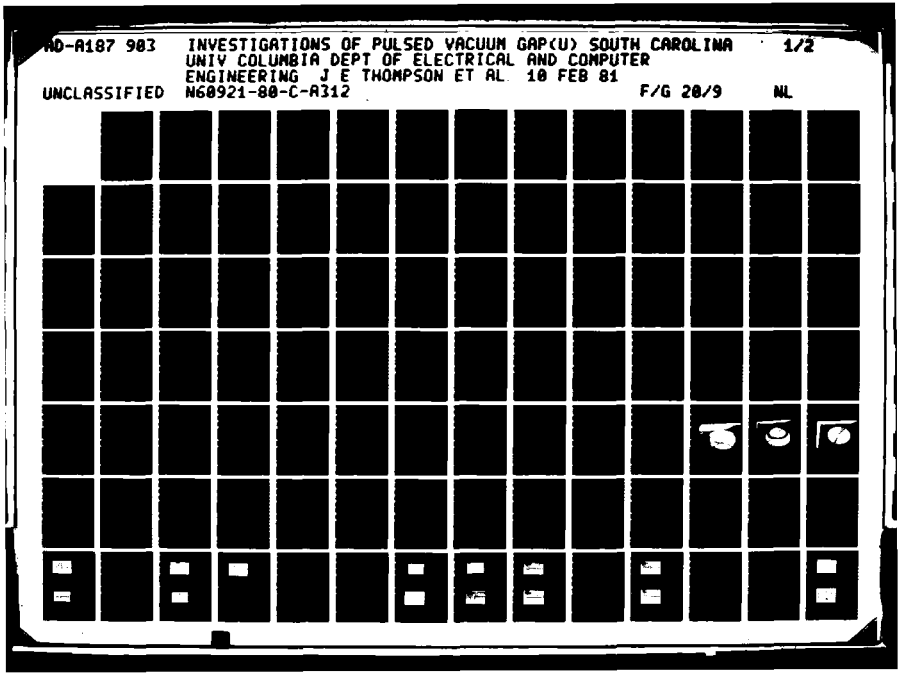
AD-A187 903 INVESTIGATIONS OF PULSED VACUUM GAP(U) SOUTH CAROLINA 1/2
UNIV COLUMBIA DEPT OF ELECTRICAL AND COMPUTER
ENGINEERING J E THOMPSON ET AL. 10 FEB 81
UNCLASSIFIED N60921-80-C-A312 F/G 20/9 NL

DEPARTMENT OF ELECTRICAL
AND COMPUTER ENGINEERING

COLLEGE OF ENGINEERING
UNIVERSITY OF SOUTH CAROLINA

INVESTIGATIONS OF PULSED VACUUM GAP

by

J. F. Thomson, T. S. Sudarshan, J. M. Butler

Final Report

Contracts N6092[illegible]-79-C-A[illegible]96 and N6092[illegible]-80-C-A[illegible]12

Naval Surface Weapons Center, Special Applications Branch

Naval Air Systems Command

Air Task No. A-350-350-F 3048/0F32-393-59

Defense Advanced Research Projects Agency

ARPA Order No. 3761

Principal Investigator: J. F. Thomson

Associate Professor, University of South Carolina

Principal Investigator: T. S. Sudarshan

Assistant Professor, University of South Carolina

February [illegible], 1986

High Voltage Laboratory

College of Engineering

University of South Carolina

Columbia, SC 29208

SECURITY CLASSIFICATION OF THIS PAGE (When Data Entered)

REPORT DOCUMENTATION PAGE	READ INSTRUCTIONS BEFORE COMPLETING FORM
1 REPORT NUMBER	2 GOVT ACCESSION NO. AD-A187903 / 3 RECIPIENT'S CATALOG NUMBER
4 TITLE (and Subtitle) Investigations of Pulsed Vacuum Gap Breakdown Mechanisms	5 TYPE OF REPORT & PERIOD COVERED Final June 1978 - December 1980
	6 PERFORMING ORG. REPORT NUMBER
7 AUTHOR(s) J.E. Thompson, T.S. Sudarshan and J.M. Butner	8 CONTRACT OR GRANT NUMBER(s) N60921-79-C-A186 N60921-80-C-A312
9 PERFORMING ORGANIZATION NAME AND ADDRESS University of South Carolina College of Engineering Columbia, SC 29208	10 PROGRAM ELEMENT, PROJECT, TASK AREA & WORK UNIT NUMBERS
11 CONTROLLING OFFICE NAME AND ADDRESS Naval Surface Weapons Center Special Applications Branch, F12 Dahlgren, Virginia 22448	12 REPORT DATE February 10, 1981
	13 NUMBER OF PAGES 152
14 MONITORING AGENCY NAME & ADDRESS (if different from Controlling Office)	15 SECURITY CLASS. (of this report) Unclassified
	15a DECLASSIFICATION/DOWNGRADING SCHEDULE

16 DISTRIBUTION STATEMENT (of this Report)

Approved for public release, distribution unlimited.

17 DISTRIBUTION STATEMENT (of the abstract entered in Block 20, if different from Report)

18 SUPPLEMENTARY NOTES

19 KEY WORDS (Continue on reverse side if necessary and identify by block number)

vacuum breakdown vacuum prebreakdown mechanisms
microparticles
pulsed breakdown
charge detection

20 ABSTRACT (Continue on reverse side if necessary and identify by block number)

Past research and the current status of understanding of electrical breakdown of vacuum is reviewed. This review includes DC, AC and pulsed vacuum gap breakdown. Measurements have been performed to determine the role of microparticles in pulsed vacuum gap breakdown. These measurements consisted of directly measuring the charge and velocity of microparticles produced using pulsed excitations up to 100kV. Measurements show that microparticles are present prior to, during, and after vacuum breakdown. Typical microparticle charge and velocity values for 100kV/cm fields are 10^{-13} C and 75m/s.

DD FORM 1473 EDITION OF NOV 65 IS OBSOLETE

TABLE OF CONTENTS

X

A-1

LIST OF FIGURES

[illegible]

[illegible]

INTRODUCTION

The breakdown voltage of a vacuum gap has increased linearly with gap spacing for small gaps (< 1 mm) and departs from linearity for large gaps (> 1 mm). For long gaps the breakdown voltage is proportional to d^{α} where d is the gap separation and α is a constant whose value is less than unity. It has been postulated that microscopic conducting particles, i.e., microparticles are responsible for this behavior.

The presence of microparticles has been verified by various investigations for DC and pulsed voltages, and various techniques have been employed to determine the characteristics of these microparticles. The objective of the work presented here is to examine microparticle prebreakdown activity using a pulsed excitation.

The first chapter of this report surveys past vacuum breakdown work for DC, AC, and impulse voltages. Chapter Two describes the experimental arrangement used to produce, measure, and characterize microparticles. Microparticles are detected using an electrostatic charge induction technique. The sensitivity of detection of a microparticle is [illegible]. In Chapter Three, experimental results are presented pertaining to the detection and analysis of both artificial and natural microparticles. Discussion of relevant observations and conclusions which can be drawn from these data are also presented. Specific microparticle characteristics which will be presented include measured charge, velocity, and calculated radius. The reported work is summarized in Chapter 4 together with suggestions for future work.

Review of Previous Research

Scientific interest in vacuum as an insulator is relatively new, with the first description of arc initiation in vacuum published in [illegible]. Since then, interest has steadily increased as technology has elicited ways in which to utilize vacuum as an insulator. Vacuum has found use in vacuum tubes, high-power switches, experimental fusion devices, and particle accelerators, to mention a few. Troubles arise using vacuum insulation because of the relative inability to prevent, or even successfully predict failure, i.e. breakdown.

Breakdown between two electrodes separated by vacuum should occur when there is sufficient charge multiplication within the vacuum. Assuming that electrode secondary emission processes do not cause cumulative production of charged particles, sufficient charge multiplication is not possible if the mean free path length of the charge carriers is much larger than the separation distance between the two electrodes. Paschen used this principle to formulate his law relating breakdown voltage between parallel electrodes in a background gas to the product of that gas's pressure and the gap separation. In nitrogen, which is the primary residual gas in a vacuum, Paschen's Law reveals minimum gap breakdown voltage should occur at $pd \approx 10^{-2}$ Torr-cm., where p is the pressure, and d is the gap spacing. The shape of the Paschen curve indicates that, at pressure values to the left of the Paschen minimum, longer gaps

will breakdown at lower voltages than shorter gaps. This is true in general. Breakdown has been observed, however, even when this product is lower by several orders of magnitude. This suggests that some mechanisms exist, within the inter-electrode space, that create charge multiplication. These mechanisms are not presently fully understood, but much research has been done to attempt to characterize, if not identify, these mechanisms.

There are two prominent phenomena which arise when the voltage across two electrodes in vacuum is progressively increased. For smaller gaps ($\lesssim$1mm), a relatively steady current begins to flow. This current has been found to be predominately due to electrons[9]. For larger gaps ($\gtrsim$3mm) small, self-quenching current pulses of charge $\geq 10^{-7}$ coulombs, lasting from about 50 us to several milliseconds[10], occur. These current pulses, called *microdischarges*, are found to be primarily due to ions[11]. Existing, high-voltage, vacuum breakdown theories attempt to relate these and other pre-breakdown phenomena to breakdown.

1.2 Factors Which Affect Vacuum Breakdown

Experimental investigators have revealed that there are several factors that affect the insulation strength of vacuum.

1.2.1 Conditioning

It was first shown by Millikan and Sawyer[2], and has been confirmed by many others[3,4,5], that as a gap is sparked, its breakdown voltage increases until it reaches a "plateau". This effect is known as conditioning. In some cases it has been observed that conditioning is not permanent, and if the voltage is removed for a time or the electrodes exposed to higher pressures, then the next breakdown value will

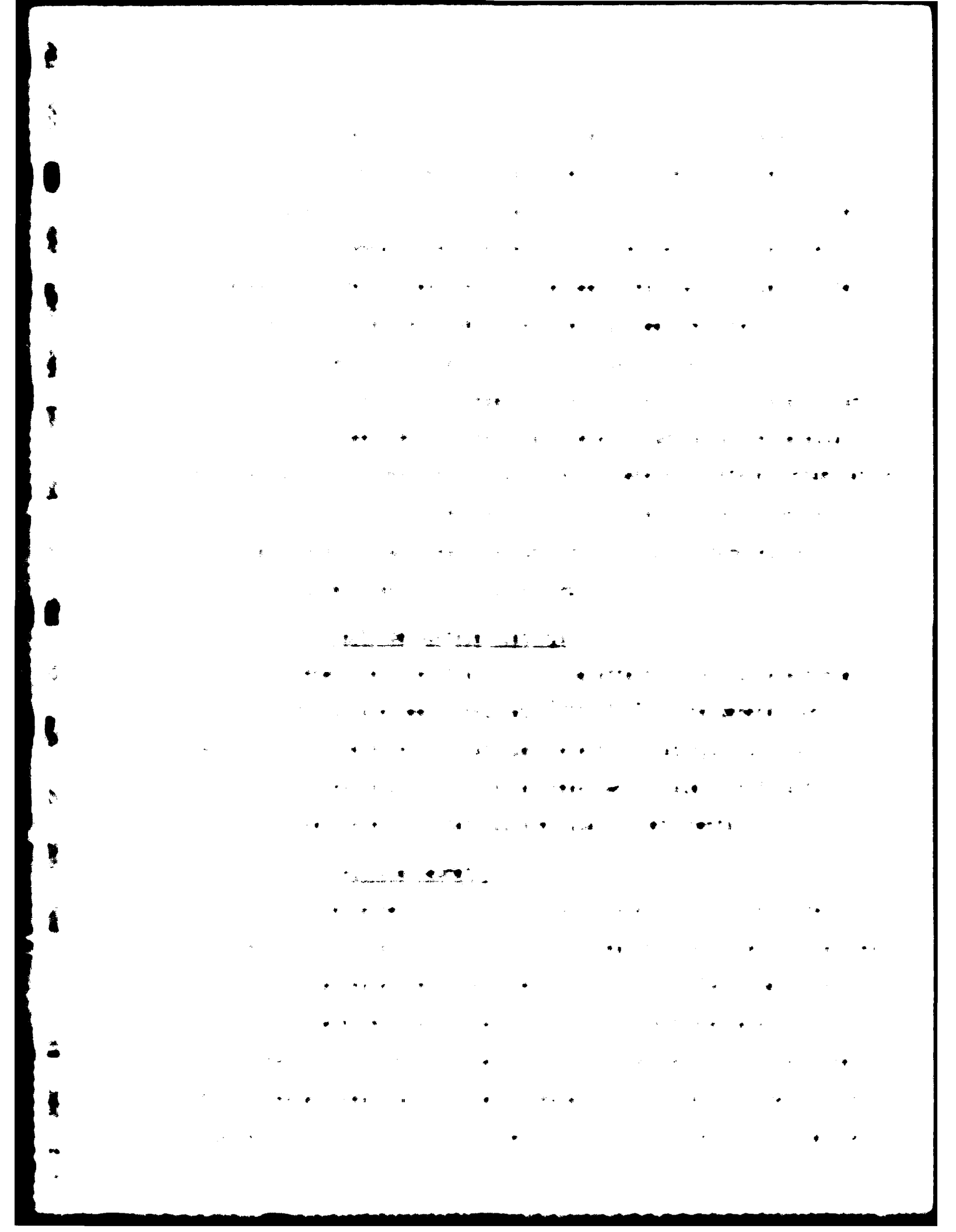

[illegible] increased, the result was an increase in breakdown voltage [illegible] increase [illegible] breakdown voltage [illegible] gaps [illegible] the [illegible] the cathode.

Cathode Temperature

Cathode temperature effects depend upon temperature range. [illegible] temperatures [illegible] several hundred [illegible] increased breakdown [illegible] the temperature range [illegible] increased breakdown voltage [illegible] cathode [illegible] has been reported [illegible] cathode temperatures [illegible] breakdown voltage [illegible] temperatures [illegible] decreases breakdown [illegible]

Residual Gas Pressure

[illegible] the effect [illegible] the breakdown voltage [illegible] residual gas pressure [illegible] observed [illegible] voltage [illegible] was [illegible] moderate pressures [illegible] between [illegible] effect was attributed to the increase [illegible] various gases [illegible]

[illegible]

[illegible]

[illegible] tage in frequency in the range of [illegible] MHz [illegible]. There are [illegible] ations that the breakdown voltage increases with applied voltage frequency for longer gaps [illegible].

[illegible] External Power Supply Circuit

Lastly, the external circuit of the power supply has been found to effect breakdown voltage[18]. It has been reported that a large resistance in series with a gap produces low and erratic breakdown voltages, and as this resistance is decreased breakdown voltages increased and became more reliable[18].

[illegible] Conclusions

[illegible] ed experiments that have [illegible] the above factors are [illegible]. Therefore, interpretations of vacuum breakdown work are [illegible] and disagreements between investigators are frequent. To date, no single vacuum breakdown hypothesis explains all of the aspects of vacuum breakdown as aforementioned. The sound reasoning behind each theory and the experimental results that support it warrant a scrutiny [illegible] each. The first vacuum breakdown mechanisms to be examined are those for DC voltages.

II. Vacuum Breakdown Hypotheses

Introduction

[illegible] ere are [illegible] east three [illegible] hypotheses [illegible] the breakdown [illegible] vacuum gap under [illegible] the three [illegible] [illegible] based [illegible] There [illegible] [illegible]

The above arguments suggest particle exchange processes do not, in themselves, cause vacuum breakdown. They are important in that the integrated effect of microdischarges appears as a relatively steady rise in drain in the high voltage power supply at voltages well below breakdown. Microdischarge phenomena are currently being investigated via computer models[48] and by determining the circuit response to a single particle.

2.2 The Field Emission Hypothesis

The vacuum breakdown hypothesis that finds the most support is the field emission hypothesis. According to this hypothesis, the pre-breakdown current and subsequent breakdown of a vacuum gap are due to field emission from the cathode. The field emission current density is governed by the Fowler-Nordheim law,[49] which, after being corrected to include temperature effects,[50] is given by[50]

$$J = \frac{A\beta^2 E^2}{\phi t^2(y)} \exp\left[\frac{-B\phi^{3/2} v(y)}{\beta E}\right],$$

where

J = [illegible],

A = [illegible],

B = Boltzmann's constant, $= 8.[illegible] \times 10^{-23}$ joules/°K,

T = temperature of the emitter in °K,

$y = \frac{[illegible]}{[illegible]}$,

ϕ = [illegible] in electron volts,

$t(y) = [illegible]$,

$v(y) = [illegible]$,

β = [illegible] constant, $= [illegible]$ electrons/[illegible],

E = [illegible] at the emitter [illegible],

βE = [illegible] at the emitter [illegible].

The factor $\frac{\sigma}{\sin\sigma}$, which takes into account the effect of temperature, remains nearly unity up to 300 K and the equation reduces to

$$j = \frac{1.54 \times 10^{-6} E^2}{\phi t^2} \exp\left(\frac{-6.83 \times 10^{9} \phi^{3/2}}{E}\right) \text{ amps meter}^{-2}, \quad (11)$$

In the normal range of interest, $t^2(y)$ may be taken to be unity and $v(y)$ may be replaced by the function $b(y)$ which was introduced by Nottingham.[38] This reduces the equation to

$$j = \frac{1.54 \times 10^{-6} E^2}{\phi t^2(y)} \exp\left(\frac{-6.83 \times 10^{9} \phi^{3/2} b(y)}{E}\right) \text{ amps meter}^{-2}, \quad (12)$$

where $b(y) = 1 - 1.89y^2 + 1.65y^4$,

and $y = \frac{3.79 \times 10^{-5} E}{\phi^2}$.

This expression was verified by Dyke and his colleagues for a point to plane gap geometry over a current density range of at least six orders of magnitude, from 6×10^{4} A m^{-2} (6 mA cm^{-2}) to 6×10^{10} A m^{-2} (6×10^{6} A cm^{-2}).[38] The shape of the point cathode, whose radius was less than 10^{-6} m, as determined with an electron microscope so that the electric field at the cathode could be accurately calculated. Furthermore, the voltage was pulsed at high current densities, to preserve the cathode shape.

For parallel gap breakdown fields observed in practice, equation (12) yields insignificant amounts of current that are orders of magnitude smaller than measured currents.[39] This discrepancy was explained by postulating the presence of microscopic field-enhancing cathode protrusions from which the current was drawn.[39] Since then, many investigators[40-47] have observed these protrusions and mathematical models have been developed for the field enhancement by the

It should be noted that some evidence suggests these protrusions are formed on the electrode surface after the application of voltage.[51] If this is so, the mechanisms responsible for their growth need to be understood.

Introducing the field enhancement factor, β, for planar gaps, the field emission current density becomes:

$$J = \frac{1.54 \times 10^{-6} \beta^2 V^2}{\phi t^2} \exp\left(\frac{-6.83 \times 10^9 \phi^{3/2} t}{\beta V}\right) \text{ amps/meter}^2, \quad (1.4)$$

where V is the applied voltage, and t is the gap spacing. Emission current is thus

$$I = J \cdot A \text{ amps}, \quad (1.5)$$

where A is the emitting area.

If the emission currents are noted experimentally for a given gap and various voltages, it follows from equation (1.3) that a plot of $\log_e I/V^2$ versus $1/V$ should be linear with slope s given by:

$$s = -\frac{6.83 \times 10^9 \phi^{3/2} t}{\beta} \quad (1.6)$$

and intercept b given by

$$b = \log_e \frac{1.54 \times 10^{-6} \beta^2 A}{\phi t^2} \quad (1.7)$$

This plot is called a Fowler - Nordheim plot.

Using the slope of the F-N plot and equation (1.6), one can estimate β and then use this estimate in equation (1.7) to find the emitting area. F-N plots have been obtained by many investigators.[39,57,59] These plots agree very well up to a current density of about 1×10^{11} amps/cm^2 [39] and to electrode temperatures of about 3000°K, thereby establishing that, within certain limits, prebreakdown conduction

is due to field emission for gaps less than a few millimeters.

A limitation of conventional F-N analysis is the inability to separate the work function from the field enhancement factor. Inconsistencies may arise if the work function of the emitting material changes,[60] or if grain boundaries and hole edges, and not sharp protrusions, are emitting sites.[61,62] The experimental results from the latter case fit Schottky[64] emission curves, which predict lower prebreakdown emission than is actually measured for low temperatures (300°C). These difficulties could be resolved if the work function of the emitting site was measured independently and F-N analysis used to determine the field enhancement.

Another apparent problem associated with F-N analysis is that the current actually comes from many different emitters, (10-40 per cm^2, typical) but the F-N plot determines only the average characteristics of the emitter surface. Since each emitter should have a different emitting area and enhancement factor, a single linear F-N plot would seem to tell very little quantitatively about an individual emitting site. Farrall[65] has shown, however, that for a random selection of emitters, a straight line F-N plot is quite conceivable. He has also shown that the effective enhancement factor measured from such a plot is close to that of the sharpest protrusion while the emitting area only crudely approximates that of the same protrusion.

There is enough experimental evidence to show that prebreakdown currents are mainly due to field emission, but the role of this current in inducing vacuum breakdown is not yet well defined. Various theoretical models have been proposed predicting either cathode or anode initiated breakdown.[62,66,67] The type of theoretical model depends on the nature

of the protrusion. In both cases, breakdown is believed to be due to the production of metal vapor in the inter-gap region which causes charge multiplication.

1.3.3 Cathode Induced Breakdown Hypothesis

In the case of cathode induced breakdown, the metal vapor is believed to be due to excessive heating and consequent local evaporation from a cathode protrusion as a result of heating by its own emitted current.[63,66,67,68,69,70] The temperature of the protrusion tip is controlled by three energy exchange phenomena:

(1) resistive heating of the protrusion, due to current flow through it;

(2) Nottingham (electron-tunnelling, heating or cooling[71]), which arises out of the difference in average energy of an electron outside the metal from that of an electron within the conduction band; and

(3) cooling of the protrusion by thermal conduction and radiation.

Radiation cooling is about three orders of magnitude smaller than conduction cooling and may be neglected.[72]

The temperature effects associated with field emission through a truncated cone protrusion, with tip radius r and cone half angle α, and through a cylindrical protrusion of height h with a hemispherical cap of radius r will be discussed. The steady state solution of the basic heat conduction equation for a truncated cone is:[66]

$$T_b - T_s = [\rho(F^2)/2K][(r/\epsilon)^2 + (1-K T_b/K)][\cot(\alpha/2)][r/\epsilon] \quad (1.3$$

where

T_b is the protrusion tip temperature,

T_b is the protrusion base temperature,

ρ_T is the effective thermal resistivity of the protrusion

λ is the thermal conductivity,

k is the Boltzmann's constant, and

β has the same meaning as in equation (1.3).

This equation is the same for a cylindrical protrusion of height h with r_0 replaced by h. The first term in (1.8) takes into account resistive heating and the second term, the Nottingham effect. Neglecting the effect of variation of thermal conductivity and resistivity with temperature, Chatterton[32] has obtained expressions for the current density necessary for cathode-initiated breakdown for a truncated cone protrusion:

$$j^2_c r_0^2 = \frac{4kT}{\xi} [1-\cos\theta(\cot\theta)^2 [1 - \frac{1}{2(\beta-1)} \cot\theta]^{-2} \qquad (1.9)$$

and for a cylindrical protrusion:

$$j^2_c r_0^2 = \frac{2kT}{\xi(\beta-2)^2} . \qquad (1.10)$$

For both equations, T is (T_g-T_b) and β is the field enhancement factor. Williams and Williams[72] included resistivity variation with temperature and the Nottingham effect in their analysis. Their expressions for necessary current density were smaller than Chatterton's by a constant factor for both protrusion geometries.

1.3.5 Anode Induced Breakdown Hypothesis

The thermal processes that control anode induced vacuum breakdown are anode spot heating caused by field-emission currents and cooling by conduction through the electrode and its support. The field-emitted electron beam that starts from a cathode protrusion spreads as it traverses the gap. The beam radius at the anode, r_a, is given as:[70]

$$R_a = 2(d\sigma r)^{\frac{1}{2}}, \tag{1.11}$$

where r is as defined earlier for both a truncated cone and cylindrical cathode protrusion. The electron beam would thus have a power density W_a given by:

$$W_a = \frac{VI}{\pi R_a^2}. \tag{1.12}$$

Combining (1.11) and (1.12), and assuming a semi-infinite plane model for the electrode, with the assumption that the back surface of the anode remains at the ambient temperature, Charbonnier, et al,[66] have derived the maximum power density from the maximum permissible temperature rise at the anode. Their calculations consider anode temperature rise corresponding to currents of different durations by defining two characteristic times, t_1 and t_2 given by:

$$t_1 = (R_r/b)^2 \tag{1.13}$$

$$t_2 = (R_a/b)^2, \tag{1.14}$$

where R_r is the effective electron penetration depth in the anode material, R_a is given by equation (1.11), and b is defined by:

$$b^2 = 2K/c\rho \tag{1.15}$$

where K is the thermal conductivity, c is the specific heat, and ρ is the anode material density.

Accordingly, for pulses of different durations, the anode

temperature rise, ΔT, is given by:

$$\Delta T = W_a t/(R_\rho c \rho) \qquad t < t_1 , \tag{1.16}$$

$$\Delta T = W_a t^2/(\pi K c \rho)^{\frac{1}{2}}, \; t_1 < t < t_2 , \text{ and} \tag{1.17}$$

$$\Delta T = W_a R_a/K , \qquad t > t_2 . \tag{1.18}$$

Furthermore, defining W_c as the critical power density corresponding to the temperature at which thermal instability, i.e., melting, occurs, the value of electric field enhancement at the cathode, β_o, which distinguishes cathode and anode induced breakdowns is given as:

$$\beta_o = (r J_c E_c/4W_c)^{\frac{1}{2}} , \tag{1.19}$$

where J_c and E_c are the critical current density and field, respectively, above which cathode protrusion evaporation begins. Cathode induced vacuum breakdown is more probable for $\beta > \beta_o$, while anode induced breakdown is more probable for $\beta < \beta_o$. Similar conclusions have been reached by Chatterton[52] and Utsumi.[67]

Thus, the hypothesis of field emission induced vacuum breakdown is well founded for at least small gaps.[67] This hypothesis is based on the attainment of a critical temperature at one of the electrode surfaces. While this appears to be a necessary condition for breakdown[73], it has been shown not to be a sufficient condition for breakdown.[74]

An alternate mechanism proposed by Boyle, et al,[55] suggests that the collective space charge of ions produced by emission currents leads to an avalanche of charge multiplication and hence, vacuum breakdown.

The sequence of events that occurs after the onset of field emission needs further experimental investigation. The final, major

[illegible]

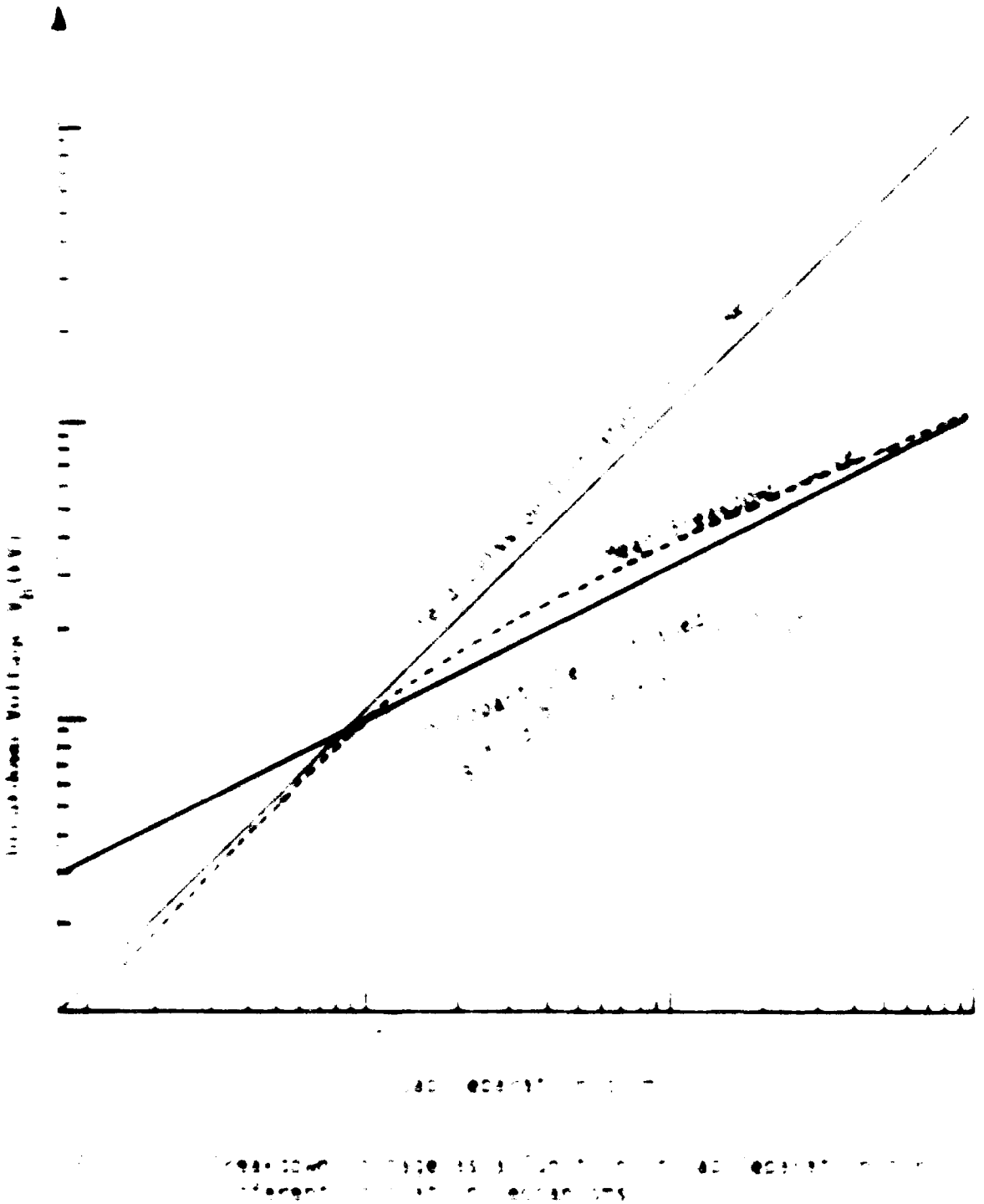

Trigger discharge field emission initiated breakdown

For the case of the trigger discharge being less than [illegible] addition of the electrode particle is not [illegible] a new mechanism for vacuum breakdown has to be produced. The trigger discharge theory of Mendel[31] is perhaps appropriate although in this theory the field is generated between the charged microparticle and the metal electrode can be large enough to cause a small trigger discharge that leads to breakdown of the main gap. Many experimental observed trigger discharges [illegible] microparticles [illegible] and small microparticles [illegible] into a vacuum gap. Two greatly different theories have been proposed that involve field emission triggered breakdown in the space between electrode and particle just prior to impact. The trigger discharge is caused by field enhancement between the microparticle and the electrode. The theory, by Vorobyov[32], proposed that the plasma produced by the trigger discharge extends into the main gap to form a positive ion sheath, which enhances the field so that the gap breaks down by conventional field emission. The alternate theory of Chatterton, et al[33], proposed that the trigger discharge melts regions on the particle and electrode. If the particle then rebounds from its impact site it pulls away some of the molten electrode material, forming a protrusion. It is further postulated that main gap breakdown occurs as a result of field enhancement caused by the protrusion. Impact melting has been observed[34]. Wenon has computer simulated a charged microparticle approaching an electrode to attempt to predict pre-impact phenomena[35]. He reported that large microparticles (>1μm diameter) emitted from the anode can generate high

enough fields at cathode protrusions to cause charge flow before impact. Calculations also indicate particle melting and gas desorption from the cathode must occur. He did not predict whether or not these conditions lead to discharge. Menon also assumed trigger discharge particle melting and predicted breakdown voltage versus gap spacing curves for particles of different radii.[30] These predictions agreed well with the results of others.[27,36]

Boreskhov and Solov'yev[36] proposed a trigger discharge breakdown mechanism similar to that of Chatterton[34] to explain trigger discharge vacuum breakdown time lags. Breakdown is proposed to occur as the particle bounces off the electrode surface after impact.

1.3.4 Microparticle Theory of Davis and Brondi

Davis and Biondi[24,103] have developed a theory to explain the breakdown of a vacuum gap that relates breakdown to microparticles and field emission. According to this theory, pre-breakdown field emission currents from a cathode protrusion heat an anode surface region to a critical temperature such that the yield stress of the anode material is equal to the force of the applied field. A positively charged microparticle is then detached from the anode hot spot and evaporated during its transit to the cathode by electron bombardment from the same cathode protrusion which caused the initial anode spot heating. If sufficient heating and evaporation of the microparticle takes place during its transit, the density of metal vapor in the vicinity of the microparticle becomes such that cumulative avalanche amplification of prebreakdown current occurs.

The authors detected neutral anode vapor in the interelectrode

volume immediately prior to breakdown.[73] They also calculated the conditions leading to the detachment of the microparticle from the anode, derived the microparticle's transit dynamics and the temperature it attains during transit, and obtained expressions for the pre-breakdown vapor density distribution.[74]

1.6 Discrepancies of the Theories of Microparticle Initiated Breakdown

Microparticle initiated breakdown is the only mechanism that has been proposed to explain vacuum breakdown of long, high voltage, gaps (>10mm). However, various aspects of the many possible theories need clarification.

The "clump" hypothesis put forward by Cranberg was based on the data of several investigators over a large range of voltages and gaps. The comparison of such varied data to form a single model could lead to wrong conclusions. Furthermore, his model has very little theoretical backing.

Slivkov's breakdown model may also be questioned. He assumes that all of the kinetic energy of the microparticle goes into heating the microparticle, and thus there is no target electrode heating. Also, substitution of numerical values of the quantities in his expressions for particle radius, equations (1.25) and (1.26), yield radius values in the 10^{-9}m range.[60] The values obtained for R_{max} and R_{min} are not only very small, they also nearly overlap. Thus Slivkov's model suggests breakdown is possible for a very limited range of very small particle sizes. Using Slivkov's model one could conclude that only ten iron atoms ($R=.12x10^{-9}$m) would be sufficient to cause breakdown.

The existence of the trigger discharge mechanisms of Dlendzkaya, Martynov, et al, are well documented for artificial microparticles, but

the application of the trigger discharge theory of vacuum breakdown is subject to various constraints. The work by Menon[39] suggests a lower microparticle radius limit of 10μm is necessary for a trigger discharge for a microparticle approaching the cathode. The radius range necessary for a trigger discharge involving rebounding microparticles was found to be 30-50μm.[94,96] However, experimental results indicate that naturally occurring particles of this size are not typically found in a vacuum gap.[50,128,129]

Finally, the breakdown mechanism proposed by Davis and Biondi involves the presence of strong field emitting protrusions. Since no appreciable pre-breakdown currents are observed for large gaps (>6mm), such a mechanism might be ruled out in discussing the breakdown of larger gaps. Some effects and experimental observations concerning the presence of microparticles in high voltage, vacuum insulated gaps will now be discussed.

1.7 Microparticle Velocity and Electrode Surface Damage Effects

If microparticles are present in a vacuum gap, and they are accelerated to velocities exceeding the plastic velocity of the target electrode, extensive surface damage is caused, leading to crater formation with sharp edges.[96] Plastic velocity is defined as the threshold velocity of the target material for plastic deformation. Typical plastic velocities are in the range 10-2[illegible]m/s. An expression for the critical microparticle radius necessary for creation of impact craters has been determined.[90] This expression derived assuming a single particle transit of the gap and a spherical particle, is

$$r_c = \frac{9.87\varepsilon_0 E^2}{v_p^2 \rho} \text{ meters,} \qquad (1.9)$$

where ε_0 is the permittivity of free space,

E is the field [illegible],

[illegible] is the particle material density, and

V_p is the electrode plastic velocity, given by $B = \frac{1}{2}$, where

[illegible] is the electrode material yield stress.

Microparticles of radii less than R_c are capable of creating impact damage on an electrode surface. R_c for stainless steel electrodes (σ_y=800m sec [illegible] in a 200 [illegible] cm gap system is 1.4μm. The impact velocity obtained by a spherical particle, of radius R, crossing the gap once is:

$$v = \frac{2qV}{m} = \frac{9.87\varepsilon_0 E^2}{\rho_p} \text{ meters/second} \quad (100)$$

The value of critical microparticle radius necessary for impact damage, R_c, can be increased by field enhancement or greater particle velocities than those found assuming single gap transits.

Equation (100) assumes no field enhancement at the microparticle site [illegible]. If an extra field enhancement is assumed, it can be caused only by an irregularity greater in length than the particle diameter, in which case the particle velocity is increased by a factor β^2. Values for β exceeding 2 are difficult to justify, for particles exceeding critical R_c values, since well prepared surfaces are smooth to that order. If, however, a region of an electrode is distorted by the electric field, larger charge to mass ratios can be achieved due to higher β values. Cornbach[96] has calculated the values of β to be expected for a protrusion which has a spherical tip and a [illegible] shank. For this type protrusion

$$\frac{\beta}{} = \frac{}{} \quad (101)$$

where h is the protrusion height, r the sphere radius, and

$$\beta = \frac{h}{1.645r} \tag{1.32}$$

These formulae suggest particle velocities an order of magnitude higher than those predicted by the sphere plane model.

Greater particle velocities, necessary for impact damage, may also be achieved by particle bouncing and charge exchange between the electrodes. This phenomenon has been demonstrated using artificial microparticles.[97,136] Bouncing or charge reversal has been found to occur in less than 10% of impact events[136] and the velocities thus achieved are limited by electrode oxide layer thickness.[98] Therefore, charge reversal is thought to occur by an electron tunnelling mechanism rather than by direct ohmic conduction.[98]

Hurley and Parnell[99] have considered the case of a microparticle which is itself field emitting. Microparticle velocities may be increased or decreased by self-field emission. The proposed theories for achieving impact damage velocities for small microparticles, and the possible situations under which large particles might be accelerated to these velocities have been considered. The mechanisms of crater formation may now be considered, where crater formation enhances field emitted currents which can lead to breakdown. This phenomenon is very complex.[100] Crater dimensions increase with particle velocity. The exact increase is dependent upon the velocity of sound, v_s, in the target material. Microparticle density and geometry also influence crater size. Typical craters [100] are hemispherical in shape surrounded by a "lip" which gives the appearance of having been splashed out of the crater. Most of the ejected material is target material. Such crater "lips" could act as emitting sites, and additionally, impact

could generate some metal vapor in the neighborhood of the crater. Local pressure build-up in the vicinity of these emitting sites could lead to trigger discharges.[90]

Investigations concerning the phenomena of intermediate-velocity ($100m/s<v<v_s$) impact by micron-sized particles (<3μm typical) on metallic targets have revealed that impact is followed by the production of a plasma.[90,101] The plasma has been found to consist primarily of micro-particle material. Expressions for the total plasma charge have been formulated, but a correlation between this plasma generation and vacuum breakdown was not attempted.

Electrode impact of ultrahigh velocity ($v>v_s$) particles(<.01μm typical) causes more or less the same type of crater damage as seen for intermediate and high velocity particle impacts.[90,102] Evaporation of such particles can lead to the creation of only an insignificant amount of metal vapor from the particle[90] and from the electrode.[102] Thus, ultrahigh velocity particle impact produces an insignificant amount of vapor to contribute to vacuum breakdown. Their presence should,therefore, not affect the insulation strength of a vacuum gap.[90]

The above discussion suggests the presence of microparticles of radii greater than about .01μm can be detrimental to the insulation strength of a dc vacuum gap. While large particles (>10μm) seem to induce breakdown by way of a trigger discharge, smaller particles (<3μm may initiate breakdown because of effects associated with impact. The

impact effects are sputtering and production of neutral vapor. Additionally, generated plasma can result from particle impact, but its significance seems small.

1.3 DC Voltage Vacuum Breakdown

Comparatively little work has been reported on the strength of vacuum gaps under alternating voltage conditions. Dennison[95] showed that over a limited electrode separation, below 1mm, in 10^{-6}-torr vacuum, the value of the dc breakdown voltage is lower than the peak ac 60 Hz breakdown voltage for several different electrode materials. One investigation,[104] however, has reported that, for a single gap spacing of 2.12 mm, using stainless steel electrodes, the ac 60 Hz breakdown voltage is lower than the dc value at a pressure of 5×10^{-5} torr.

Hackam and Kitchen[103] conducted extensive tests using several electrode materials and concluded that, for the gap range of 0.10 - 3.00mm and the pressure range of 10^{-6} - 2×10^{-2} torr, the ac 60 Hz breakdown strength is always greater than the dc strength at pressures where the breakdown voltage is independent of gas pressure. Only in the pressure range around 10^{-3} torr, where dc breakdown voltage maxima occur, is ac 60 Hz breakdown strength lower than dc strength.

Another difference between power frequency ac voltage breakdown and dc breakdown is that the pre-breakdown current for power frequency 50 or 60 Hz applied voltage is higher than that with dc applied

oltage [104,106]. The reasons for the observed differences between ac 50 and 60 Hz and dc breakdown have not been clearly explained.

Two vacuum breakdown studies to ascertain the functional dependence between gap spacing and breakdown voltage for ac voltages reported a gap distance to breakdown voltage dependence given by [103,105]

$$V = Cd^{n}, \qquad (33)$$

which is as postulated by Cranberg, et al, for the microparticle breakdown hypothesis. Mackam and Altonen[103] reported values of n between .8 and .86, dependent upon electrode material. Their gap separations are, however, in the range of .13 - 4.57 mm which may be too small to assume microparticle initiated breakdown. Allan and Bordoloi[105] reported values of n between .73 and .85, again for small gaps (.1 - .3mm), which compares favorably with the value of .7 found by assuming field emission breakdown[69]. Allan and Bordoloi[105] also determined that pre-breakdown currents could be described by the Fowler-Nordheim Law, and suggested that, for their short gaps, breakdown was field emission initiated. Analysis by Huston[107] has showed that the differences between ac 50 and 60 Hz and dc breakdown cannot be explained on the basis of the time period of the ac voltage. Additionally, Theophilus, et al,[106] have found that the ac pre-breakdown electrode microprojections differ in number, shape, and distribution from those formed by dc voltages.

There have been few high-voltage ac vacuum breakdown studies at frequencies other than power frequencies (50 or 60 Hz). Mackam, et al[103], have reported that for gaps up to 2 mm, there is no dependence of breakdown voltage on frequency, in the range 60 to

[illegible] There are indications[33,34] that, for [illegible] under gaps, breakdown voltage increases with applied voltage frequency. [illegible][34] has conducted studies at [illegible] using aluminum alloy electrodes at [illegible] Torr. The gap range studied was [illegible] mm, and he concluded that the value [illegible] in equation 1.33 was [illegible]

1.9 Pulsed Voltage Vacuum Breakdown

1.9.1 Introduction

Many studies have attempted to characterize the behavior of vacuum gaps under the influence of pulsed high voltage excitations. These studies are necessary to clarify breakdown mechanisms and to characterize the operation of devices that either operate using pulsed voltages or experience pulsed voltages during operation. Devices that operate under pulsed voltages in vacuum include klystrons and diodes used in high-energy particle beam accelerators.

Surge arrestors, which are used by the power industry to prevent lightening damage, are typical examples of devices that may experience pulsed voltages during operation.

1.9.2 Relation Between Gap Length and Breakdown Voltage

A vacuum gap, in general, can withstand significantly higher field strengths under pulsed voltages than either continuous or alternating voltages. The notable exception occurs in the pressure range of 10^{-3}-10^{-4} Torr. Dennolm[35] first determined this fact by studying the performance of small gaps (.1 - 1 mm) under pulsed, continuous, and alternating voltages in a vacuum of 10^{-6} Torr. He found the breakdown voltage obtained using a 12μs rise, 50μs decay pulse was approximately double the dc value.

Lee, using longer gaps, demonstrated a doubling of operating stress between dc and shorter pulses having durations on the order of 1 μs.[108] He derived an empirical relationship for this pulse duration, relating the breakdown voltage, V, to the gap length, d, given by:

$$V = C\, d^{\alpha} \text{ volts}, \tag{1.34}$$

where $C=6\times10^6$, $\alpha=.8$, and d is in meters. Other investigators have found similar results for various gap lenghts, and pulse durations. Using a pulse of risetime .3μs, Parkins[109] found α to be .54 and .5, respectively, for copper and tungsten electrode gaps, with d in the range of .1 to 2 mm. Leader[18] found α to be .73 for 20 mm diameter sphere electrodes and d between .04 and .3 mm for a 1.5x70μs pulse (risetime of 1.5μs, and decay time of 70μs). Rozanova and Granovskii[110] studied breakdown in a vacuum gap formed by a 10 mm diameter anode disk and a 10 mm hemisphere under the influence of a pulse with decay time of .125μs. They found that α depends upon electrode material, for d in the range .2-1 mm. Using a 1.5x40μs impulse, Slivkov[88] found α to range between .36 and .92 for various combinations of planar and spherical steel electrodes with d between 1 and 10 mm. Nandagopal[111] measured breakdown voltage of a point-plane gap for d between 1 and 12 mm and found α = .5 for a 1.5x50μs pulsed excitation. Note that most of the above results are similar to dc results for short gaps,[69] indicative of field emission breakdown initiation, and longer gaps,[76,88] characteristic of discharge initiation by microparticles.

1.9.3 Parameters of Pulsed Vacuum Breakdown

Several investigators, most of them Russian, have attempted to

characteristic impulse vacuum breakdown. Most of their work was conducted at relatively low voltages (10-100 kV) for short gap lengths. A brief survey of their work follows.

Kassirov and Nesterikhin[112] have conducted experiments to measure the time to breakdown and the voltage fall times at breakdown for nanosecond excitations. They found the breakdown delay time, τ, to be a non-linear function of gap length, d, given by

$$\tau = \frac{c\, d^2}{V_{SB}} \text{ sec}, \qquad (1.35)$$

where c is a constant dependent upon electrode material and electron penetration depth, and V_{SB} is the pulsed breakdown voltage. They also measured voltage fall times at breakdown and found there was an increase in fall time with increasing over-voltage ratio $\beta = V/V_{SB}$ for pulsed/V_{SB} for dc. This is in contrast to a reduction in fall time with increase in β for gas gaps.

Kassirov and Koralchuk[113] have obtained gap breakdown data using pulse risetimes of 4ns. They found that the breakdown delay, τ, decreased as excitation voltage increased. They also obtained the dependence of τ on the over-voltage ratio β. Their results show that τ decreases with β and τ is very dependent on gap length for small β but relatively independent of gap length for large β.

Kalyatskii, Kassirov, and Smirnov studied pulsed vacuum gap breakdown for .5μs risetime pulses.[114] They discovered a conditioning effect for impulse voltages, and showed that pulsed gap breakdown voltage is independent of residual gas pressure over the range 5×10^{-6} torr 10^{-2} torr.

Kalyatskii and Kassirov[115] have conducted experiments to determine the effect of electrode material on the pulsed strength of a

vacuum gap. The excitation source had a minimum risetime of .2μs. Their results indicate:

1. the gap breakdown delay depends on electrode material and increases with material mechanical strength,
2. the delay time to breakdown depends on the anode material,
3. the temporal form of the predischarge voltage depends on the cathode material.

Kalyatskii, Kassirov, Smirnov, and Frolov have conducted pulsed breakdown experiments using nanosecond risetime excitations.[116] They showed that breakdown voltage decreases as T increases. Thus, for a given gap, the shorter the pulse length the larger the self-breakdown voltage.

1.10 Long Pulse (>ms) Voltage Vacuum Breakdown Hypothesis

1.10.1 Introduction

Farrall made one of the first attempts to explain the initiation of pulsed voltage breakdown.[117] He assumed microparticles to be the initiating factor for long-gap pulsed breakdown and derived a breakdown criterion based on voltage rise type. According to Farrall, applying a pulse of constant rise rate should result in a gap breakdown voltage which depends upon the 5/6 power of gap spacing d. Moreover, breakdown voltage should be related to the 5/2 power of d for gap impulse voltages with constant risetime. This hypothesis has little experimental support. The experimental results of Wijker,[118] and even the results of Dennolm,[35] which were used in formulating this hypothesis, do not agree with Farrall's conclusions.

Experimental results seem to support breakdown mechanisms which are gap length and pulse length dependent, and not voltage rise de-

pendent. Plots of breakdown delay times versus gap spacing[...] and [...] suggest a possible breakdown mechanism change at d=.5 mm for very short gaps (<1mm). Results for longer gaps (1<d<12mm) suggest a mechanism change at d=12mm.[...]

Suggested vacuum gap breakdown mechanisms for long (>msec.) pulsed excitations include: (1) ion exchange; (2) cathode projection vaporization by field emission; (3) anode vaporization by field emission; and (4) microparticle discharge initiation.

1.10.2 Ion Exchange Hypothesis

Smith and Mason[119] have examined the impulse breakdown of a 2 cm gap between large stainless steel electrodes (≈2000 cm^2), at a pressure of $2x10^{-6}$Torr. The applied waveform had a 4us risetime and a discharge time constant of 5ms. Breakdown occurred at 290 kV. The investigators noted three types of breakdown:

(1) a sharp, complete breakdown with voltage collapse taking less than 1us and with a time lag averaging about 24 us. A few time lags were less than 4 us;

(2) an incomplete breakdown characterized by a smooth drop of about 100 kV over a period of 10 us. The voltage fall slope corresponded to an initial discharge current of 20 amperes followed by a flow of 3 amperes near the end of the voltage collapse. This was accompanied by a pressure increase to about $1.5x10^{-3}$Torr;

(3) a combination of (1) and (2), beginning as (2) and changing to (1).

The breakdown described in (1) is seen as a bright localized spark, whereas that in (2) is a diffuse, glow-like discharge. In later

papers,[120,121] the investigators state the breakdown mechanism is ion exchange with the same breakdown criterion as for the dc case.

3.3.3 Anode and Cathode Vaporization and Microparticle Initiation Hypotheses

Ronrbach[122] has studied the impulse breakdown between titanium electrodes of area 80 cm^2 at a pressure of 10^{-8} torr. A 400 kV pulse, having a risetime of 100 ns and a decay time constant of 132 ns, was superimposed on a 300 kV dc voltage to supply a total possible pulse magnitude of 700 kV. Some 50,000 measurements, involving 3000 discharges between the electrodes, were taken. The measurements were analyzed by computer to give breakdown probability and time lag at different gap lengths and total applied voltage.

At gap lengths less than 9 mm, plots of breakdown voltage versus gap spacing followed Fowler-Nordheim plots. At gap lengths between 9 and 10 mm, there was a transition region, after which (for longer gaps) the breakdown field fell significantly.

Analysis of the time lag distributions of Ronrbach's data suggest the existence of three breakdown initiation mechanisms:

(1) very short time lags (.1 - 1.0 us), independent of voltage and gap length, are characteristic of cathode microprojection vaporization. The calculated heights of these projections are between .4 and 1.2 um;

(2) very long time lags (miliseconds), linearly dependent upon gap spacing are characteristic of the vaporization of anode microprojections of heights between .2 and 2.0 um;

(3) intermediate time lags (1 - 100 us) are characteristic of discharge initiation by microparticles.

Ronrbach defined the transition gap region as: the gap region where the three mechanisms are most likely to occur simultaneously at a voltage close to the dc breakdown voltage.

1.11 Short Pulse (< μs) Voltage Vacuum Breakdown Hypotheses

1.11.1 Introduction

Suggested vacuum gap breakdown mechanisms for short (<μs) pulsed excitations include: (1) electron induced anode ions, for long gaps, and (2) cathode emitted electrons and subsequent explosion of the emitting site for short gaps.

1.11.2 Anode Ion Hypothesis for Long Gaps

Milton[123] used a low impedence, 50 nanosecond pulse generator to investigate the time correlation between prebreakdown current and voltage in a 1.27 cm vacuum gap. The excitation duration was controlled so that it was similar to transit times for ions in the gap. It was shown that five separate stages exist prior to and including the initial part of the breakdown. The time stages are:

(1) a quiet initial stage where the voltage rises but no predischarge current exists;

(2) a period of time in which a series of microdischarges are present. The microdischarges are not reproducible and apparently do not play a vital or necessary role in breakdown;

(3) a period of time during which the current is not space charge controlled and is exponentially related to the voltage, as predicted by cathode field emission theory;

(4) a stage during which the current-voltage relationship is space charge controlled, as predicted by both the field

emission equations and the Child-Langmuir relationship; and

(5) a final stage where the current becomes sustaining at a high level even though the voltage has dropped by an order of magnitude. This stage appears to be time dependent. The elapsed time to this stage is dependent upon the rise-time of the applied voltage and the gap spacing.

Milton theorized, based upon his results, that electron induced anode ions caused electrical breakdown as a consequence of regeneration effects near the cathode after anode ion arrival. His results show that greater than 10% of the metal atoms vaporized from the anode are ionized in the intergap region. He also states that the time to sustaining current (breakdown) can be predicted if the mass to charge ratio of the accelerating ions are made. Milton did not, however, make this measurement.

1.11.3 Cathode Explosive Emission Hypothesis

Vacuum gap breakdown, as a result of short (<us) impulses, is associated with the explosion of microscopic projections on the cathode surface and the progress of the resultant plasma flare across the gap. Mesyats[124] has shown this process occurring, together with a corresponding current growth associated with electron emission from the plasma flare. The term "explosive emission" has been coined for this current from the flare, and at least one study has attempted to characterize these emissions.[125]

The speed with which the vacuum gap breaks down, when subject to pulsed overvoltages (and also in many dc voltage cases), is determined by the velocity of the cathode flare as it moves toward the anode. This speed has been measured for several cathode materials to be in the range

of 1.6 km/s to 3 km/s.[124] In addition, cathode flare velocity has been observed to be relatively constant in time and only weakly dependent on the applied voltage.

Pavary and Goldman[126] have examined the closing time of a negative point to positive plane gap with a 10ns risetime pulse generator. They have concluded that, for gap lengths less than 0.5cm, the closure time was proportional to the gap length and independent of electrode materials. With gap lengths less than 1cm, their results agreed with those of Mesyats and imply cathode electron emission dominated breakdown.

Kalyatskii, Kassirov, and Smirnov[127] studied breakdown with pulses of 0.5μs risetime. Their data show an approximately linear relationship between breakdown voltage and gap length, d, for d<1.2 cm. This result can be interpreted as implying, for the conditions investigated, breakdown was initiated by cathode emitted electrons.

Mentzone, Buttner, Pucharov, Ronrbeck, and Wolff have conducted experiments with nanosecond excitations and gap lengths of between 1 and 5 mm.[128] They determined:

(1) electron emitting microprotrusions are destroyed by explosions caused by high electron current densities, and that new potential explosion sites can be formed in nanoseconds;

(2) melting occurs at the explosion site but no craters are immediately formed; and

(3) only after 2-3 ns is there electrode cratering with the formation of droplets and micropoints at the crater boundaries.

1.12 Summary of Pulsed Voltage Vacuum Breakdown Work

The results reported in the above references imply the following concerning pulsed vacuum breakdown:

1. The breakdown of short gaps (<6mm) in nanoseconds or a few 10's of nanoseconds, and the breakdown of gaps of lengths 1mm<d<25mm, in μsec., are due to explosions of cathode microprotrusions. A change in the relationships between time lag and degree of over-voltage and between time lag and gap length have been observed at gap lengths near 1cm. This implies the detailed breakdown mechanism may have changed at this gap length.
2. The pulsed breakdown mechanism for longer, and hence higher voltage, gaps (>1cm) appears to change at a gap spacing of approximately 1 cm.
3. Anode vaporization and subsequent Paschen type breakdown is thought to become important for gaps with lengths 1<d<25mm only after milliseconds of excitation.
4. Anode originating ions are believed to participate in the breakdown of 1.27 cm gaps in ten's of nanoseconds.
5. An ion exchange mechanism is believed to initiate breakdown of 2 cm gaps under the influence of a 3 μsec pulse.
6. Microparticles are believed to participate in breakdowns for excitation times of between a few microseconds to a few hundred microseconds.

1.13 Future Goals of Pulsed Voltage Vacuum Breakdown Work

The discussion of impulse vacuum breakdown indicates that further research work is needed, particularly at high voltages and longer gaps, before a complete understanding of breakdown is achieved. In parti-

cular, measurements of time delay to breakdown as a function of cathode emission (both electronic and microparticle) characteristics are required. Additionally, existing initiation models need to be extended to cover not only the initiation processes but also the later stages of breakdown, including the establishment of the vacuum arc.

1.14 Detection of Microparticles

1.14.1 Introduction

The discussions of dc and impulse vacuum breakdown suggest that microparticle activity may be a plausible cause or at least contribute to dc and pulsed voltage vacuum breakdown. Artificial microparticles have been studied to determine their effects upon vacuum breakdown, as concerns trigger discharges and impact damage. Naturally occurring microparticles have been observed, and in a few cases characterized with respect to charge, size, and velocity, using optical and electrostatic charge induction methods. The optical methods, used to observe naturally occurring microparticles, include scanning electron microscopy and two types of laser scattering techniques.

1.14.2 Scanning Electron Microscopy

Hurley and Parnell[128] were able to confirm microparticle transfer by interposing a plastic film between planar electrodes in the prebreakdown phase. The film on examination showed the presence of trapped particles 3-40μm in diameter.

Menon[50] used a shielded collector placed under a partially transparent cathode to collect prebreakdown microparticles. The electrodes in Menon's 7mm gap were of different materials to determine which electrode is favorable for producing microparticles. The collector, which was also

a different material, had a lapped alumina finish of .6um. The applied dc voltage was raised until at least one microdischarge was observed (38-80 kV) then brought down to zero. The collector was then removed and examined under the SEM and a microprobe analyzer. Examination of the collector revealed that microparticles of diameter $\leq$3um were produced at voltages as low as 30% of the gap breakdown voltage (=150 kV). The majority, although not all, of the particles were of the anode material.

Theophilus, Srivastava, and van Heeswijk[129] observed microparticles produced in a 1mm gap which consisted of two planar electrodes (one perforated) separated by an insulator. The collector surface used was vacuum-deposited aluminum on optical glass. Dc voltages, at levels below breakdown, of both polarities were applied to the gap. Subsequent SEM analysis of the collector revealed the presence of small (1-3um diameter) electrode microparticles and insulating particles.

1.14.3 Laser Scattering Techniques

Rohrbach[96] and Piuz[130] developed a laser scattering technique which allowed particles of diameter greater than 3um to be detected, while in flight between the electrodes in a planar gap (6-22mm length), after application of a 600 kV impulse voltage. The light from a non-Q-switched ruby laser (m sec pulse length) was passed through the inter-electrode area after the application of the impulse. Any particle in transit between the electrodes would scatter light. The difference between this scattered light and the non-scattered light was measured to search for a microparticle response, which would appear as a spike. Several events which could possibly be identified as microparticles were observed, but the frequency of observation was low and

many breakdown events occurred which had the characteristics of a microparticle induced event but in which no microparticles were detected. Burtt [xxx] reported the measurement of single 1 micron microparticle prior to a vacuum breakdown.

Smalley [xxx] also used a laser technique to attempt to detect microparticles in transit between the electrodes of a vacuum gap. The technique used caused microparticles to traverse a pattern of fringes formed by the interference of two laser beams. Scattered light was detected with a photomultiplier. The fringe pattern determined the detecting sensitivity of the system. This was experimentally confirmed. Smalley used both a 100 ns and a 10 μs pulse-time impulse voltage as gap excitations. He observed no microparticles. This failure could, however, be a result of the small gap spacings used (1 - 2mm) and the small volume sampled by the laser.

Jenkins and Chatterton [xxx] observed microparticles using forward scattering from a focused 4w argon ion laser that illuminated 10% of the cathode surface. The investigators gave the system sensitivity as 1μm. Jenkins and Chatterton conducted high and low energy dc and impulse tests.

The dc tests were made for a gap separation of 6mm. The results are as follows for the low energy tests. Pulses were seen which corresponded to particles of diameters between 1 and 10 μm when the voltage was raised. These low particles were not associated with breakdown. Upon breakdown many microparticles were detected. However as the voltage was raised, through breakdown, fewer and fewer breakdown microparticles were seen until a final value was

The additional discovery was that once breakdown occurred, no slow microparticles were produced. The results for the high energy dc tests were the same, but in general more microparticles were released at breakdown.

For the impulse tests the gap was set at 3mm, and the excitation source was a 220 kV Marx Generator with a 20μsec risetime and a decay time constant of 200μsec. In 3 out of 60 breakdown events particles were observed crossing the gap prior to the initial collapse of the voltage. The particles had upper velocities in the range of 78-375m/sec. These results indicate that particles cross the gap prior to every breakdown (if one assumes the statistical information can be extrapolated).

The microparticle laser detection results are inconclusive in that the frequencies of microparticles detected and their appearance prior to breakdown vary widely among investigators.

[illegible] - Electrostatic Charge Induction Techniques

The electrostatic charge induction detection scheme works as follows: a small cylinder of length [illegible] is located within another cylinder. A microparticle of charge q moving through the inner cylinder induces a voltage pulse in the cylinder. The magnitude of the pulse is proportional to q and the length of the pulse is proportional to the particle velocity. If one assumes a spherical microparticle, resting on a [illegible] surface, the particle mass and radius can be calculated from the charge q and the velocity [illegible].

[illegible] were the first to use this method to attempt to measure microparticles [illegible] places. Lenon and [illegible] work on pressure gap [illegible] and gap distance was between [illegible]. The [illegible] was [illegible] transparent [illegible] cylinder

disk under which the detecting cylinder was mounted. A microparticle removed from the anode would approach and pass through the cathode, and then through the detecting cylinder. The detecting cylinder was connected to the input of a low noise (30mV), wide band (7MHz) amplifier, whose output was taken out of the vacuum system. The charge detecting sensitivity of the detecting system was 6×10^{-14}C, which corresponds to a microparticle of about 8um diameter, resting on an electrode surface where the field is 200 kV/cm. Repeated attempts using voltages up to 170 kV and different anode materials showed that no microparticles in the detectable range were generated prior to breakdown.

Texier[134] next used electrostatic induction in an attempt to detect and characterize dc microparticles. His working pressure was 10^{-5} Torr, and his gap distance was 5mm. His cathode was a grid made of stainless steel parallel wires 0.15mm in diameter and 1.5mm apart. His detection system consisted of two operational amplifier stages, the first a voltage follower (non-inverting with a gain of 1), and the second a non-inverting stage with a gain of 10. Texier states his charge sensitivity as 10^{-15}C. It must be noted that the accuracy of this number is doubtful, since the input capacitance of his first stage alone was 10^{-11}F[135]. The minimum total system noise for a noise to signal ratio of one would had to have been .1mV which is lower than for any presently available commercial operational amplifier. Texier, in contrast to Menon, produced numerous prebreakdown microparticles for voltages up to only 60 kV. The size of detected microparticles ranged from less than 1um to more than 10 um (only a few cases). Velocities

ranged from a few m/s to 200 m/s. When different electrode materials were used, examination of a collector mounted under the detecting cylinder revealed both anode and cathode microparticles, the former always smaller than the latter.

Further research by Texier and Boulloud[137] showed that the outgassing of electrodes at high temperatures, which is necessary to achieve high vacuum, reduces the number of microparticles emitted from an electrode. This reduction was by about a factor of 10 when compared to the non-outgassed electrodes. This effect could have affected the results of Menon or Smalley.

Griffith, Kivlin, and Eastman[138] have found microparticles in submodules of accelerator tubes using an electrostatic induction system similar to Texier's. System charge sensitivity was 5×10^{-15}C. Microparticles of both polarities have been observed. Microparticle charges ranged from $<5 \times 10^{-15}$C to 10^{-12}C but less than 30 of the total of 351 particles of both polarities had charges less than 10^{-14}C. Particle velocities range from 10 to 200m/s but 90% were in the 20-100 m/s range. Particles were produced only after a tube voltage increase, and most were produced between 300 kV and 600 kV (1.5×10^{8} V/cm and 3×10^{8} V/cm). One note of caution concerning the results of Griffith, Eastman, and Kivlin is that their electrode surfaces were prepared by abrasion with 100um diameter alumina. Most, or some, of the observed microparticles could, therefore, be alumina particles. X-ray microprobe analysis revealed many of them on the electrode surfaces.

1.15 Comparison of Detection Techniques

Naturally occurring microparticles have been observed prior to breakdown using optical, laser, and charge induction methods. Each

method has advantages and disadvantages.

The scanning electron microscope can be used to directly determine the actual shape and size of microparticles, and identify and characterize impact damage. SEM analysis, however, tells nothing of the temporal production of microparticles, and quantitative energy measurements are impossible.

Laser detection schemes are advantageous in that they are fairly sensitive, they can be used to sample all the microparticles produced in the inter-electrode region, and the measurement technique does not affect gap activity and is exterior to the vacuum. Furthermore, electric field calculations are easier and more exact, and there is no dependence on the continuous operation of electronic devices which may easily fail in the presence of a high voltage discharge. Laser alignment however, is tricky and usually temporary, and for pulsed excitations timing is very critical. Charge cannot be directly measured and thus size calculations depend upon the intensity of the light scattered by the microparticle. The intensity of the scattered light is proportional to particle radius as r^m by the Mie-Lorenz theory of light scattering where m can range between 6 and 2 for small and large particles, respectively.

Electrostatic charge induction schemes are easily calibrated. The effective input capacitance can be measured using capacitive voltage division, and the system noise is directly measureable. Thus charge sensitivity is easily found. Both charge and velocity are measured so size can be easily calculated if particle geometry can be assumed. Since one electrode must be leaky in order for particles to escape, regenerative effects are reduced. Additionally, there are no timing problems associated with the use of pulsed voltages. One major disadvantage with the use of an electrostatic induction scheme is that is is mutually

exclusive. Any particle that is detected probably does not affect or initiate breakdown. Therefore, more than one microparticle must be produced, in order to relate them to breakdown. The leaky electrode changes the gap field slightly and, therefore, field values must be approximated. Only anode or cathode microparticles can be detected, and regenerative effects can probably not be studied. Reducing the effective input capacitance below some value, determined primarily by wire connections and amplifier input capacitance, is difficult. Additionally, electronic devices are very sensitive to voltage discharge noise.

Naturally occurring microparticles have been postulated to be one possible cause of vacuum, high voltage, dc and impulse breakdown. Microparticles have been detected and in some cases characterized for both dc and impulse voltages. They have been detected prior to and during vacuum breakdown. No definite correlation relating vacuum breakdown to microparticles has been established. The research results to be presented in this report are an attempt to correlate the production and characteristics of microparticles to vacuum breakdown.

CHAPTER 2

EXPERIMENTAL APPARATUS

It has been postulated that microparticles play an important role in the breakdown of high voltage vacuum gaps. Experimental measurements have, therefore, been conducted to determine the charge, velocity, mass, and radius of microparticles generated in a pulsed vacuum gap. These measurements have been made by directly measuring the microparticle charge and velocity using an electrostatic charge detection technique. The experimental arrangement consists of a vacuum chamber, high voltage power supply, electrode assembly, and the charge detector.

2.1 Vacuum Chamber

A schematic diagram of the high vacuum system is shown in Fig. 2.1. The vacuum chamber is a stainless vessel of cylindrical shape with a volume of 63 liters. The chamber consists of two pieces, a top, removable, section and a bottom section. The seal between the two pieces is made with either a copper or Viton O-ring. The bottom section has a 6 inch port which connects to an ion pump and 12 smaller half-nipple ports, only half of which are used. These six are used for electrical feedthroughs, connecting an ionization guage, and the roughing lines. The top section has 6 half-nipple ports, but only one is used, to provide the high voltage input. All the half-nipple ports are fitted with standard "Varian" flanges and employ copper gasket seals.

An ion pump (Varian model 912-7001) with pumping speed of 140 liters-sec^{-1} serves as the main pump. A cryogenic (sorption) pump (Varian model 941-6501) and a 3/4 hp mechanical pump (Vac Torr model 150), with a pumping speed of 300 liters-sec^{-1} and an ultimate pressure of 15 microns of Hg, serve as roughing pumps.

Vacuum measurements are made using a thermocouple tube (Teledyne Hastings Raydist, type DV-6M), an ionization tube

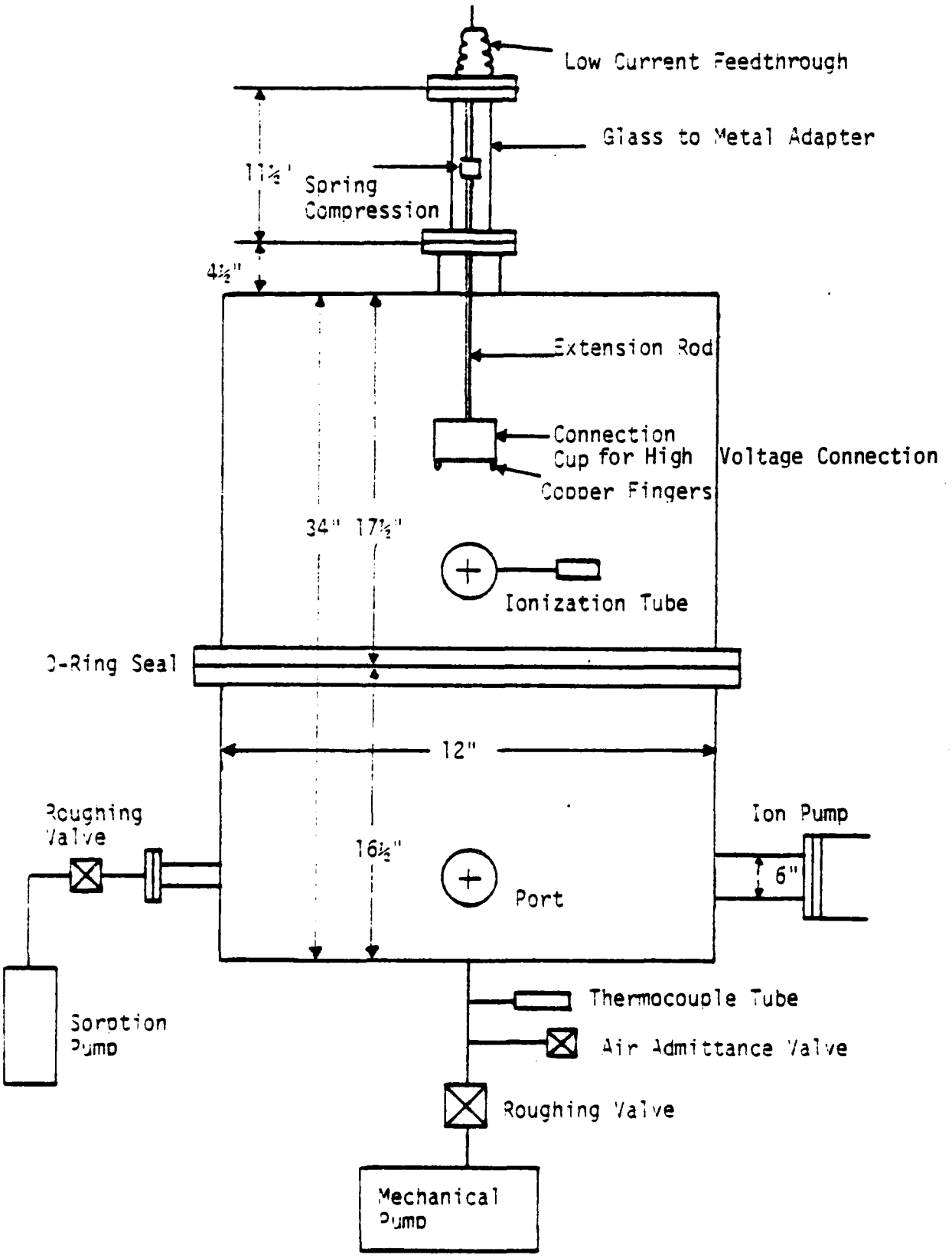

Fig. 2.1 Schematic Diagram of the Vacuum System and High Voltage Connection.

(Huntington Type 4336KLL), and the pressure meter scale of the ion pump control unit (Model # 921-0034). Ultimate system pressure is 1×10^{-6} Torr with the Viton O-ring seal.

2.2 High Voltage Connection

Details of the high voltage connection scheme are also shown in Fig. 2.1. A Varian medium current feedthrough (model # 954-5019) serves at the high voltage vacuum feedthrough. This feedthrough is isolated from the rest of the vacuum chamber by a glass to metal adapter made from two 'Huntington' glass to metal half nipples (VPF-150). A spring compression connector joins the 1/4" center conductor of the feed through to a metal rod extending into the vacuum chamber. The extension rod connects to a cylindrical stainless steel cup whose bottom rim is encircled with beryllium-copper fingerstock. The cup sits atop the anode plate, surrounding the rod used for gap spacing adjustment. Electrical continuity between the anode plate and the hv feed through is made when the top section of the vacuum chamber is lowered into place.

2.3 High Voltage Power Supply

The primary voltage source employed is a Universal Voltronics ac source. The input transformer is an UVC model B-3-10-915 with specifications: 115 volts, 60 HZ, .69 KVA. The output is an UVC model B-3-10-916 transformer with specifications: 200 KV RMS, 0.5 KVA. Output duration can be regulated from a single half cycle to several cycles by use of the triggering circuit whose schematic is seen in the Appendix. An unusual characteristic of the excitation is that

a single half cycle pulse has a duration of 15 m sec. instead of the expected 8.3 m sec.

2.4 Electrode Assembly

Fig. 2.2 shows the vacuum gap. The gap consists of a top plate to which a stainless steel upper electrode is attached and a bottom plate which contains the transparent electrode. The two plates are separated by a Delrin hollow cylinder insulator. The upper electrode is shown in Fig. 2.3 and has a 1 1/2" (3.8 cm) diameter. The upper electrode surface finish is a 000 grit emory cloth polish for all of the experimental work. The lower transparent electrode is shown in Fig. 2.4 and consists of a clear aperture having a 3" diameter which is covered with a 45% transparent perforated screen. The screen is Buckbee-Mears .005" thick, 304SS Micro-Etch Screen with hole openings of 305 μm diameter. A copper transparent wire mesh electrode with square openings of width 1600 μm is also available for use. Most of the experimental results are obtained using the perforated screen electrode because it is thought this electrode will yield more uniform gap fields.

2.5 Electrostatic Charge Induction Microparticle Detector

2.5.1 Introduction

It was stated in the first chapter that, at least in the case of long high voltage, vacuum gaps ($\gtrsim$ 6mm), there are strong indications that microparticles are responsible for the initiation of vacuum breakdown.

Naturally occuring microparticles have been observed, using laser and electrostatic charge induction methods, and characterized

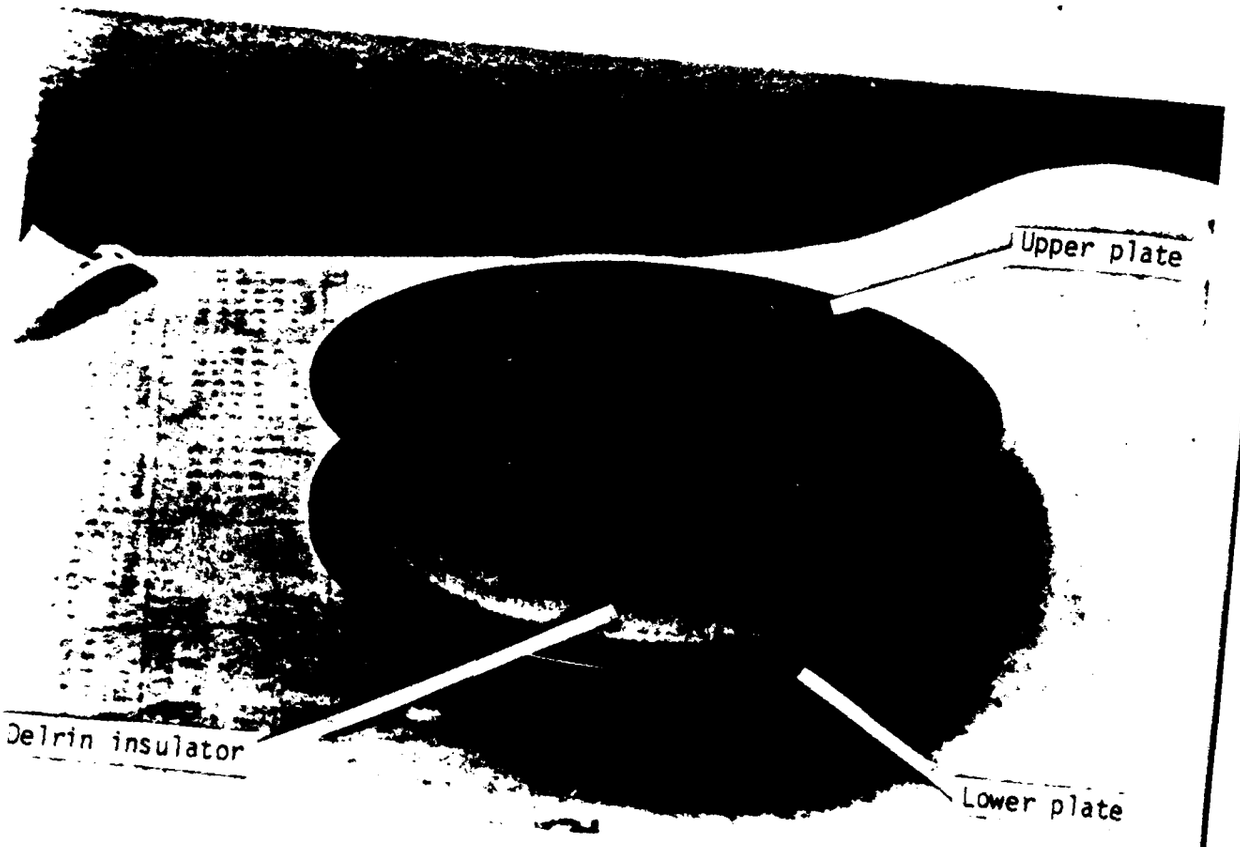

Fig. 2.2 Vacuum Gap Showing Plate Supporting Upper Electrode and Lower Plate Containing Transparent Electrode.

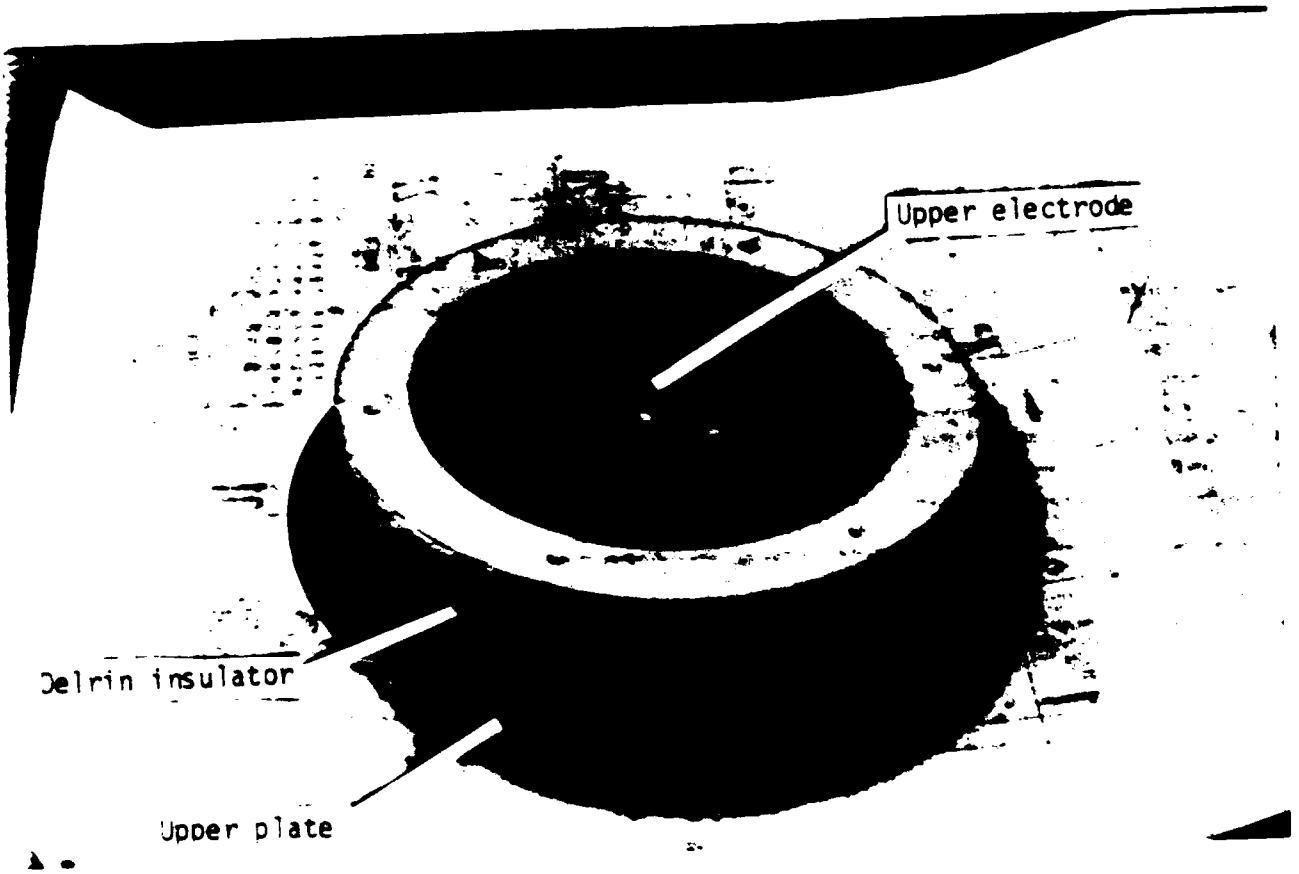

Fig. 2.3 Upper Stainless Steel Electrode On Upper Plate with Delrin Insulator.

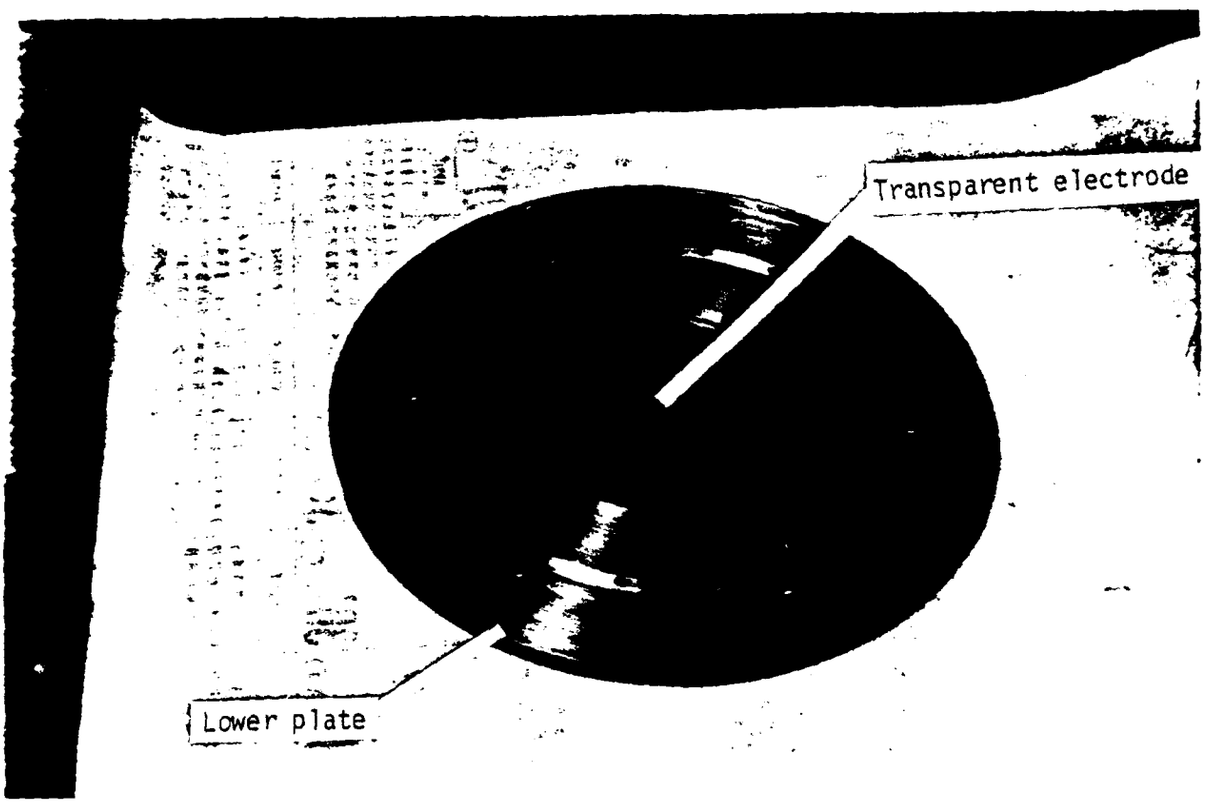

Fig. 2.4 Lower Transparent Electrode.

with respect to number, vacuum breakdown, charge, velocity, and size. The objective of this work is to determine mechanics and to specifically relate microparticle production to vacuum breakdown.

The detection method chosen was the electrostatic charge induction method used by Texier and others. This detector was chosen because: (1) the sensitivity as reported by other investigators could be improved because of the development of lower input electronic devices; (2) numerous microparticles can be generated and thus a statistical sampling technique could relate microparticle production and characteristics to vacuum breakdown; and (3) this measuring technique is easily calibrated and therefore gives more quantitative information than do the other detecting schemes.

2.3.2 Basic Principle of Operation

The principle of operation of the electrostatic charge induction scheme is based on the rise in potential of a conducting, hollow cylinder when a charged particle moves through it.

Fig. 2.3 (a) shows a cylindrical electrode situated coaxially inside another cylinder. If a microparticle of charge Q is allowed to pass through the inner cylinder, the voltage induced, V, is given by:

$$V = Q/C_{in} \text{ volts} , \qquad (2.1)$$

where C_{in} is the effective capacitance at the detector terminals. The voltage so induced will appear only so long as the particle remains within the inner cylinder and thus the output waveform of this

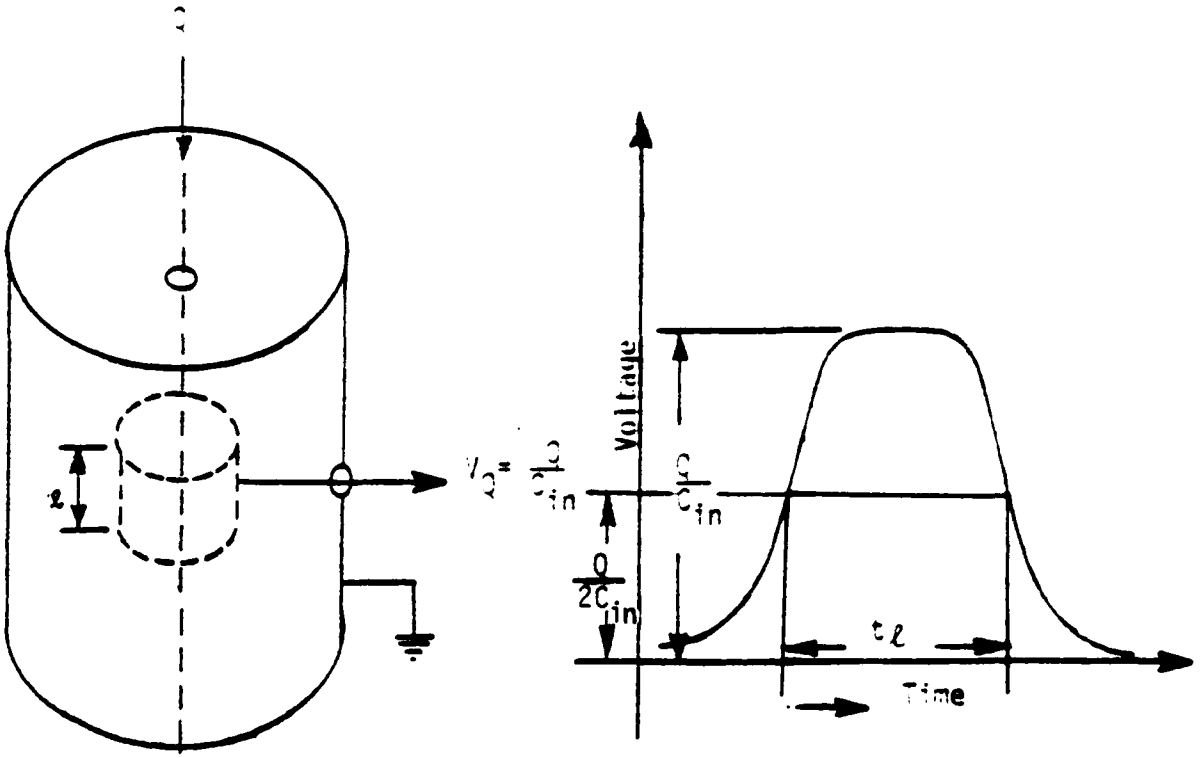

(a) (b)

Fig. 2.5 (a) The Basic Detector.

(b) Output Waveform.

configuration should be as shown in Fig. 2.5 a). The velocity of the particle is given by:

$$v = \frac{\ell}{t_c} \text{ m/sec}, \tag{2.2}$$

where ℓ is the axial length of the inner cylinder. The quantity t_c is the observed time between the half maximums of the charge detector response. This definition of t_c has been found to be necessary due to the observed, non-zero detector risetime. If V is the applied voltage which accelerates a microparticle through the gap, the mass of the particle is given by:

$$M = \left(\frac{2QV}{v^2}\right) = \frac{2QV\, t_c^2}{\ell^2} \text{ Kg}. \tag{2.3}$$

Furthermore, if the microparticle can be assumed to be spherical and of the same material as the parent electrode whose density is ρ, the radius of the particle is given by:

$$r = \left(\frac{3M}{4\pi\rho}\right)^{1/3} \text{ meters}. \tag{2.4}$$

2.5.3 Detector Sensitivity

It can be seen from equation (2.1) that the sensitivity of the detector is inversely proportional to the input capacitance, C_{in}, at the detector terminals. This capacitance includes the capacitance of the connecting cables and circuit elements, the input capacitance of the voltage measuring device, C_i, and the capacitance between the inner (detecting) cylinder and ground, C_g. Capacitance C_{in} can be reduced and hence the detector sensitivity reduced by:

1. placing the voltage measuring circuit as close as possible to the detecting (inner) cylinder,
2. chosing a low input capacitance voltage measuring device, and
3. reducing or eliminating the capacitance between the detecting

cylinder and ground, C_g.

C_g is reduced by dividing it into two parts, C_1 and C_2 as seen in Fig. 2.6, and eliminating one part with a bootstrapping method and the other part by placing it in parallel with the output voltage. Capacitance C_1 is given by:

$$C_1 = \frac{2\pi\varepsilon_0 \ell}{\ln(\frac{r_1}{r_2})} \quad F, \tag{2.5}$$

where ℓ is the detecting cylinder length, and r_1 and r_2 are the radii of the detecting cylinder and the coaxial cylinder, respectively. The coaxial cylinder will henceforth be referred to as the inner cylinder. The value of C_1 for the system in Fig. 2.6 is .67 pF. This capacitance is cancelled by a bootstrapping method. Capacitance C_2 is the capacitance between the inner cylinder and the outer grounded cylinder. The value of this capacitance is on the order of a few hundred pF. The electronics configuration effectively places this capacitance in parallel with an output voltage. This capacitance is easily driven by the electronic devices used in the detection system.

2.6.4 Microparticle Detection Electronics System

The microparticle detection electronics consist of two operational amplifier stages. The first stage is a voltage follower with unity gain, and the second stage is an inverting circuit with gain of either unity or ten (actual measured gains are .87 and 9.48). Fig. 2.7 shows a schematic of the detection electronics. Unless otherwise stated, all of the experimental results reported are obtained

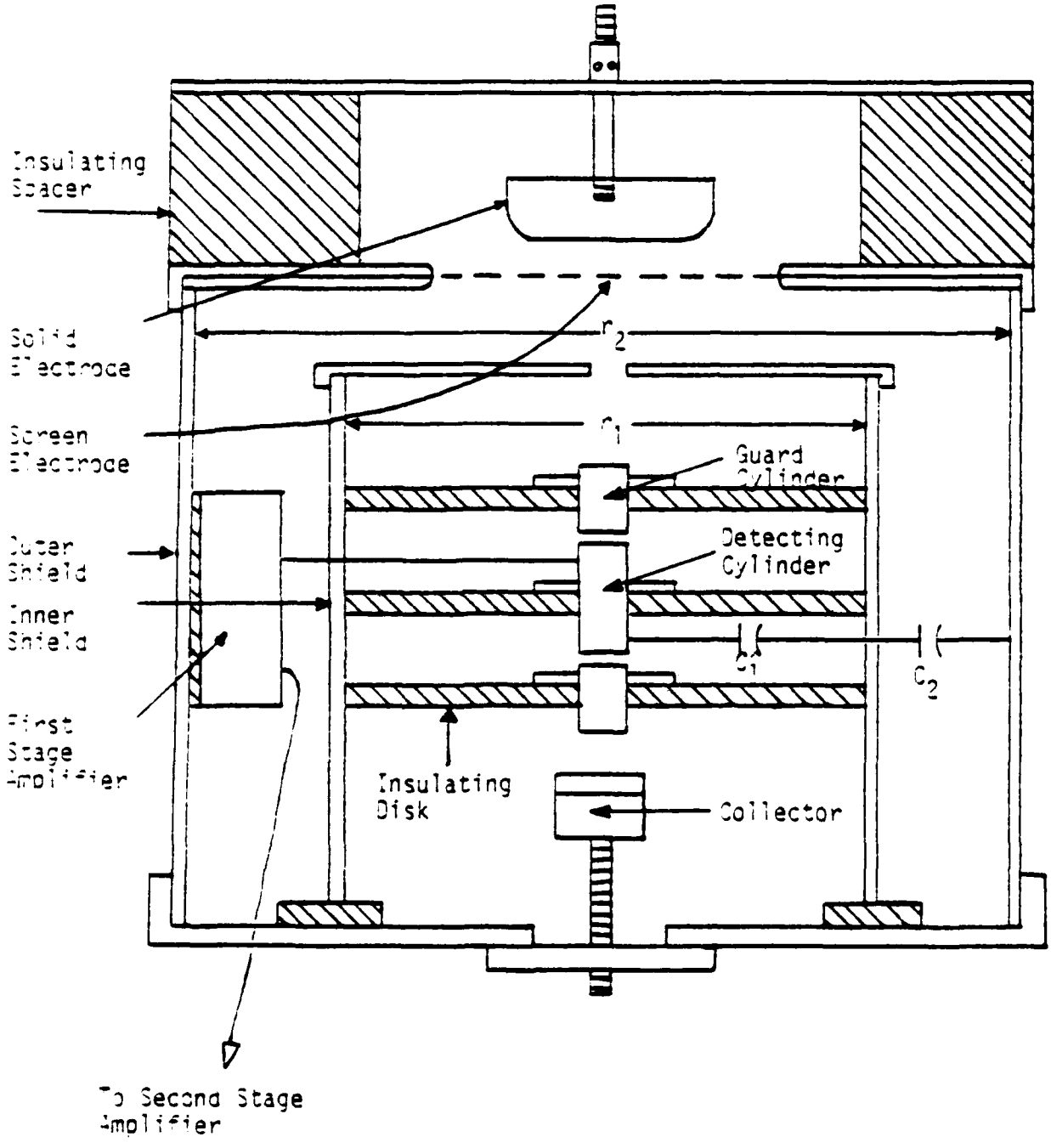

Fig. 2.6 Microparticle Detection System Arrangement.

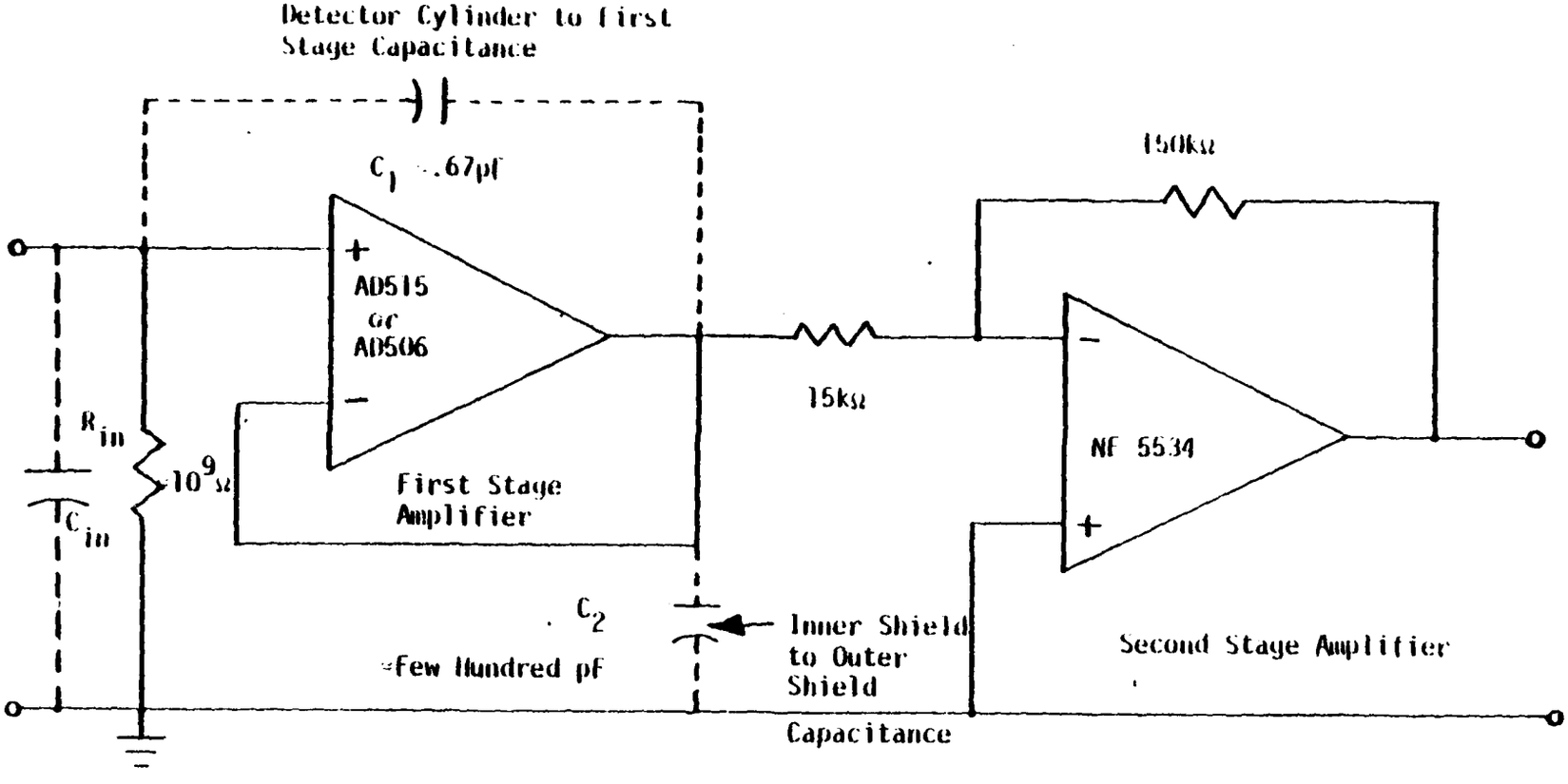

Fig. 2.7 Diagnostic Electronics.

with a system gain of 10.

The first stage was constructed using an AD515 operational amplifier (manufactured by Analog Devices) in a "bootstrap" configuration, with C_1 as a feedback capacitor. This configuration effectively cancels the capacitive effect of C_1 and reduces C_{in}.

The AD515, an FET input operational amplifier, was chosen for two reasons. First, it has the lowest common mode input capacitance, i.e. C_A, of any commercially available op-amp (.3 pF). This value was reduced to .2 pF by an appropriate circuit layout scheme.[139] Second, the AD515 also has the lowest input biasing currents of any commercial op-amp. This keeps the magnitude of any dc offset voltage, which is the product of R_{in} and the biasing current, small. A typical offset voltage value is 2mV. R_{in}, a glass coated carbon resistor, was chosen such that the time constant associated with the droop of a microparticle signal ($\tau = R_{in} C_{in}$) would remain large compared to the anticipated microparticle pulse durations.

The bandwidth of the AD515, used in a unity gain circuit, is 100 kHz. This allows measurements of particle velocities up to 3000 m/s. However, if the AD515 is used in a circuit of gain N, bandwidth reduces by 1/N. Furthermore, the small signal (mV) risetime is approximately .35/bandwidth. These two considerations determined that any signal gain must be accomplished by a second stage.

Occasional availability problems with the AD515 necessitates the use of an AD506 op-amp[140] in the first stage circuit. The performance of the AD506, which has the second lowest C_{in} and biasing currents commercially available, is similar to that of the AD515. The AD506's common mode input capacitance is 1.4 pF in the first

stage circuit, and its bandwidth is approximately 350 kHz.

The op-amp used in the second state inverter circuit is the NE5534A[14] (manufactured by Signetics Corporation), a low noise amplifier with bandwidths of approximately 300 kH_z (X10 gain) or 1 MHz (X1 gain), dependent upon the second stage gain. Total system bandwidth is thus limited by the first stage. Additionally, if necessary, the NE5534A can be capacitively compensated to drive a high impedence load. It is important that the system electronics be shielded and grounded very carefully to reduce noise pickup and to prevent possible ground loop current surges caused by the high voltage excitation. The first stage is shielded by a copper box which is mounted on the inner wall of the outer grounded cylinder in Fig. 2.6. The second stage, which is located outside the vacuum chamber, is also shielded by a copper box. Possible ground loops were eliminated by grounding the entire vacuum system, including the ion pump and measuring oscilloscopes, at a single point at the input of the first stage and by using batteries for the op-amp power supplies.

The use of a single point ground necessitated the fabrication of two shielded vacuum feedthroughs whose electrical throughput lines and shielding are isolated from the vacuum chamber wall. One feedthrough is used to provide power to the AD515, and the other is used for the first stage output. A picture and description of these feedthroughs are included in the Appendix.

Inductive noise pickup is reduced by using twisted pair, low inductance, shielded cables for interconnections between amplifier stages. Electrical shielding is made as complete as possible by

clamping the shielding of this cable to the feedthrough shield and to the first and second stage copper boxes.

2.5.5 Details of the Microparticle Detector

A detailed schematic of the test arrangement used to detect microparticles and to determine their characteristics is shown in Fig. 2.6. The vacuum gap is formed by the solid top electrode and the bottom grid electrode. The vacuum gap is supported atop an outer grounded cylinder. The outer cylinder serves as a detector shield and as a first stage mount. Microparticles produced at the top electrode escape through the transparent electrode to the analyzer section of the detector.

The analyzer section contains two guard cylinders and the detection cylinder. These cylinders are supported within a floating inner cylinder by insulating Delrin disks. The inner cylinder is also mounted on an insulating Delrin disk so as to allow the bootstrapping of capacitance C_1 (refer to Fig. 2.6). The guard cylinders are used to increase the risetime of the microparticle induced charge potential. The effect of the guard cylinders will be discussed further in section 2.5.6.

A collector electrode is also shown in Fig. 2.6. The top removable section has a 1 μm mirror finish and is designed to fit the sample holder of the University of South Carolina's SEM-Microprobe Analyzer. Thus, optical analysis of generated microparticles is also possible.

Pictures of the complete microparticle detection system and the individual parts, are included in the Appendix.

2.5.6 Detector Input Capacitance Effects

As mentioned in section 2.5.3, the microparticle sensitivity is inversely proportional to the input capacitance, C_{in}, at the detector terminals. The capacitances due to connecting cables, circuit elements, and operational amplifiers are the major contributers to C_{in}.

The contributions to C_{in}, caused by the first stage electronics, cannot be reduced below certain values. These values are .2 pF for the AD515 and 1.4 pF for the AD506. The magnitudes of the remaining contributions to C_{in} were determined using a capacitive voltage division scheme.

The primary circuit element contributing to C_{in} is the first stage input resistor R_{in}. The use of an AD506 in the first stage requires R_{in} be the carbon resistor described in section 2.5.4. The first stage circuit board leakage resistance can, however, be used for R_{in} if an AD515 is used. Using board leakage for an input biasing current path, however, causes randomly changing dc offsets. Thus the usual procedure for both op-amps is to use the carbon resistor for R_{in}. The use of this resistor adds about 1.2 pF to C_{in}.

The use of guard cylinders also adds to system input capacitance. A system of analog measurements, described in the Appendix, determined that the decrease in risetime of a microparticle signal with the use of grounded guard cylinders more than compensates for the addition to C_{in}. The use of grounded guard cylinders adds 1 pF

to C_{in}.

The remining portion of C_{in} ($\sim$ 1.2 pF) is due to the wire connections of the first stage and cannot be reduced or eliminated except by negative parallel capacitance simulation which was not attempted. It must be noted that the above capacitance numerical values are typical and are subject to change for individual system amplifiers.

The effective input capacitance at the detector terminals can be as low as 1.5 pF, but problems arise due to dc offset voltages and slow microparticle signal risetimes. More typical values of C_{in} are 3.7 pF and 4.8 pF when an AD515 or AD506, respectively, is used in the first stage electronics.

The minimum detectable microparticle charge is determined by the value of C_{in}, and the magnitude of system electronic noise. The first stage generated, high frequency noise (1 MHz) ranges in magnitude from 1mV to 5mV for both the AD506 and the AD515.

Thus, assuming a signal to noise ratio of unity, the minimum values of detectable charge are 3.7×10^{-15}C (AD515) and 4.8×10^{-15}C (AD506), for typical system sensitivities. These charges correspond to microparticles of radii 1.4 μm and 1.6 μm, respectively, produced in a planar vacuum gap of 1 cm at a voltage of 100 kV.[50]

CHAPTER 3
EXPERIMENTAL RESULTS

3.1 Introduction

The experimental arrangement and measurement technique described in the previous chapter have been used to directly measure the charge and velocity of microparticles generated in a pulsed, high voltage, vacuum gap.

The experimental results are presented in three sections. Each section represents an advancement in experimental technique with the ultimate goal being to relate microparticle activity to vacuum breakdown. Experimental procedures progress from determining detector system response to small charged beads, to the characterization of artificial microparticles, to the detection of naturally occurring microparticles.

3.2 Detection System Characterization

Beginning experimental procedures were designed to show detection system response to any conceivable microparticle activity. These early tests, which were conducted outside the vacuum chamber, determined the detection system response to charged balls, the influence of the guard cylinders, and the effects of charged particles directly hitting the detecting cylinder, a guard cylinder, and the floating inner cylinder.

Metal balls, charged with a given polarity, have been dropped through the detecting cylinder. The balls were charged using a 1 cm parallel plate arrangement and a voltage source, as shown in Figure 3.1. Positive and negative dc voltages up to 4 kV were applied across the plate. A small (2 mm diameter) lead ball was dropped between the plates. The ball rolled in contact with the bottom plate, either acquiring or losing electronic charge, and then dropped through the guard cylinders

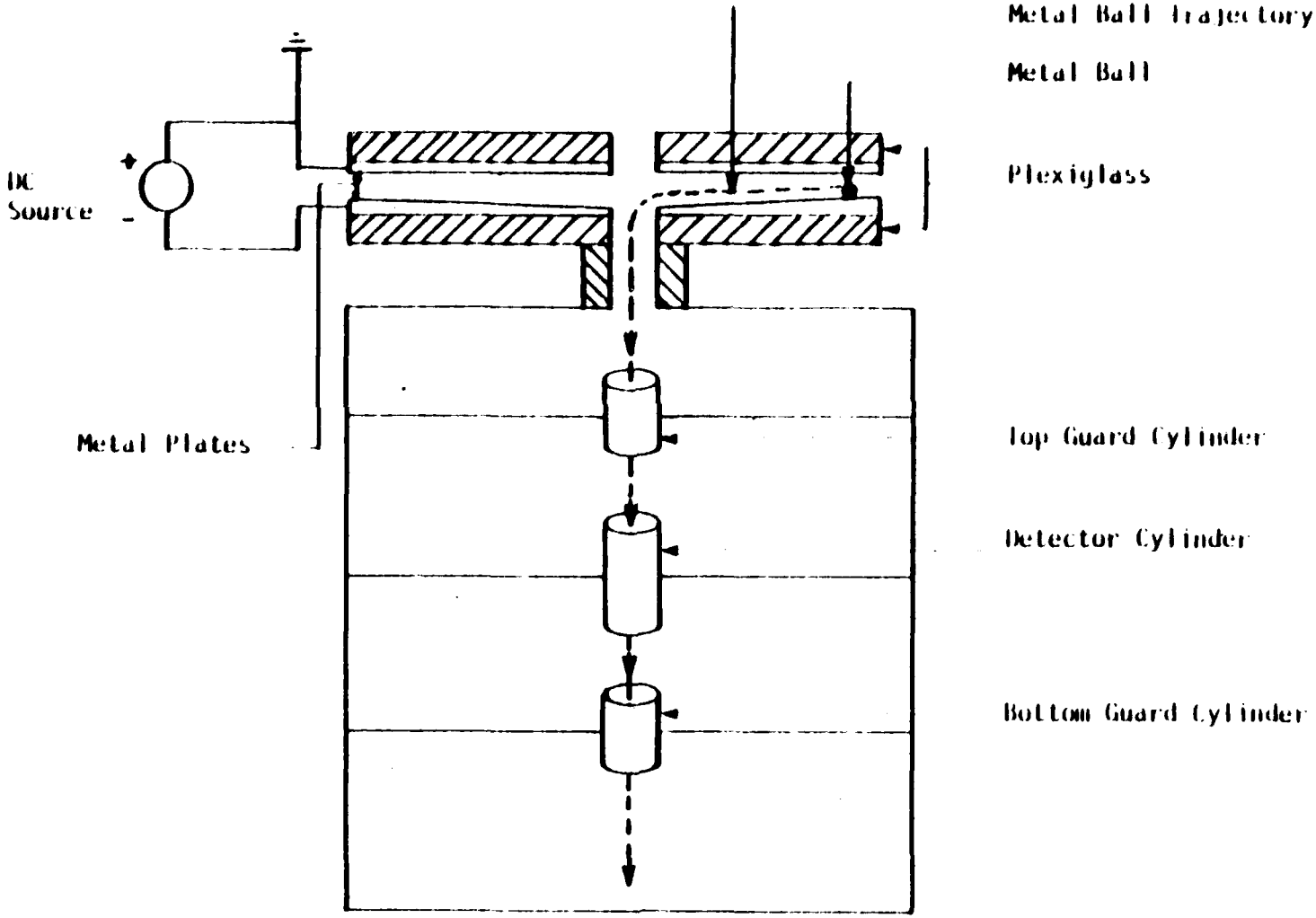

Fig. 3.1 Test Arrangement for the Detection of Charged Metal Balls.

and the detecting cylinder. The signal response at the output of the second stage was observed using a Tektronix type 549 Storage Oscilloscope.

The transit time of a metal sphere falling through the detecting cylinder is found using energy conservation. This time is given by:

$$t = \left(\frac{d^2}{2gh}\right)^{\frac{1}{2}} \text{ sec}, \qquad 3.1$$

where g is the acceleration due to gravity, d is the detecting cylinder length, and h is the height from which the ball is dropped (bottom plate to detecting cylinder separation). For the experimental arrangement of Figure 3.1, d = 3.0 cm and h = 10.0 cm, so that t = 21.0 ms. The signal response for a ball passing through the detector cylinder should therefore have a pulse width of approximately 21 ms.

Figure 3.2 shows the detector response to a 2 mm ball charged by a negative plate potential. It should be noted that, due to the second stage inverting circuit, a negatively charged ball gives rise to a positive signal. Additionally, the input capacitance for the microparticle simulation tests was increased to 100 pF by placement of an externally connected capacitor in parallel with the detector input. This was done to decrease sensitivity to a level where the electronics did not saturate in response to the large ball charges.

The signal pulse width, measured at half total magnitude, is approximately 27 ms. The signal droop and undershoot decay with the system input RC time constant.

Figure 3.3 shows the detector response to a positively charged 2 mm ball. The response is similar to the negative ball response with a voltage inversion.

The effect of the upper and lower guard cylinders has been determined

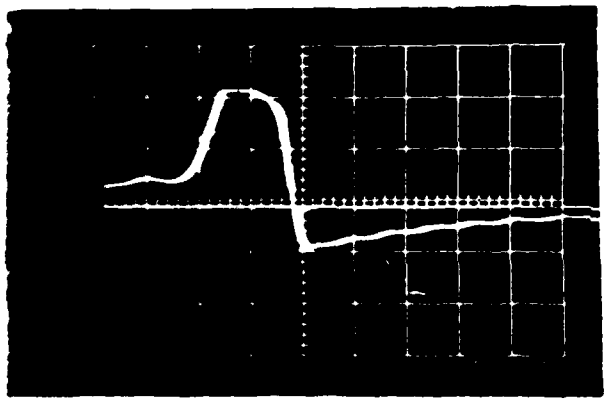

Scales:

Detector Response: 5 V/cm

Horizontal: 20 ms/cm

Detector Response to a Negatively Charged 2 mm Lead Ball.
Floating Guard Cylinders.

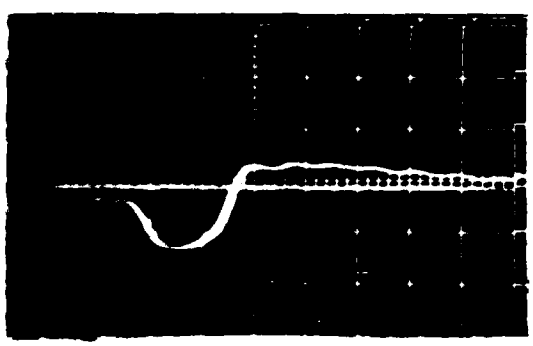

Scales:

Detector Response: 5 V/cm

Horizontal: 20 ms/cm

Detector Response to a Positively Charged 2 mm Lead Ball.
Floating Guard Cylinders.

using the charging scheme in Fig. 3.1. Fig. 3.4 shows the detector response to a negatively charged lead ball. In this case the guard cylinders were grounded. Figures 3.2, 3.3, and 3.4 were obtained with the same oscilloscope triggering level. The low level plateau of Fig. 3.2 is smaller in Fig. 3.4. This implies that the detector output risetime is faster with the guard cylinders grounded. It is also clear that the detector cylinder responds earlier (the low level plateau) to the charge if the guard cylinders are not grounded. Fig. 3.5 shows detector response to a negatively charged ball with no guard cylinders are in place. Note the slow signal rise and conspicuously long tail. The results seen in Fig. 3.2 through 3.5 imply a faster signal risetime with grounded guard cylinders and agree with the results of the analog measurements described in section 2.5.6. The diameter of the center hole in the top of the inner floating cylinder, 15/32 inches (≈ 1.2 cm), is smaller than the 1.5 cm opening of the detector cylinder. Thus, the chance of a particle entering the inner cylinder and then hitting the detecting cylinder is small. Regardless, the detector system response to a charged ball directly hitting the detecting cylinder has been determined. The detecting cylinder was cupped and then a charged ball was allowed to hit the cylinder. Fig. 3.6 shows system response to a charged 2 mm ball directly hitting the detecting cylinder. Note, the signal rises and then decays with the detector input time constant.

Additionally, the effects of charged balls directly hitting a cupped guard cylinder and the inner shielding cylinder were measured. No signals were measured for either of these events implying that no microparticle signals occur due to particles directly hitting the containment cylinder or guard cylinders.

The detector system response to 2 mm lead balls has been determined. It has been concluded that:

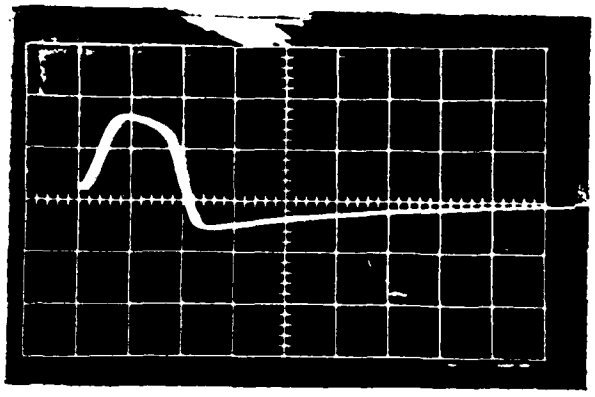

Scales:

Detector Response: 2 V/cm

Horizontal: 20 ms/cm

Fig. 3.4 Detector Response to a Negatively Charged 2 mm Lead Ball. Grounded Guard Cylinders.

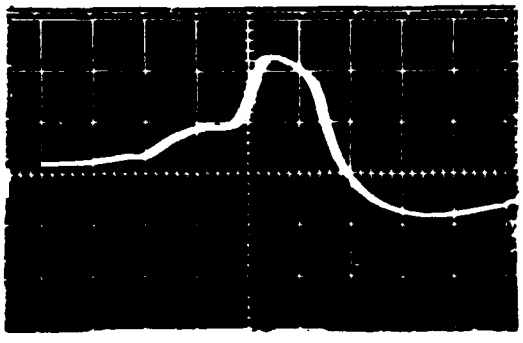

Scales:

Detector Response: 2 V/cm

Horizontal: 20 ms/cm

Fig. 3.5 Detector Response to a Negatively Charged 2 mm Lead Ball. No Guard Cylinders.

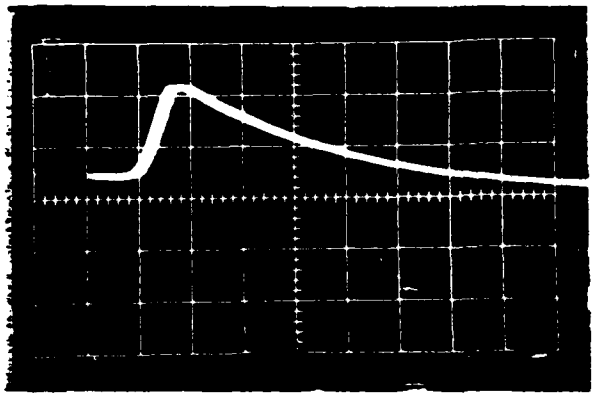

Scales:

Detector Response: 5 V/cm

Horizontal: 20 ms/cm

Fig. 3.6 Detector Response to a Negatively Charged 2 mm Lead Ball Directly Hitting the Detecting Cylinder.

(a) The presence of guard cylinders sharpened signal rise time.

(b) Grounding the guard cylinders further sharpened signal rise time, but not as much as (a).

(c) Positively charged balls gave rise to negative detector response as expected. The response polarity changed as the charge on the ball changed polarity.

(d) Negligible signals were produced by the balls striking the guard cylinders or the floating inner shield.

(e) Ball velocities were measured and found to have reasonable values.

3.3 Detection and Characterization of Artificial Microparticles

The second phase of experimental work involved the characterization of artificially introduced microparticles for low excitation voltages, which did not cause breakdown, and for higher excitation levels, where gap discharge did occur.

The artificial microparticles were certified zinc metal dust (Zn-99.5%, Ni-.5%) from Fisher Scientific. The zinc dust was observed under a microscope to consist primarily of spherical particles having radii between 1 and 5μm.

Electrode preparation for the artificial microparticle measurements consisted of degreasing using trichloroethylene, followed by methanol and distilled H_2O baths. The top electrode was coated with a thin layer of low-vapor pressure Varian vacuum grease. Zinc dust was then lightly sprinkled on the greased surface to provide the source of artificial microparticles.

The vacuum gap spacing for all of the artificial microparticle data was 8.0 mm. The bottom electrode was the perforated, 305μm hole diameter, screen. Additionally, the system pressure was approximately

4×10^{-6} Torr. All measurements were made with an AD506 as the first stage amplifier and a system gain of 10 (9.48).

Low voltage data were first obtained with the guard cylinders not grounded and a system input capacitance of 6.2 pF. The ungrounded condition was inadvertant, but the results will be reported. Results obtained were similar to those seen in Figures 3.7 and 3.8 for positive gap excitation. The two responses in Fig. 3.7 imply particle charge magnitudes of 0.12 pC and 0.09 pC, respectively, and velocities of approximately 25.0 m/s and 10.0 m/s. These particles have calculated radii of 6.0um and 9.0um, respectively. The particles in Fig. 3.8 imply charges of aporoximately 0.07 pC and 0.06 pC and velocities of 12.0 m/s. Conditioning was apparent in that further gap excitations at the same voltage level, produced particles of lower charge, and ultimately no response. Additional particle responses were produced only after a voltage increase.

Detector system response, with ungrounded guard cylinders, to negatively charged zinc particles, has also been determined. Again a conditioning effect was apparent. Fig. 3.9 shows the detector response to a negatively charged zinc particle. The excitation trace was inverted to solve a triggering problem.

All subsequent microparticle data have been produced using grounded guard cylinders. The system input capacitance increased to 7.2 pF for this configuration. All other conditions remained unchanged. Fig. 3.10 is typical of the positively charged artificial microparticle data. The particle in Fig. 3.10 was produced at 36 kV, has a charge of 0.2 pC, and a velocity of 14.0 m/s. Fig. 3.11 shows several positive microparticle responses, and an additional response that is similar to the response of

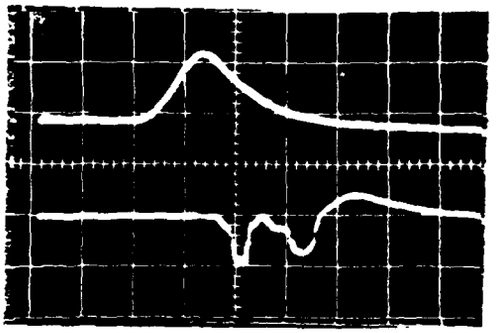

Scales:

Top: Excitation, 20 kV/cm

Bottom: Detector Response, .2 V/cm

Horizontal: 5 ms/cm

Fig. 3.7 Detector Response to Positive Zinc Particles. Ungrounded Guard Cylinders.

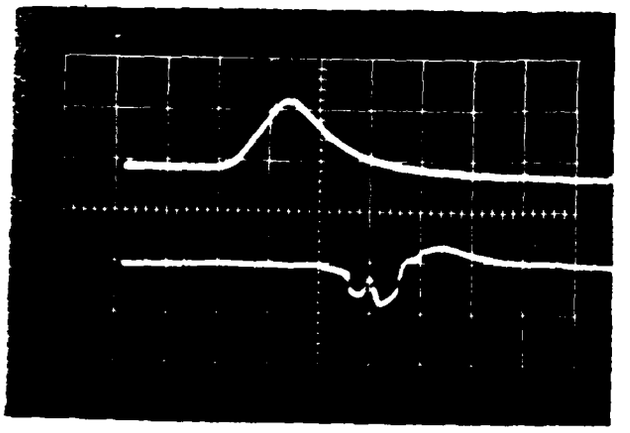

Scales:

Top: Excitation, 20 kV/cm

Bottom: Detector Response, .2 V/cm

Horizontal: 5 ms/cm

Fig. 3.8 Detector Response to Positive Zinc Particles. Ungrounded Guard Cylinders.

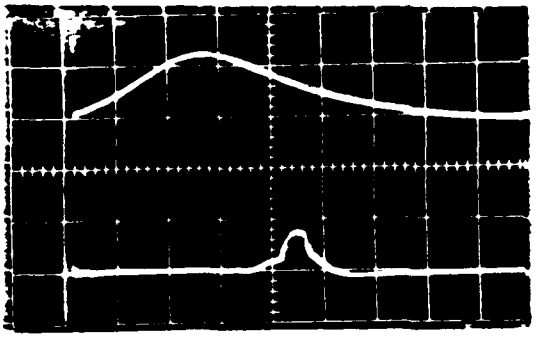

Scales:

Top: Excitation, 20 kV/cm (inverted)

Bottom: Detector Response, .2 V/cm

Horizontal: 2 ms/cm

Fig. 3.9 Detector Response to a Negative Particle. Ungrounded Guard Cylinders.

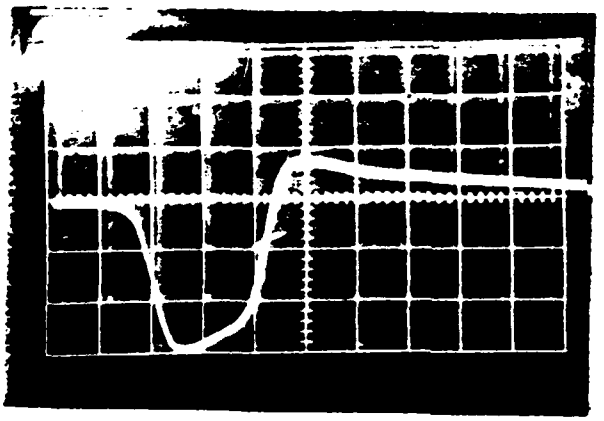

Scales:

Detector Response: .1 V/cm

Horizontal: 1 ms/cm

Fig. 3.10 Detector Response to a Positive Particle Guard Cylinders Grounded.

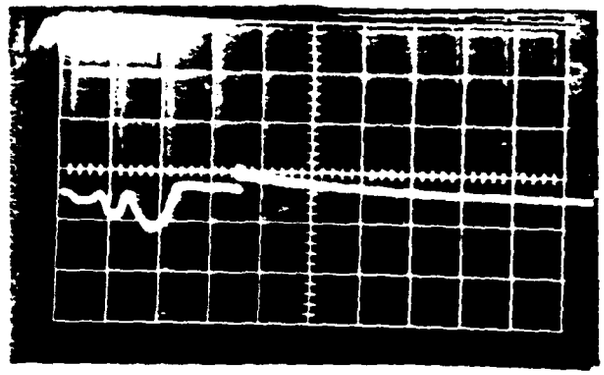

Scales:

Detector Response: .2 V/cm

Horizontal: 2 ms/cm

Fig. 3.11 Detector Response to a Positive 30 kV Peak Voltage. Guard Cylinders Grounded.

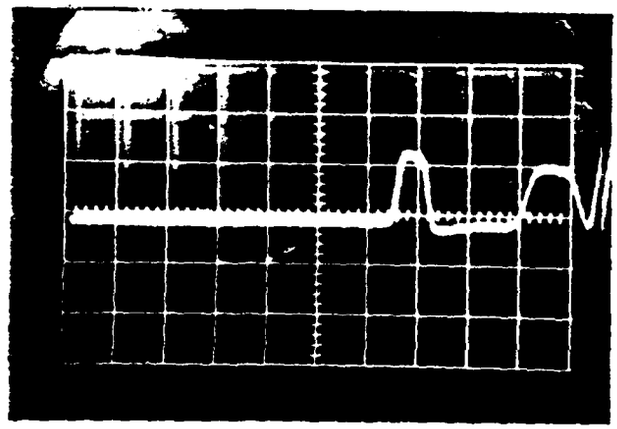

Scales:

Detector Response: .1 V/cm

Horizontal: 1 ms/cm

Fig. 3.12 Detector Response to a Negative 36 kV Peak Voltage. Guard Cylinders Grounded.

a particle hitting the detector cylinder. This response, which is seen only occasionally, is seen for positive and negative excitations, and usually is positive irrespective of gap voltage polarity. Later investigations attempt to explain this fast rise, slow decay detector response.

Fig. 3.12. shows a typical detector response to negatively charged zinc microparticles. This trace is only a small section of the total detector response to a half-cycle excitation. The gap voltage, which is not shown, was viewed using another oscilloscope. The first particle, which was produced at a gap voltage of 36.0 kV, has a charge of 0.085 pC, a velocity of 50.0 m/s, and a calculated radius of 4.3um. The second particle, which has a charge of 0.07 pC, a velocity of 30.0 m/s, and a radius of 5.8um, was also produced at approximately 36 kV. Fig. 3.13 shows a negative particle produced at 16.0 kV and a fast rise, RC decay response. Note that the response is positive and it occurred before the microparticle entered the detecting cylinder. The failure of this response to change polarity with gap voltage polarity change confirmed that it was not produced by a particle striking the detecting cylinder. There was no apparent pattern connected with the appearance of this response. It was observed prior to, after, and without accompanying microparticle signals. An initial attempt to describe these responses is described in the following paragraph.

One possible interpretation of the detector responses seen in Figures 3.11 and 3.13 is that they are noise arising from microdischarges in the intergap region. This possibility was investigated by replacing the screen electrode with thick solid foil, applying gap voltage, and monitoring the detector response. The detector response to positive and negative voltages near and above breakdown levels was always a fast rise time

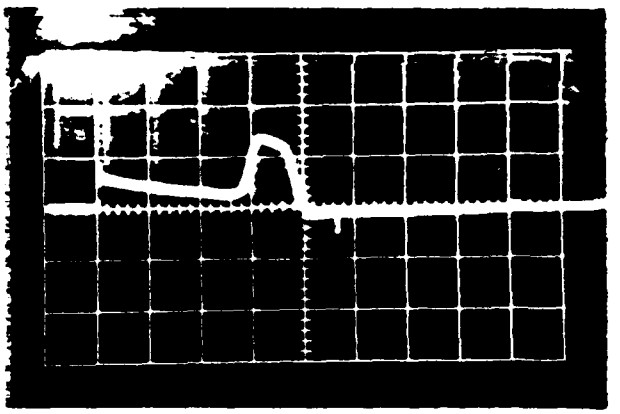

Scales:

Detector Response: .2V/cm

Horizontal: 2 ms/cm

Fig. 3.13 Detector Response to a Negative Particle.

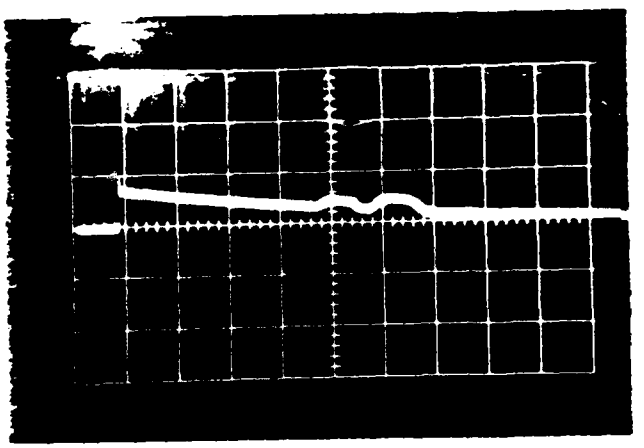

Scales:

Detector Response: .2V/cm

Horizontal: 1 ms/cm

Fig. 3.14 Detector Response to Negative Particles.

positive impulse, which then decayed with the detector system input time constant ($\tau = R_{in}C_{in}$). For positive gap voltages, this response appeared with or without apparent gap voltage collapse as viewed across a resistive voltage divider consisting of series 2 watt carbon resistors. This response did not occur for negative excitation, without definite partial gap voltage collapse. When this response appeared, with breakdown excitation of both polarities, it appeared before, after, and simultaneously with the voltage collapse. These results support the interpretation that intergap activity cause these "noise" responses.

Closer examination of the data in Fig. 3.13 reveals a possible connection between microparticle production and the appearance of noise responses. The charge of the observed microparticle is approximately 0.18 pC, and its velocity is 19.0 m/s. This particle would have required approximately 5.0 ms to travel the 10.0 cm from the top electrode to the detecting cylinder, and thus would have left the top electrode at the same time of the noise response. This implies either the microparticle was produced by the discharge or that the discharge was caused by the removal of the particle from the top electrode. However, additional data, an example of which is seen in Fig. 3.14, show too long a time delay between noise response and microparticle signal to make either of these inferences. Measurements at higher voltages, where gap breakdown obviously occurred, were conducted to further investigate the noise phenomenon.

The microparticle detector response to artificial microparticles, produced by voltages which caused partial gap voltage collapse, have also been studied. These partial voltage collapses were observed using the resistive voltage divider. The following situations were observed for

positive overvoltages:

(1) a gap voltage perturbation followed by a microparticle signal, with no noise signals

(2) a voltage perturbation preceded by a noise signal and microparticle signals

(3) a voltage perturbation and a simultaneous noise response, and

(4) a voltage perturbation preceded and followed by noise responses. There were no microparticles produced for this situation.

There were cases when no voltage perturbation was observed. Detector response for these cases consisted of noise and microparticle signals.

Fig 3.15 shows the detector response for case (1). Voltage collapse associated with an intergap discharge is seen to occur at a excitation field of 56.0 kV/0.8 cm = 70.0 kV/cm. This discharge is followed, after approximately 0.6 ms, by a single microparticle signal and then several large microparticle signals. The shape of the detector signal, as the gap voltage goes to zero, is not understood.

Fig. 3.16 shows the detector response for overvoltage situation (2). A positive noise signal precedes the voltage perturbation, and is followed by microparticle responses. Again, the detector response, as the gap voltage approaches zero, is not understood.

Case (3) detector response is seen in Fig. 3.17. Two noise responses are seen on the detector output trace. The voltage collapse apparently introduces the first response, but the cause of the second is not known.

Fig. 3.18 shows the detector response described by the fourth observed situation. The cause of the negative noise response is not known. Previously, all such noise responses were positive irrespective

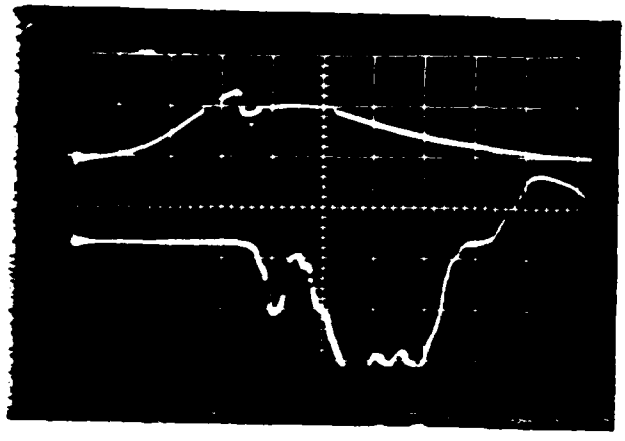

Scales:

Top: Excitation, 40 kV/cm

Bottom: Detector Response 1V/cm

Horizontal: 2 ms/cm

Fig. 3.15 Detector Response to a Positive Voltage with Partial Gap Breakdown.

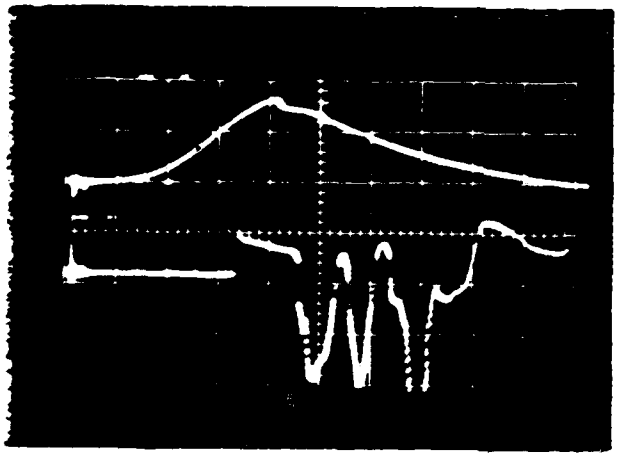

Scales:

Top: Excitation, 40 kV/cm

Bottom: Detector Response, .2 V/cm

Horizontal: 2 ms/cm

Fig. 3.16 Detector Response to a Positive Voltage with Partial Gap Collapse.

AD-A187 903 INVESTIGATIONS OF PULSED VACUUM GAP(U) SOUTH CAROLINA 2/2
UNIV COLUMBIA DEPT OF ELECTRICAL AND COMPUTER
ENGINEERING J E THOMPSON ET AL 10 FEB 81
UNCLASSIFIED N60921-80-C-A312 F/G 20/9 NL

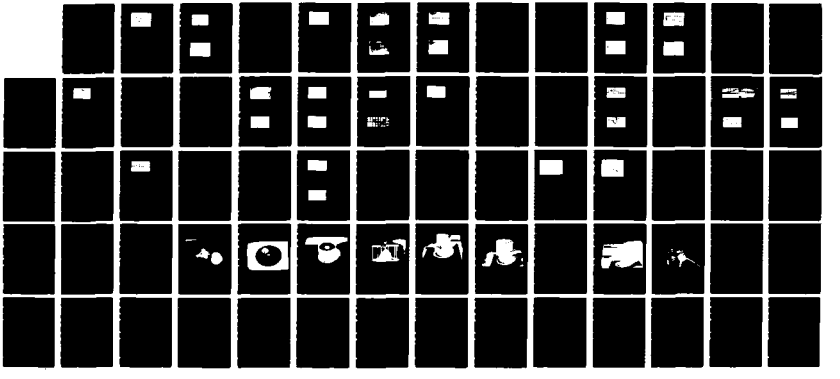

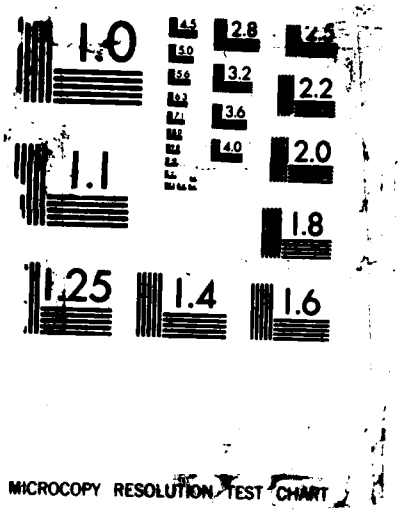
1.0
1.1
1.25
1.4
1.6
1.8
2.0
2.2
2.8
3.2
3.6
4.0
MICROCOPY RESOLUTION TEST CHART

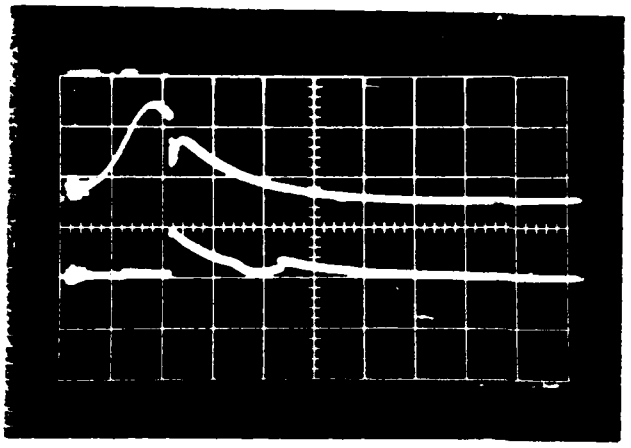

Scales:

Top: Excitation Voltage,
40 kV/cm

Bottom: Detector Response,
0.2 V/cm

Horizontal: 5 ms/cm

Fig. 3.17 Detector Response to a Positive Overvoltage.

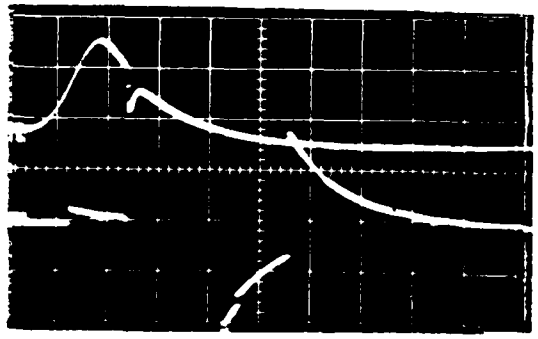

Scales:

Top: Excitation, 40 kV/cm

Bottom: Detector Response, .2 V/cm

Horizontal: 5 ms/cm

Fig. 3.18 Detector Response to a Positive Overvoltage.

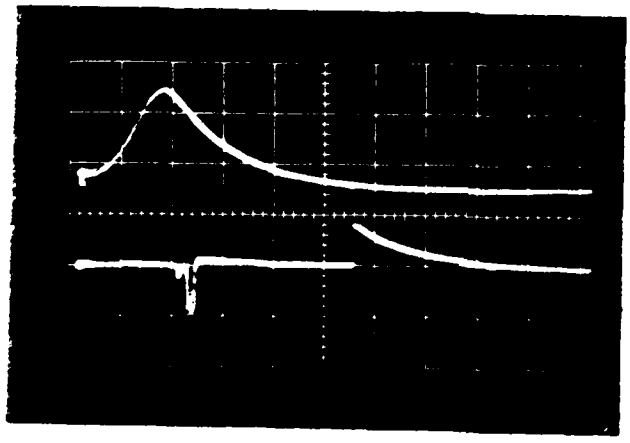

Scales:

Top: Excitation, 40 kV/cm

Bottom: Detector Response, .2 V/cm

Horizontal: 5 ms/cm

Fig. 3.19 Detector Response to a Positive Voltage with No Apparent Gap Voltage Perturbation.

of voltage polarity. This was the only negative noise observed during the artificial zinc microparticle tests.

Finally, Fig. 3.19 shows the detector response when the gap voltage was not observed to collapse. A microparticle signal appears after the excitation peak and a noise response is seen to appear approximately 16 ms later after the voltage has apparently reached zero. A small voltage does, however, probably exist across the gap and is sufficient to propagate pre-breakdown mechanisms started by higher field values.

Overvoltaged-gap,artificial microparticle data have also been obtained using negative voltages. Negative gap breakdown voltages were in general only two-thirds the magnitude of the positive breakdown voltages, so direct comparisons between positive and negative data may not be possible. The only detector response to negative overvoltages was the noise response indicative of a interelectrode region microdischarge. This noise response appeared before, simultaneously with, and after observed gap voltage perturbations. No microparticle signals were observed. The lack of microparticle signals could be a result of gap conditioning, but the actual cause could not be determined. A typical detector response to a negative gap overvoltage is shown in Fig. 3.20.

The final test,involving the detection of artificial microparticles, is concerned with improving the risetime of the detector response. The detector signal risetime, when used in conjunction with grounded guard cylinders, is longer than expected. Typical data are shown in Figures 3.21, 3.22, 3.23, and 3.24. The ratios of the length of the pulse flat top to the risetime in each of these cases are given in Table 3.1. It was expected that this ratio should be rather constant and dependent only upon geometry (size of detecting cylinder and distance between guard and detecting cylinder). The distance between the guard and detecting cylinder was measured and found to be 7 mm. The gap, which could conciev-

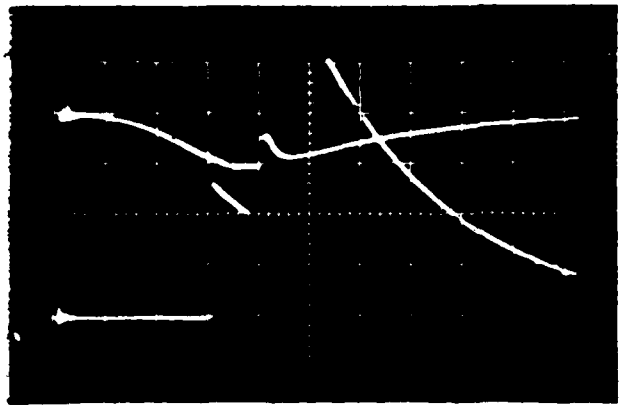

Scales:

Top: Excitation, 40 kV/cm

Bottom: Detector Response, .2 V/cm

Horizontal: 2 ms/cm

Fig. 3.20 Detector Response to a Negative Gap Overvoltage.

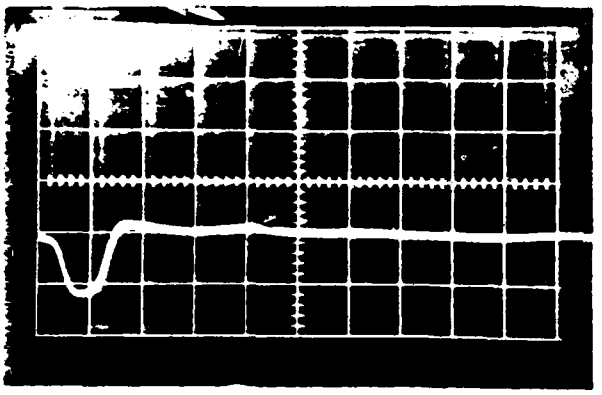

Scales:

Detector Response .2 V/cm

Horizontal: 2 ms/cm

Fig. 3.21 Detector Response to a Positive Zinc Particle. 7 mm Detecting Cylinder to Guard Cylinder Separation.

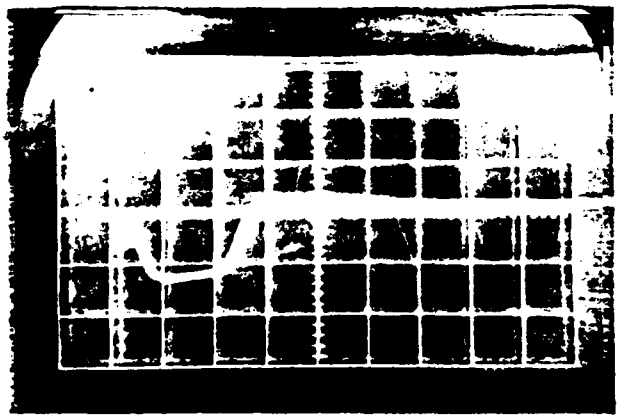

Scales:

Detector Response, .1 V/cm

Horizontal: .5 ms/cm

Fig. 3.22 Detector Response to a Positive Zinc Particle. 7 mm Detecting Cylinder to Guard Cylinder Separation.

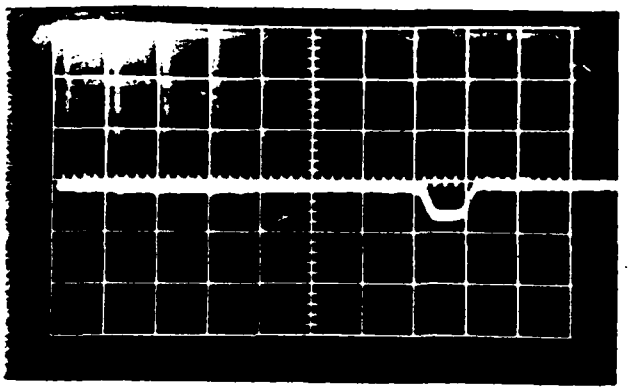

Scales:

Detector Response: .05 V/cm

Horizontal: .5 ms/cm

Fig. 3.23 Detector Response to a Positive Zinc Particle.
7 mm Detecting Cylinder To Guard Cylinder Separation.

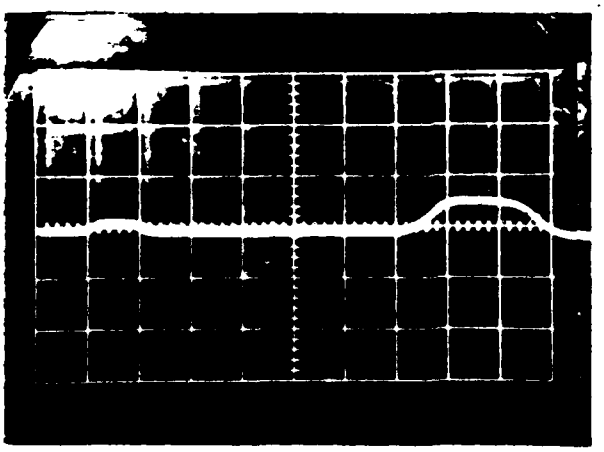

Scales:

Detector Response: .2 V/cm

Horizontal: .5 ms/cm

Fig. 3.24 Detector Response to Two Negative Zinc Particles.
7 mm Detecting Cylinder to Guard Cylinder Separation.

Figure Number	Flat Top/Rise Time
3.21	1.2 ms/0.8 ms = 1.5
3.22	0.75 ms/0.25 ms = 3
3.23	0.35 ms/0.1 ms = 3.5
3.24 (second pulse)	0.75 ms/0.35 ms = 2.14

Table 3.1. Ratios of Pulse Flat Top Duration to Rise Time for 7 mm Distance Between Guard and Detecting Cylinders.

ably contribute to slow rise time, was reduced to 1 mm and microparticle data again produced. Typical detector outputs for this arrangement are seen in Figures 3.25, 3.26, 3.27, and 3.28. All of these responses were obtained using a positive excitation.

The ratios of flat top duration to rise time are tabulated in Table 3.2. In general, there is slight improvement. The analog measurements mentioned in section 2.5.6 further investigate the cause of the slow detector signal rise time.

The detector system response to artificial zinc particles of radii 1.0um to 5.0um has been determined. Results are as follows:

(a) Square microparticle signals have been obtained for both positive and negative excitations, from which microparticle velocity and charge can be easily determined. Typical values are 0.02 pC to 0.2 pC and 10.0 m/s to 70.0 m/s.

(b) Fast rise time, exponentially falling signals have been observed, together with the microparticle signals for positive and negative excitations. Using a solid bottom electrode, these signals were shown not to be detector responses to microparticles. It was postulated that these noise signals are associated with gap microdischarge activity. Noise responses have been observed to occur before and after microparticle detection. In some cases it was possible to relate the noise signals to microparticle signals.

(c) The detector response to overvoltages has been determined for positive and negative excitations. Voltage perturbations, related to partial or complete gap voltage collapse have been observed together with microparticle and microdischarge noise signals for positive excitation. The relationship, if any,

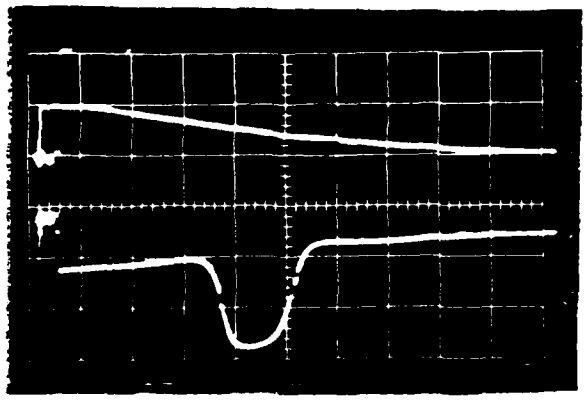

Scales:

Top: Excitation, 40 kV/cm

Bottom: Detector Response, .1 V/cm

Horizontal: 1 ms/cm

Fig. 3.25 Detector Response to a Positive Zinc Particle.1 mm Detecting Cylinder to Guard Cylinder Separation.

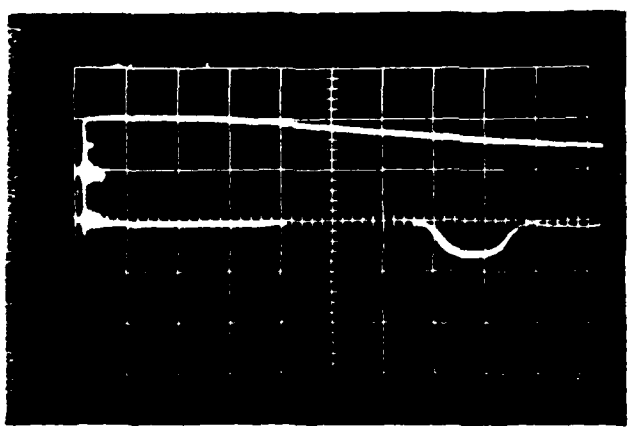

Scales:

Top: Excitation, 40 kV/cm

Bottom: Detector Response, .05 V/cm

Horizontal: .5 ms/cm

Fig. 3.26 Detector Response to a Positive Zinc Particle.1 mm Detecting Cylinder to Guard Cylinder Separation.

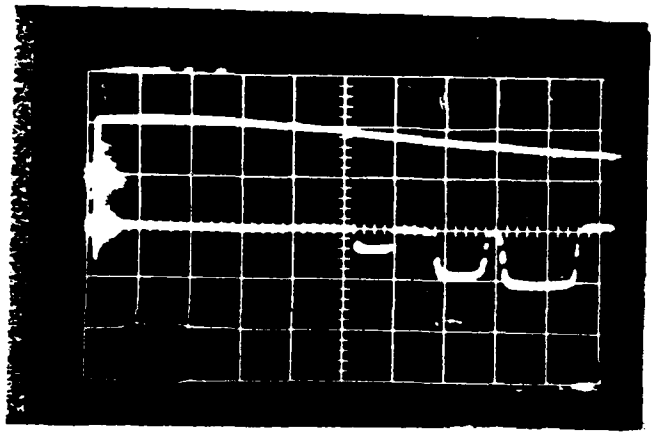

Scales:

Top: Excitation, 40 kV/cm

Bottom: Detector Response
.05 V/cm

Horizontal: .5 ms/cm

Fig. 3.27 Detector Response to Positive Zinc Particles. 1 mm Detecting Cylinder to Guard Cylinder Separation.

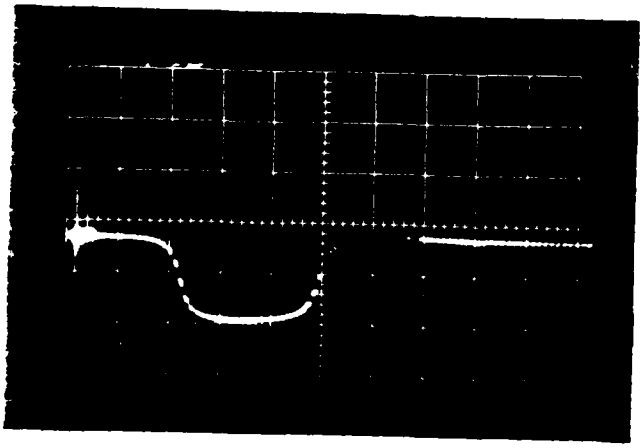

Scales:

Detector Response: .05 V/cm

Horizontal: .2 ms/cm

Fig. 3.28 Detector Response to a Positive Zinc Particle. 1 mm Detecting Cylinder to Guard Cylinder Separation.

Figure Number	Flat Top/Rise Time
3.25	1.0 ms/0.6 ms = 1.7
3.26	0.5 ms/0.2 ms = 2.5
3.27 (last pulse)	0.75 ms/0.2 ms = 3.8
3.28	0.42 ms/1.0 ms = 4.2

Table 3.2. Ratios of Pulse Flat Top Duration to Rise Time for 1 mm Distance Between Guard and Detecting Cylinders.

between these events could not be determined. Only microdischarge signals were observed for negative excitation, but this could be due to a conditioning effect.

(d) The microparticle signal rise time has been investigated as a function of spacing between the guard and detecting cylinders. Slight improvement was seen for a reduction in this spacing from 7.0 to 1.0 mm.

Although the detector system response to artificially produced microparticles is important, the objective of this research is to attempt to determine the role of naturally occurring microparticles in vacuum breakdown.

3.4 Detection and Characterization of Naturally Occurring Microparticles

The primary objective of the presented research was to determine the characteristics of microparticles produced in a planer high voltage vacuum gap using pulsed excitation. Specifically, particle mass, velocity, charge and size were determined. Furthermore, for some data, the vacuum gap current and voltage were simultaneously measured, together with the detector response, with the intent of relating breakdown phenomena to microparticle production.

The experimental conditions, for the initial attempt to detect naturally occurring microparticles, were as follows. The top electrode was thoroughly cleaned, and the gap set at 10 mm. The bottom electrode was the 45% transparent screen. An AD506 served as the first stage amplifier. The input capacitance was 7.2 pF (for all other cases, Cin = 4.8 pF for an AD506). The system background, high frequency, noise was 5 mV. This background noise reduced system input charge sensitivity to 3.6×10^{-14} C.

The total electronics system gain was always approximately 10. The guard cylinder to detector cylinder spacing was 1 mm, and the guard cylinders were always grounded. The gap voltage was viewed using the previously described resistive voltage divider. The gap voltage and detector response were viewed using 3, series 549, Tektronix storage oscilloscopes. For all data runs, except one, these scopes were externally triggered 5 ms apart, with the first scope triggered at the beginning of the gap voltage rise.

For the initial experiment, positive gap voltage of magnitudes between 5 kV and 120 kV was applied a total of 87 times. No detector response was seen until the first partial gap voltage collapse at 60 kV. Detector response to this collapse was the microdischarge noise type signal described in section 3.3. The same response is shown in Fig. 3.29 for the next partial voltage collapse at 72 kV. Sometime after the 87th voltage application the first stage amplifier was destroyed.

The first stage op-amp destruction was normally accompanied by a large change in dc offset voltage (milivolts to volts). After any such change, the first stage op-amp was replaced if it was found to be defective. Any one of the following conditions usually indicated the first stage op-amp was not operating correctly:

(1) a non-unity first stage gain

(2) an incorrect frequency response

(3) a signal could not be capacitively coupled into the first stage input as seen in Fig. 3.30.

The circuit seen in Fig. 3.30 is the one used to measure detector system

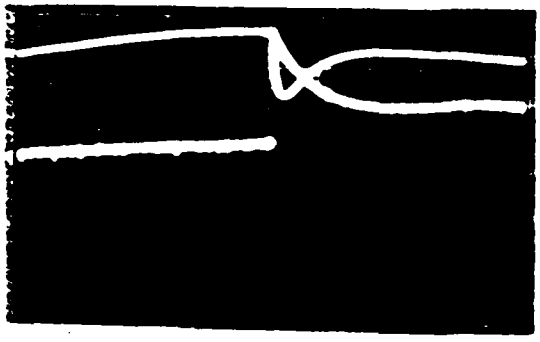

Scales:

Top: Excitation, 40 kV/cm

Bottom: Detector Response, .05 V/cm

Horizontal: .5 ms/cm

Fig. 3.29 Detector Response to Partial Gap Voltage Collapse.

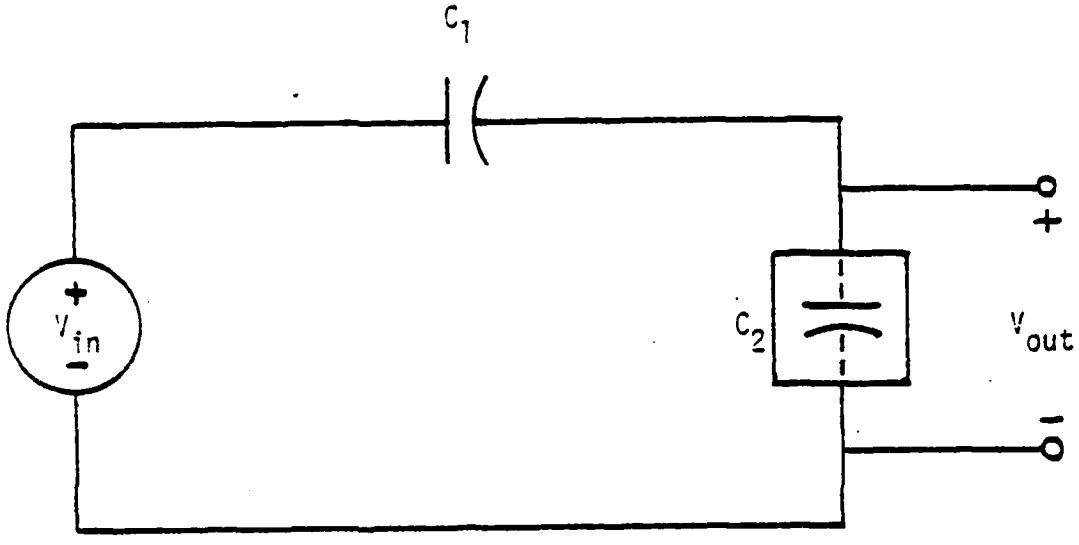

Fig. 3.30 Circuit Used to Measure Microparticle Detection System Input Capacitance.

input capacitance. V_{in}, the known input voltage, is related to V_{out}, the first stage output voltage, by:

$$V_{out} = \frac{V_{in}\ C_1}{C_1 + C_2} \quad ,$$

where C_1 is a known capacitance and C_2 is the effective input capacitance of the microparticle detection system.

The operational amplifier was replaced with an AD515 amplifier and more measurements were made. The top electrode was roughened slightly using 000 grit emory paper for subsequent measurements. The electrode was then thoroughly cleaned and the gap set at 5 mm. The 45% transparent screen was used as the bottom electrode. System input capacitance was 3.24 pF and the background noise was 1.5 mV. The resulting system sensitivity, for a unity noise to signal ratio, was $q = 4.9 \times 10^{-15}$C. The gap voltage and detector response were viewed for 1 ms prior to and 2 ms after the peak gap voltage.

Positive voltage of magnitudes between 80 kV and approximately 120 kV was applied to the gap. The most prevalent detector response, over this entire voltage range, was a microparticle signal large enough to saturate the second stage amplifier ($q > 2.9$ pC). A typical saturation response is seen in Fig. 3.31. It should be noted that two microparticle saturation signals are shown. This type response was seen before and after smaller microparticle signals.

Smaller, non-saturating, microparticle signals were also observed. Figures 3.32 through 3.37 show typical responses. The microparticle data does not appear "square." The reason for this is unknown.

The measured charge and velocity, and calculated mass and radius

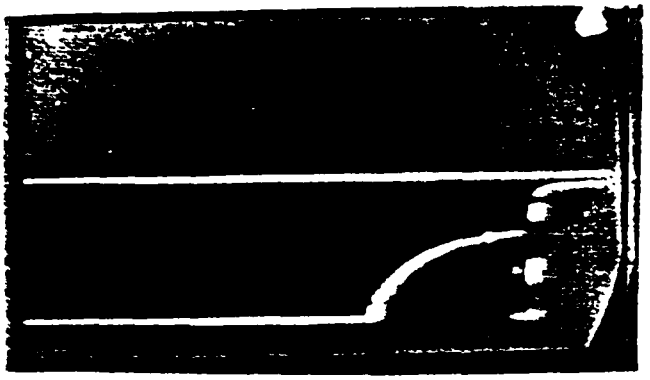

Scales:

Detector Response: 5 V/cm

Horizontal: 100 μs/cm

Fig. 3.31 Microparticle Causing Amplifier Saturation.

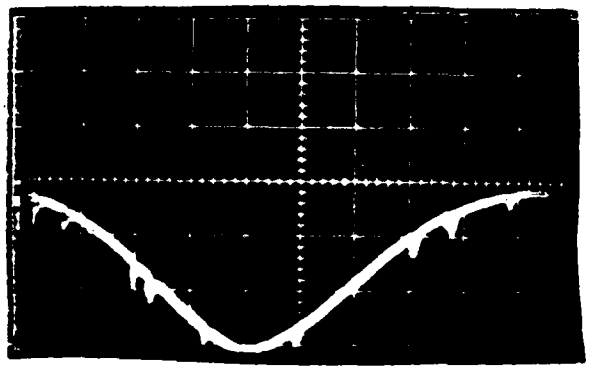

Scales:

Detector Response: 1 V/cm

Horizontal: 100 μs/cm

Fig. 3.32 Microparticle Signal. Peak Voltage = 92 kV.

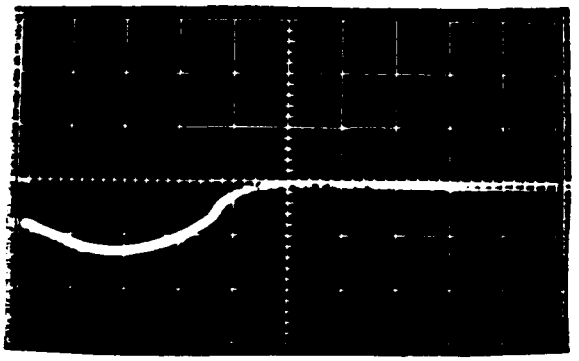

Scales:

Detector Response: .3 V/cm

Horizontal: 100 μs/cm

Fig. 3.33 Microparticle Signal. Peak Voltage = 92 kV.

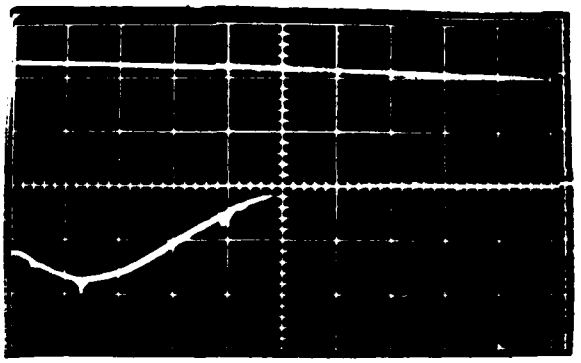

Scales:

Top: Excitation, 40 kV/cm

Bottom: Detector Response, .2 V/cm

Horizontal: 100 μs/cm

Fig. 3.34 Microparticle Signal.

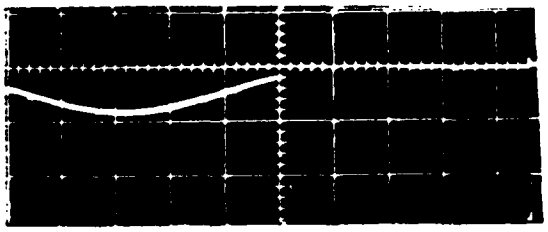

Scales:

Top: Excitation, 40 kV/cm

Bottom: Detector Response, .5 V/cm

Horizontal: 100 us/cm

Fig. 3.35 Microparticle Signal. Peak Voltage = 80 kV.

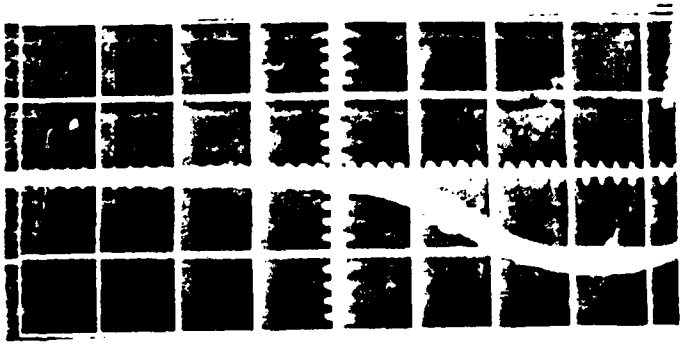

Scales:

Detector Response: 5 V/cm

Horizontal: 100 us/cm

Fig. 3.36 Microparticle Signal. Peak Voltage = 30 kV.

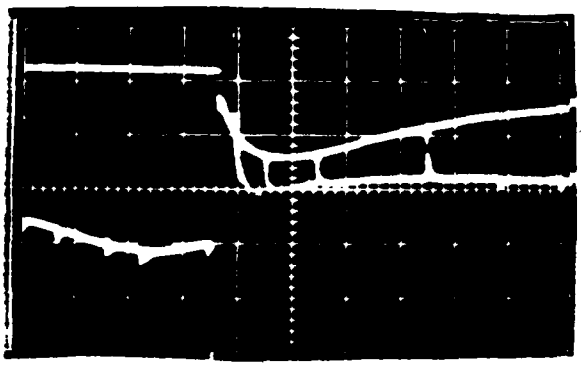

Scales:

Top: Excitation, 40 kV/cm

Bottom: Detector Response
.1 V/cm

Horizontal: 100 μs/cm

Fig. 3.37 Microparticle Signal With Gap Voltage Breakdown.

values for the microparticle signals shown are listed in Table 3.3.

The data of Fig. 3.37 illustrates different conditions from those of the other data. Gap breakdown occurred while the microparticle was within the detecting cylinder. The subsequent detector response is not understood. The typical detector response to a partial voltage collapse is a positive noise response similar to that seen in Fig. 3.29.

Because of the large positive microparticle signals, the second stage electronics were altered to allow for a gain of one. Subsequently, a vacuum feedthrough was damaged before negative gap voltage could be applied. This prevented continuation of these data, and thus comparison of positive and negative microparticle data.

An additional diagnostic technique, involving current measurement, was added in an attempt to relate microparticle production to vacuum gap breakdown. A 60 kΩ current measuring resistor was installed in the ground return from the bottom transparent electrods. This electrode was insulated from the outer ground cylinder by a Delrin ring. This scheme measured both displacement and conduction (discharge) currents.

Typical voltage and current measurements, obtained without vacuum breakdown or prebreakdown, are shown in Fig. 3.38. The current trace is due solely to displacement current. It should be observed that the current zero occurrs simultaneously with the voltage maximum as is expected for a capacitive system.

Typical results obtained for voltage levels where vacuum breakdown did occur are shown in Fig. 3.39. The current trace of Fig. 3.39 shows two small positive spikes which occur at 7 ms and 7.6 ms, a large negative spike at 10 ms, and a positive and negative spike at 12 ms. The events at 10 ms and 12 ms are associated with voltage collapses. It is believed the small current pulses (90 A), not associated

Figure Number	Charge (pC)	Velocity (m/s)	Mass (kg)	Radius (μm)
3.32	.972	67	3.9×10^{-11}	10.6
3.33	.21	85	5.4×10^{-12}	5.5
3.34	.11	≈100	1.8×10^{-12}	3.8
3.35	.13	75	3.7×10^{-12}	4.8
3.36	1.9	≈90	3.8×10^{-11}	10.4
3.37	.039	≈60	1.7×10^{-12}	3.7

Table 3.3 Characteristics of Naturally Occurring Microparticles.

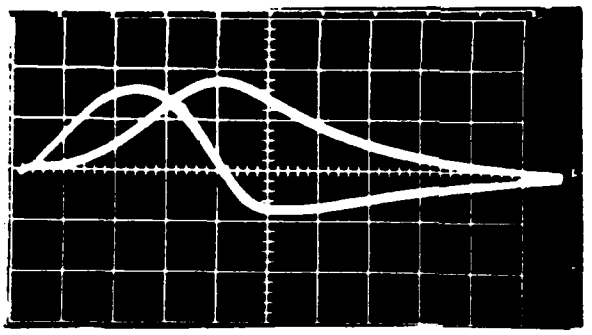

Scales:

Voltage: 20 kV/cm

Current: 83 μA/cm

Horizontal: 2 ms/cm

Fig. 3.38 Vacuum Gap Current and Voltage with no Discharge or Breakdown.

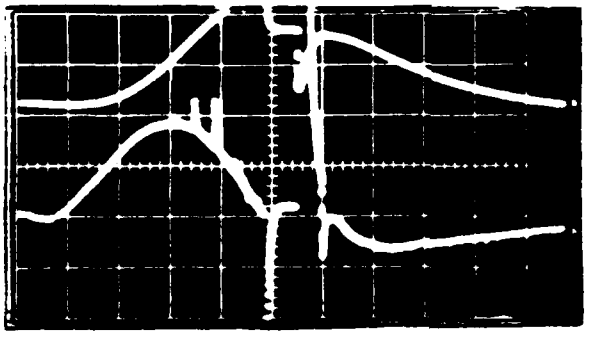

Scales:

Voltage: 20 kV/cm

Current: 83 μA/cm

Horizontal: 2 ms/cm

Fig. 3.39 Vacuum Gap Current and Voltage with Discharges and Breakdowns.

with voltage collapse are self-quenching microdischarges, and that the larger spikes are total-gap discharge currents.

The initial data, taken measuring both detector response and gap current, were inadvertently collected with a defective first stage, thus revealing no useful microparticle information. However, two observations could be made:

(1) positive self-breakdown voltage was larger than negative, and

(2) after application of negative voltage, the positive self-breakdown voltage was lowered.

No attempt was made to verify result (2), for a switch from positive to negative excitation.

Typical, simultaneously acquired, current, voltage, and microparticle data for positive gap excitation are shown in Figures 3.40 and 3.41. These figures show two of the three microparticles produced in a 5 mm gap for 43 total gap excitations, for voltages between 20 kV and 90 kV. Thirty-seven similar voltage applications for a 10 mm gap produced no microparticles. C_{in} was 4.8 pF (AD506) and the background noise was 1.74 mV, for these 80 voltage applications. Additionally, the top electrode was roughened slightly with 000 emory paper prior to vacuum gap assembly. The only notable difference between the 5 mm and 10 mm data was that the bottom electrode was the 1600μm square-hole mesh for the 5 mm data and the 305μm diameter hole screen for the 10 mm data.

No voltage breakdown or current discharges occurred for the data of Fig. 3.40. Microdischarges are, however, seen on the current trace. The first microdischarge current spike occurs simultaneously with the noise response of the detector. Every noise response of the detector corresponds to a microdischarge current spike, the converse is, however, not true.

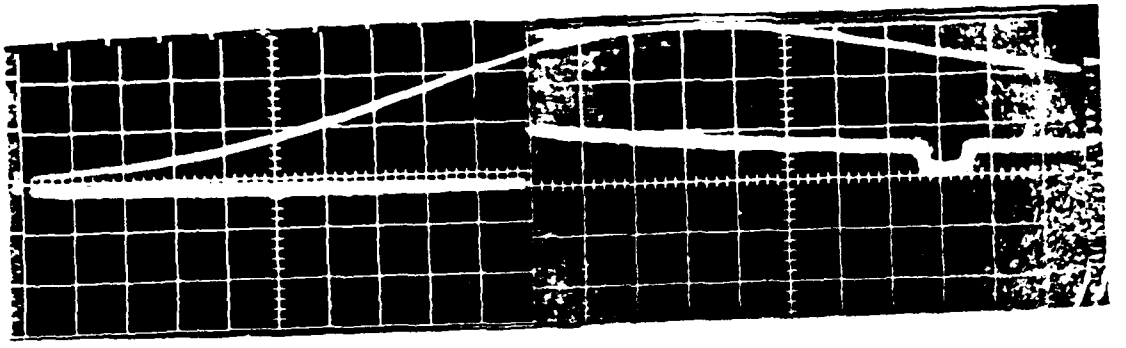

Scales:

Top: Excitation, 20 kV/cm

Bottom: Detector Response, 50 mV/cm

Horizontal: .5ms/cm

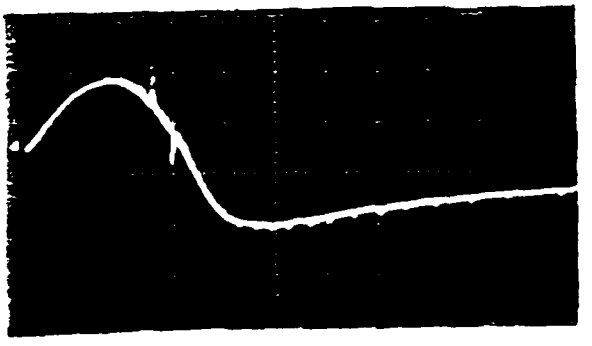

Current: 30 μA/cm

Horizontal: 2 ms/cm

Fig. 3.10 Gap Voltage, Detector Response and Gap Current, 6mm Gap.

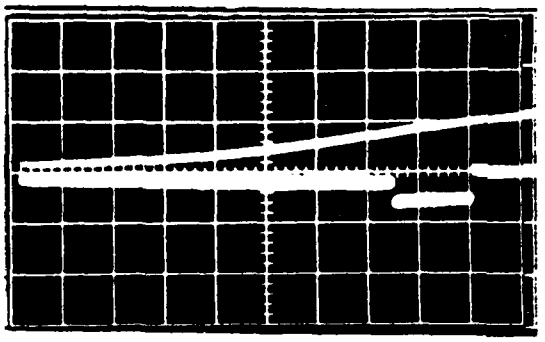

Scales:

Top: Excitation, 40 kV/cm

Bottom: Detector Response
50 mV/cm

Horizontal: .5 ms/cm

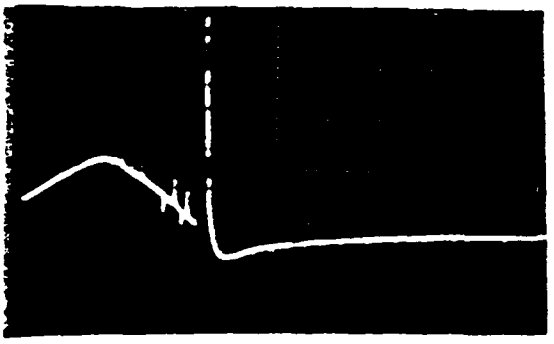

Current: 166 μA/cm

Horizontal: 2 ms/cm

Fig. 3.41 Gap Voltage, Detector Response and Gap Current, 5mm Gap.

The microparticle , having charge q = 9.6 x 10^{-15}C and velocity 60 m/s, traveled the 100 mm between the top electrode and detector in 1.6 ms and thus was pulled off the top electrode at a voltage of 60 kV. There was no current discharge response at this voltage.

For the data of Fig. 3.41, a voltage breakdown and associated current discharge occurred after detection of the microparticle. The microparticle, which has a charge of 1.4 x 10^{-14}C and a velocity of 43 m/s, was produced at 16 kV.

The microparticle detector response most often observed during the simultaneous measurement of gap voltage, detector response, and gap current, was a positive noise signal, indicative of a microdischarge. Small positive and negative current spikes were seen on the current trace with no breakdown and only large positive spikes were seen at breakdown. The small negative current spikes were not seen until peak gap voltages of approximately 60 kV(56 kV for the 5 mm gap, and 66 kV for the 10 mm gap) were reached. It should be noted that the observed negative polarity, for the positive excitation, is not presently explainable.

The microparticle detector response, gap voltage, and gap current were also simultaneously viewed for negative excitations of a 5 mm gap. The conditions were the same as for the positive excitation case, and the system pressure was 6 x 10^{-6}Torr. The top electrode surface was not roughened again. No microparticles were seen for a total of 10 voltage applications between 28 and 68 kV, where breakdown occurred. The only detector response was positive noise signals that occurred simultaneously with small negative current spikes.

Destruction of the first stage amplifier by a gap voltage collapse, which had been an occasional problem before the addition of the

current viewing resistor, became more of a problem after its addition. The discharge current, which is limited by a 10 MΩ series resistance, was believed too small to explain this change, so the remaining data was taken without the current viewing resistor.

Initial data, with no current viewing resistor, were taken for a 5 mm gap using an AD506 as the first stage amplifier. C_{in} was 4.8 pF and background noise was 1.74 mV. System pressure was 2 x 10^{-5}Torr. The first 34 positive voltages applications,between 16 kV and 72 kV,produced only positive and negative microdischarge signals. The last voltage application, which destroyed the AD 506, and the associated detector response, is shown in Figure 3.42. At least two microparticle signals are seen. Their charges are 8.2 x 10^{-14}C and 6.2 x 10^{-14}C, respectively, and their velocities are both approximately 400 m/s. The small positive signal,seen before the first microparticle,precedes the particle arrival at the detector by approximately .25 ms. If this signal is a microdischarge signal, it would have been produced at approximately the same time as the microparticle.

Additional data taken for a 10 mm gap using an AD515 as the first stage with sensitivity of c = 5.6 x 10^{-15}C gave only positive noise signals for 20 positive voltage excitations between 54 kV and 80 kV. Initial partial gap voltage collapses at 72 kV did not harm the first stage op-amp, but one at 80 kV destroyed it. Because of the repeated failure of both stages of the electronics at gap breakdown, a protection scheme was devised to protect them from large transiet voltages.

This protection scheme is shown incorporated in the electronics in Fig. 3.43. Diodes D_1 and D_2 and resistor R_1 were added to protect the input of the first stage op-amp. At gap breakdown, a large positive or negative input voltage would forward bias either D_1 or D_2.

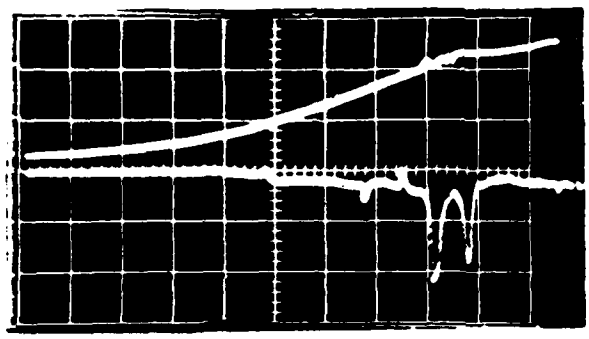

Scales:

Top: Excitation, 40 kV/cm

Bottom: Detector Response, 100 mV/cm

Horizontal: .5 ms/cm

Fig. 3.42 Gap Voltage and Microparticle Signal.

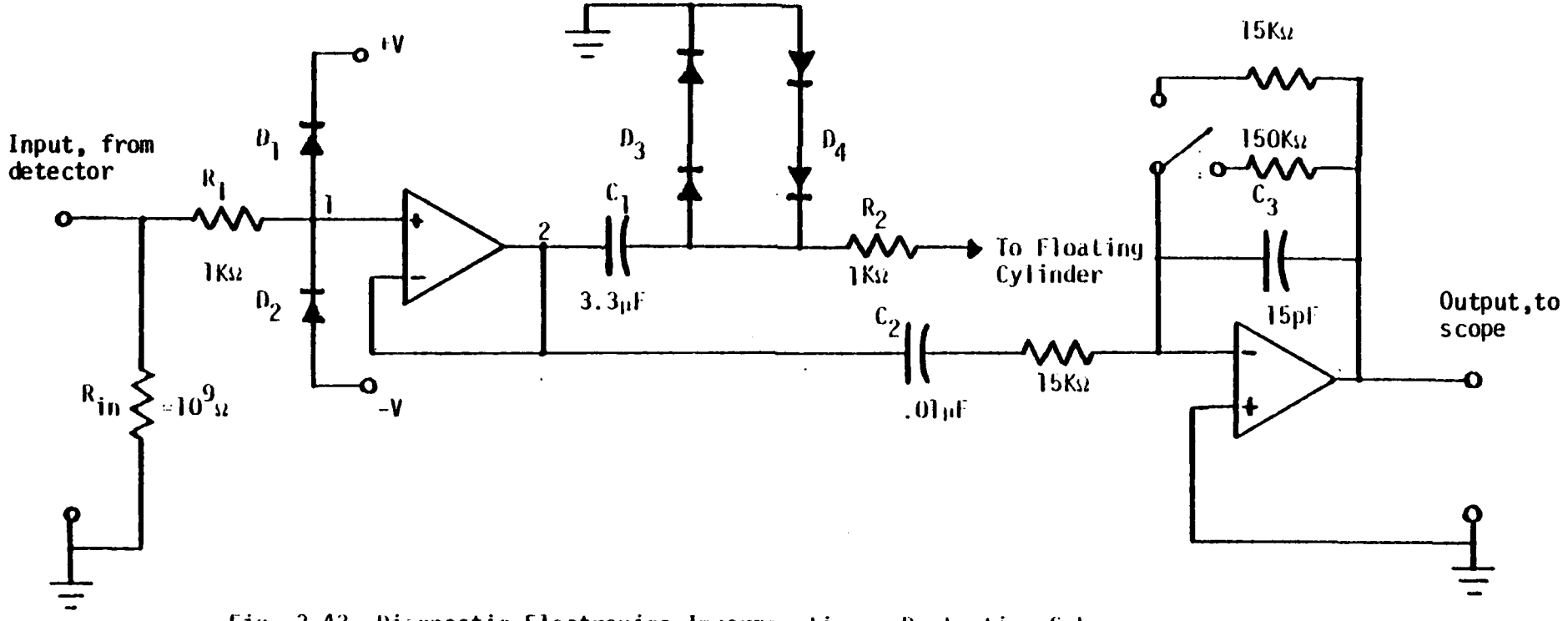

Fig. 3.43 Diagnostic Electronics Incorporating a Protection Scheme.

The voltage at node 1, the op-amp input, would then be limited to approximately V minus the diode voltage drop. The major portion of the breakdown induced input voltage would then be dropped across R_1.

A gap breakdown may raise the floating inner cylinder to a high potential. In this case diodes D_3 and D_4 clamp the output of the first stage to 2 V_{diode} (approximately 1.4 volts), and the output of the second stage to approximately 14V. Both voltage magnitudes are easily withstood by their respective op-amps.

A mis-match in the leakage currents of diodes D_1 and D_2 caused a 5V offset at the output of the first stage amplifier. C_1 was added to prevent this offset from continually forward biasing D_3 or D_4. C_2 was added to prevent saturation of the second stage output. Both C_1 and C_2 could be replaced by a single capacitor placed to the left of node 2 in Fig. 3.43, but the first stage board layout prevented this. One additional circuit change, the addition of C_3, was made for stability purposes. System input conditions for the electronics as seen in Fig. 3.43 are C_{in} = 4.8 pF and 1 mV background noise. A total of 92 positive voltage applications, of magnitudes between 13 kV and 54 kV for a 10 mm gap, have been applied after the addition of the protection circuitry. These excitations produced many discharge noise signals but only two definite microparticle signals. One of the signals is shown in Fig. 3.44. This particle, which was pulled off the upper electrode at 40 kV, has a charge of 2.4 x 10^{-14}C, a velocity of approximately 21 m/s, and a calculated radius of 5.14 μm. Neither of the two particle responses were associated with gap breakdown. Application of negative gap voltage followed immediately.

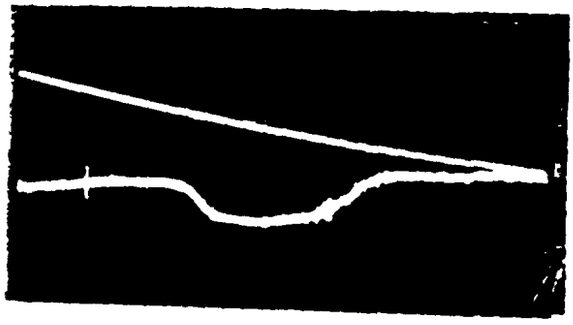

Scales:

Top: Excitation, 10 kV/cm

Zero is 1 cm below center reference line.

Bottom: Detector Response, .05 V/cm

Horizontal: .5 ms/cm

Fig. 3.44 Positive Microparticle Signal.

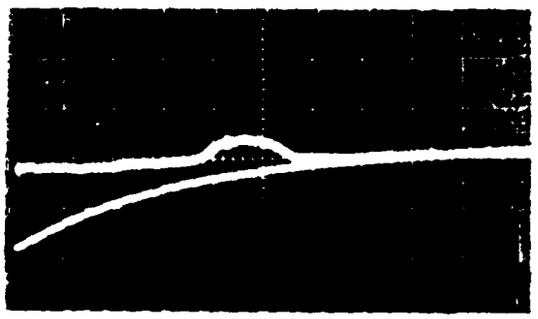

Scales:

Top: Detector Response, .05 V/cm

Bottom: Excitation, 10 kV/cm

Horizontal: .5 ms/cm

Fig. 3.45 Negative Microparticle Signal.

Negative gap voltage was applied a total of 70 times for voltage magnitudes between 13 kV and 44 kV. The only detector response was the microparticle signal seen in Fig. 3.46. This particle, which was produced at 13 kV, has a charge of 9.6×10^{-15}C, a velocity of 50 m/s, and a radius of 1.6 μm. This particle was not associated with a gap breakdown. Further voltage applications at higher voltages produced discharge noise responses. The large noise responses prevented any produced particles from being viewed.

Naturally occurring microparticles, produced by a 16 ms pulse, have been detected and their characteristics have been determined. Additionally, for some data, the vacuum gap current has been measured with the intent of relating vacuum breakdown to microparticle production. It has been concluded that, for the experimental conditions and detecting sensitivities described:

(a) Positive microparticles are produced for voltages between ≈ 16 kV and >100 kV for a 5 mm and a 10 mm gap.

(b) These positive microparticles have charges between > 2.9 pC and 9.6×10^{-15}C (.0096 pC), and velocities which range from ≈10 m/s to ≈400 m/s. Their radii range from 10 μm to ≈1.2μm.

(c) Only a few positive microparticles are produced for voltages ≤100 kV.

(d) There is a possible correlation between electrode surface roughness and production of microparticles.

(e) Only one negative microparticle was detected for gap voltages between 13 kV and 68 kV. This microparticle,

which was produced at 18 kV, had a charge of 9.6×10^{-15} C, a velocity of 50 m/s, and a radius of 1.6 m.

Breakdown occurred, consistently, at lower voltages for the negatively excited gaps. Breakdown occurred at voltages lower than values needed for substantial microparticle production.

(f) The measurement of gap current revealed microdischarges which were sometimes associated with a detector "noise" response. These microdischarges were seen with and without microparticle production.

A Marx generator has been constructed and is currently being used to excite the vacuum gap. The Marx is capable of producing pulses up to 150 kV with durations between 10 us and 50 ms. A typical Marx generator output is shown in Figure 3.46.

Preliminary data have been obtained using the Marx generator. These data are shown in Figure 3.47. The top trace is the uncrowbared voltage excitation and the lower trace is the amplifier output. The detector output is seen to increase positively, upon application of the excitation and to decay towards zero. This initial rise is due to excitation coupling to the amplifier. Attempts are being made to eliminate this initial rise. What can be interpreted as microparticle signals occurs at 4.3 cm on the grid shown. The trace shows three small microparticles followed by a larger microparticle at 5.8 cm. Additional, small microparticles are seen at 5.8 cm and 7.7 cm. A microdischarge occurs at 7.8 cm. The data shown in Figure 3.47 is preliminary but does indicate the presence of microparticles for the Marx excited vacuum gap. It should, however, be added that noise problems still exist and that the data or Figure 3.47 is among the best yet obtained.

Data similar to that shown in Figure 3.47 have been obtained for crowbared Marx outputs. Noise, however, continues to be a major problem, especially at the time of Marx output termination (see Figure 3.46). Grounding and shielding are being improved to reduce the induced transient noise levels.

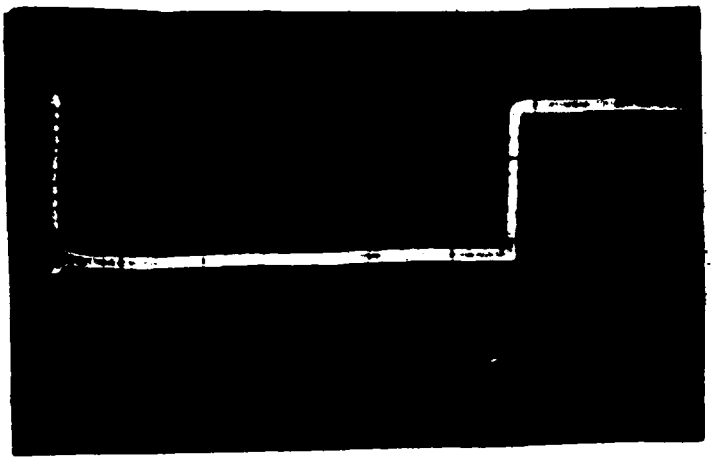

Horiz Scale - 2 ms/cm

Vert Scale - 50 KV/cm

V_{CH} - 35 kV/stage

Delay - 11½ms

Figure 3.46. Marx Generator Output.

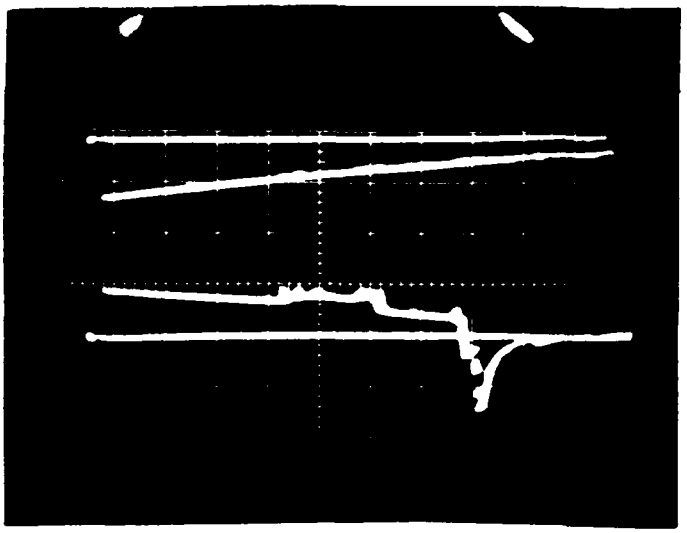

Marx output voltage
60 kV/cm

Detector output 5 V/cm

Horizontal scale
5 ms/cm

Figure 3.47. Marx Generator and Microparticle Detector Output.

CHAPTER 4

SUMMARY AND SUGGESTED FUTURE WORK

Microparticles generated in a vacuum gap by positive and negative pulsed voltages have been detected and characterized using a technique based on the principle of electrostatic charge induction. Typical charge sensitivity for the detector is $\approx 10^{-15}$C.

The detector response to a particle of a given polarity has been determined by dropping charged 2 mm lead balls through the detection system. The detector response to these balls had the correct polarity. Positively charged balls gave rise to negative signals, and the reverse was true for negatively charged balls. The detector response had the expected shape as shown in Fig. 2.5(b). Additionally, the ball velocities were found to be in agreement with calculated values.

The detector response to charged zinc particles of radii between 1 μm and 5 μm has been determined. "Square" microparticle signals have been obtained for positive and negative excitations. The charge and velocity ranges determined from these signals are .02pC to .2pC and 10 m/s to 70 m/s. Fast risetime, exponentially decaying signals, microdischarge noise responses, have been observed together with the microparticles. These responses have been shown not to be detector responses to microparticles. These signals were postulated to be associated with gap microdischarge activity. In some cases the appearance of the noise responses corresponds to the time at which the charged particles were removed from the upper electrode. The detector response to overvoltages

has been determined. Microparticles were produced before and after noise responses which in turn occurred prior to, simultaneously with, and after partial gap voltage collapse. Sufficient data have not been acquired to permit correlation.

Naturally occurring microparticles have been generated from stainless steel electrodes subjected to positive and negative 16 ms pulsed excitations. Positive and negative microparticles have been produced for voltages between 16 kV and >100 kV for a 5mm and a 10mm gap, for the experimental conditions described. Typical values of charge, velocity, and radius for these microparticles lie between >2.9pC and 9.6×10^{-15}C, $\simeq$ 10m/s and $\simeq$400 m/s, and > 10um and $\simeq$ 1.2 um. The number of microparticles increased after roughening the electrode surface. This implies that the surface condition does play a role in microparticle production. Positive microparticles are easier to produce than negative microparticles. This is consistent with the observations of Griffith, et al.[138] Breakdown occurred for negative excitations at lower voltages, before substantial particle productions occurred. Most positive microparticles were produced for voltages exceeding 100 kV.

Simultaneous gap voltage, current, and microparticle data have been produced to determine the correlation between the microparticles and gap breakdown. Microparticles have been observed which cause or are caused by microdischarges in the gap. However, present data imply that the breakdown and microparticle production mechanisms are somewhat random. This further implies that substantial data must be taken and statistically analyzed.

A Marx generator, capable of producing 150 kV pulses of variable duration, has been constructed and is currently being used to excite the vacuum gap. The Marx works well, however, noise, induced by the high Marx

generator currents, preclude the acquisition of interpretable data. Grounded and shielding are being improved to reduce the transient noise.

Work completed and reported here has developed techniques for measuring microparticle activity in a vacuum gap. Techniques have also been developed for measuring discharge current and gap voltage simultaneously with microparticle activity. Preliminary data have been obtained which show that microparticles are present in vacuum gaps and are related to vacuum breakdown. The observed microparticle characteristics have been determined.

Future tasks should concentrate on the extension of the present work to short duration excitation pulses of length between 100 us and 5 ms with voltage magnitudes up to 300 kV. It is believed these excitations will facilitate the production of microparticles and allow for a temporal study of their evolution. Additional parameters which may affect either the generation of microparticles or their role in vacuum breakdown need to be investigated. These parameters include: gap spacing, electrode surface condition, and pressure. The sensitivity of detection of microparticles must be improved or a radically new scheme developed so as to determine the role, if any, of sub-micron sized particles in vacuum breakdown. The results of these future investigations should form a basis for determining the role of microparticles in high voltage vacuum gap breakdown.

Appendix A

High Voltage Source Trigger Circuit

The circuit used to trigger the high voltage ac source is seen in Figure 1. The solid state switch is closed by a positive low voltage pulse. The voltage-setting variable transformer has a 2000:1 turns ratio. S_1 is a double-pole, double-throw switch wired so as to allow either power supply operation or voltage setting. The circuit breaker, main switch, solid state switch, the DPDT switch, and the variable transformer are contained within a control box. The main switch pilot light, and the voltage setting meter are mounted on the control box front.

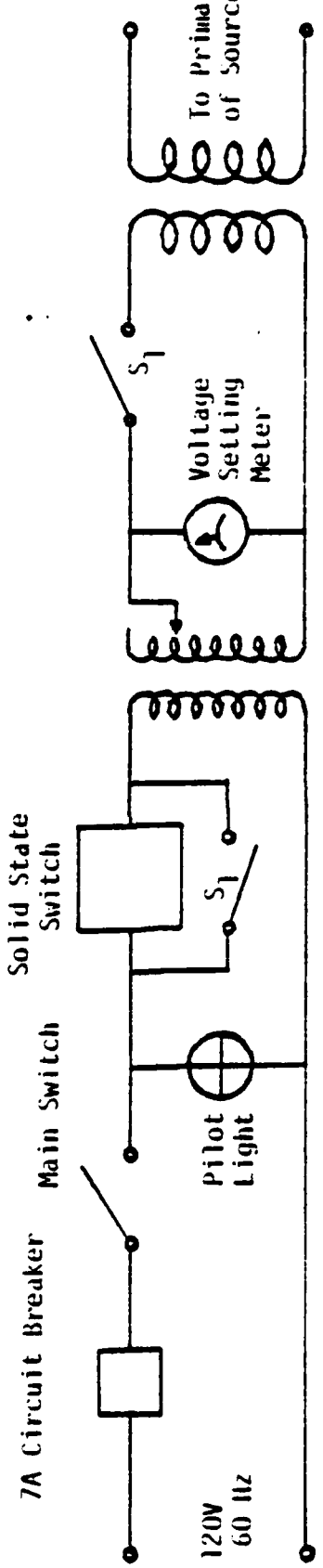

Fig. 1. High Voltage AC Power Supply Triggering Circuit.

Appendix B

Microparticle Detection System

The second section of the Appendix contains additional photographs of portions of the microparticle detection system.

Figure 2 shows the high voltage connection cup, and one of the vacuum feedthroughs used for the electrical connection between the first and second amplifier stages. The feedthrough was manufactured by replacing the bore of the conductor of a high current feedthrough with a glass tube through which two 0.040" diameter tungsten wires were passed. The bore was then sealed using a vacuum epoxy.

Figure 3 shows one of the guard cylinders and the Delrin ring which supports this ring within the inner floating shield (cylinder).

Figure 4 is a view of the floating inner shield. Each Delrin ring is held in place by 3 positioning screws. The circumference of the inner shield is vertically calibrated to ease determination of guard and detecting cylinder separation.

Figure 5 shows the mounting support for the microparticle detector. Also shown is the collector electrode which is mounted beneath the guard and detecting cylinders. The collector support is screwed into the base of the microparticle detector. Barely visible above the detector base plate is the inner shield insulating ring.

Figure 6 shows the inner floating shield mounted atop the detector base and mounting support.

Figure 7 shows the outer ground cylinder which surrounds the inner shielding cylinder. The first stage electronics are mounted on the interior of the outer cylinder, and the test gap assembly (Figure 2.2) is placed on top of the outer cylinder. When currents are measured, a thin Delrin ring separates the outer cylinder from the lower electrode

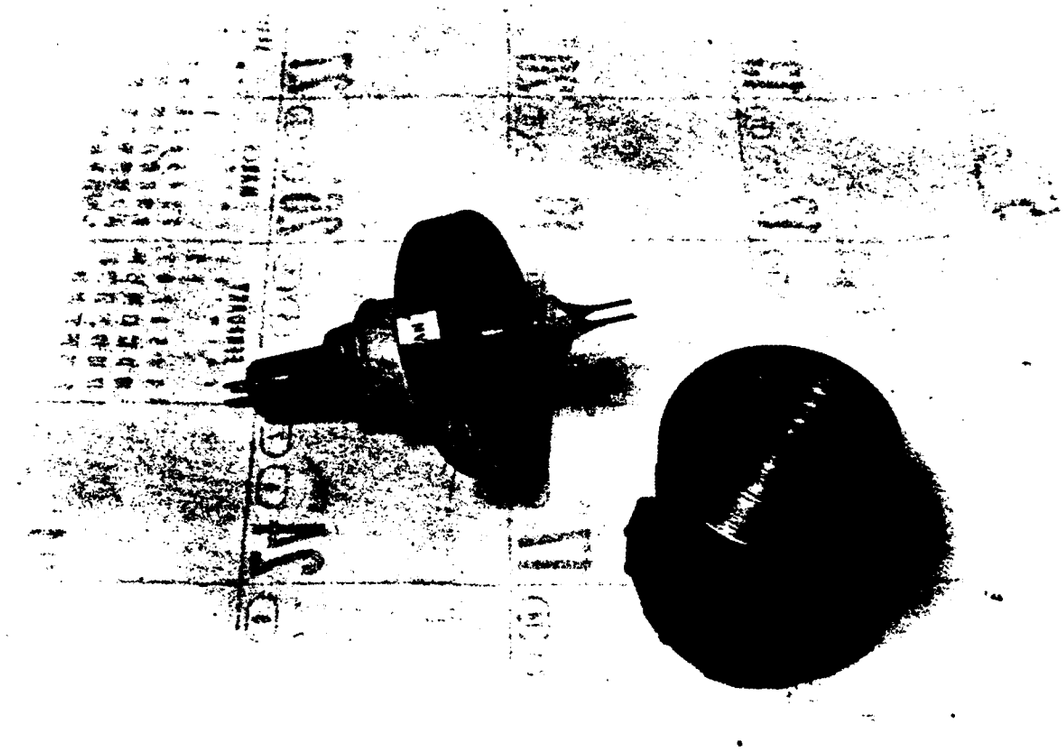

Fig. 2. Electrical Feedthrough and Voltage Connection Cup.

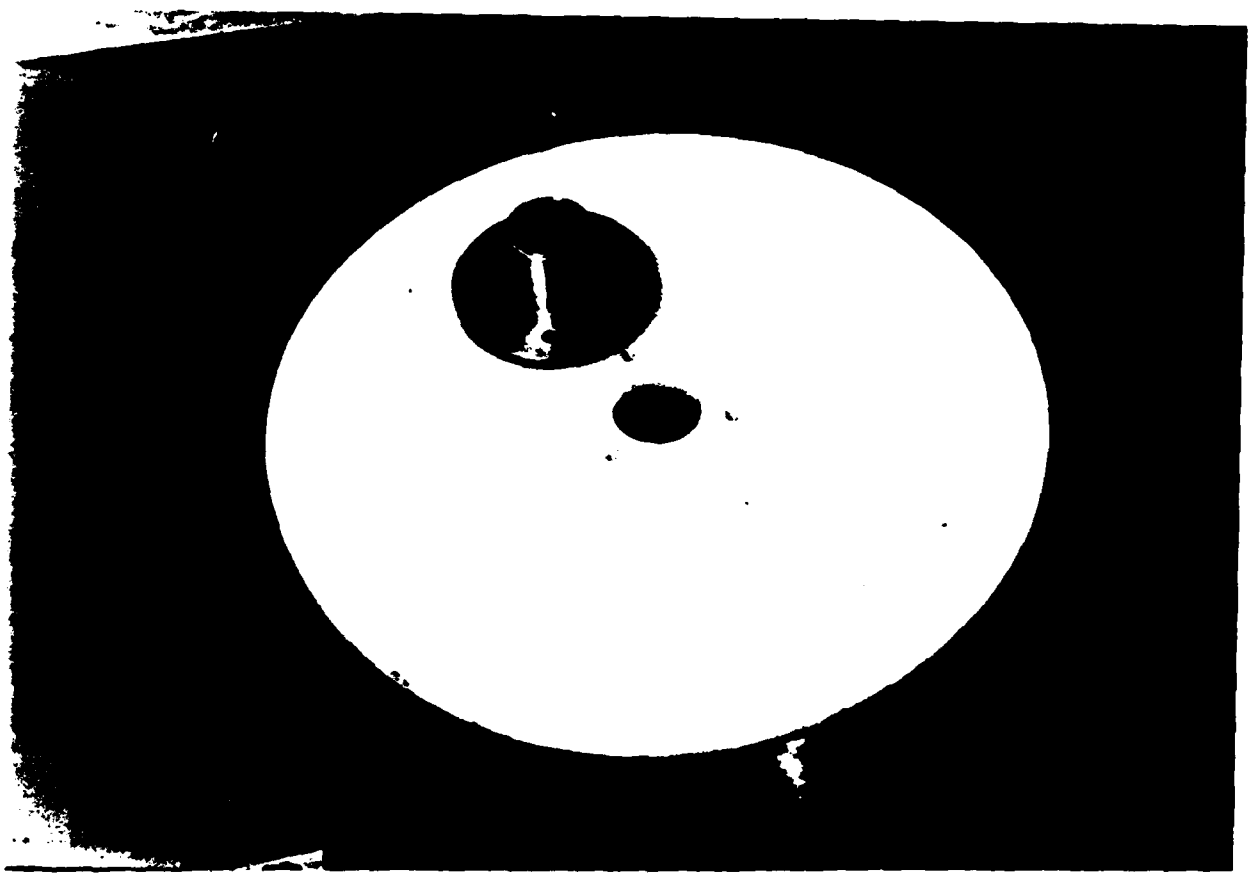

Fig. 3 Guard Cylinder and Mounting Delrin Ring.

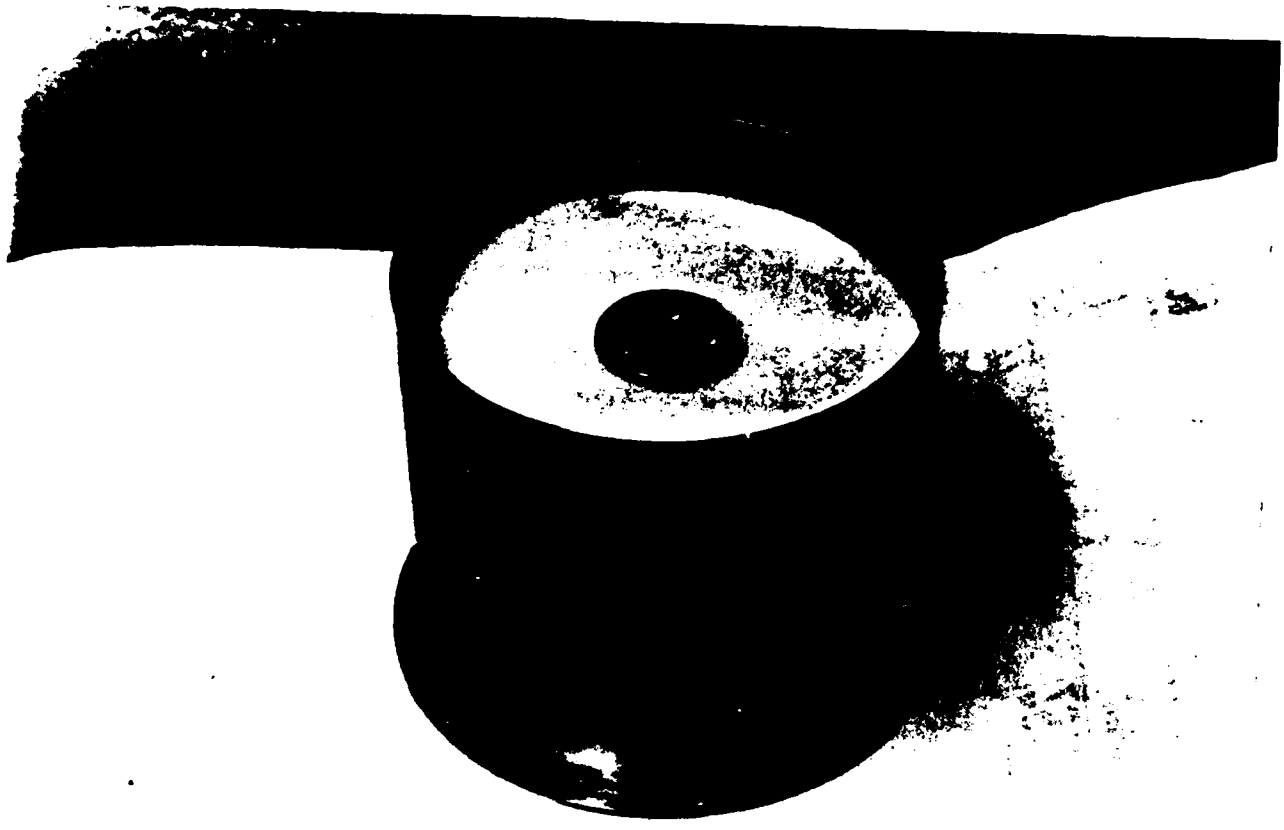

Fig. 4 Floating Inner Shielding Cylinder.

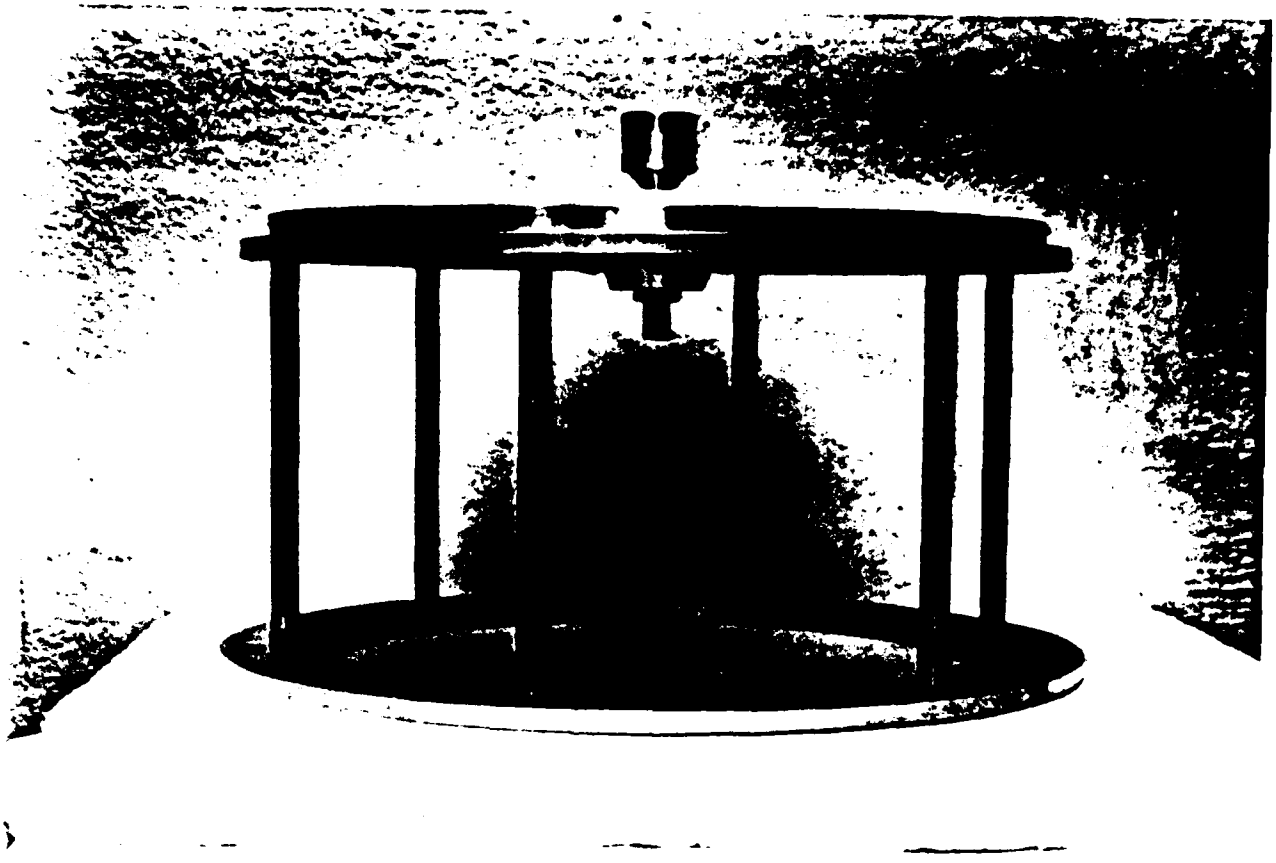

Fig. 5 Mounting Support and Collector Electrode.

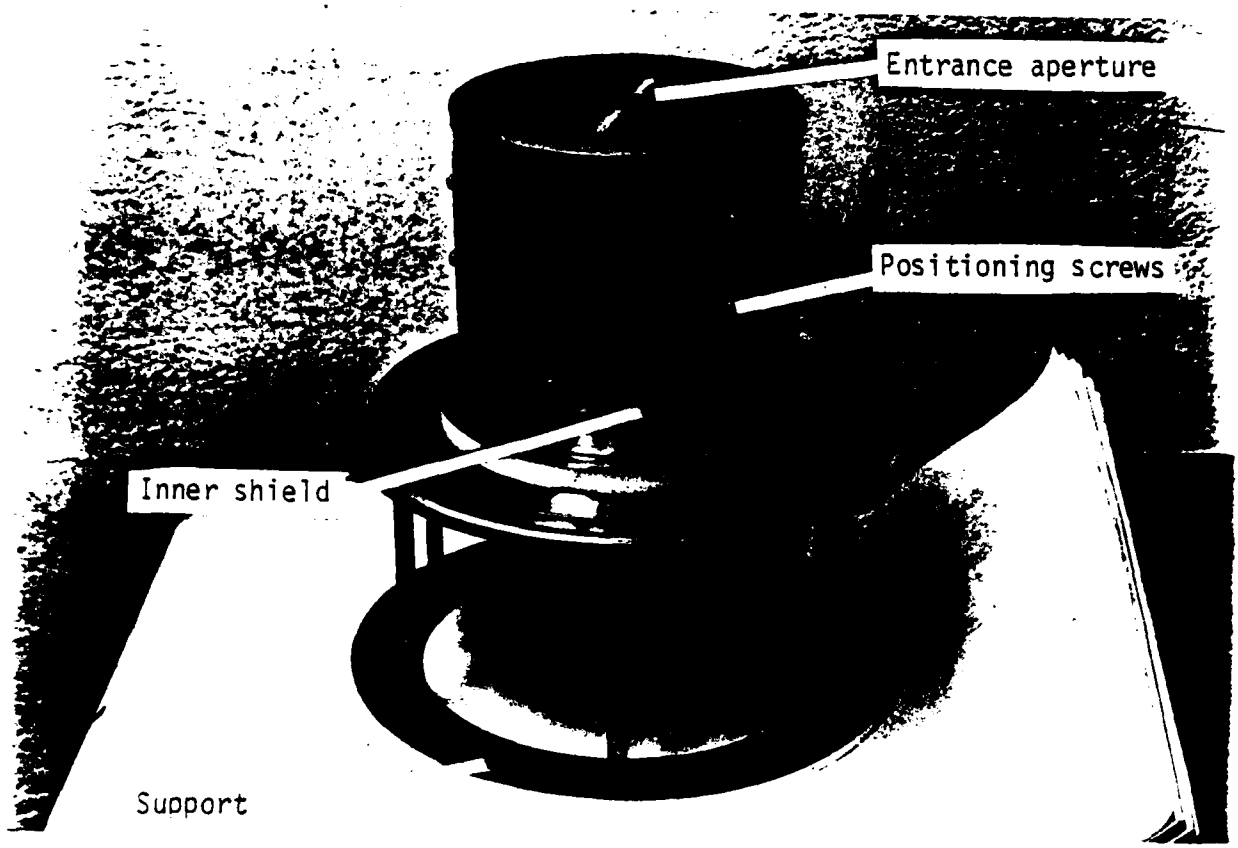

Fig. 6 Detector Inner Shield Assembly.

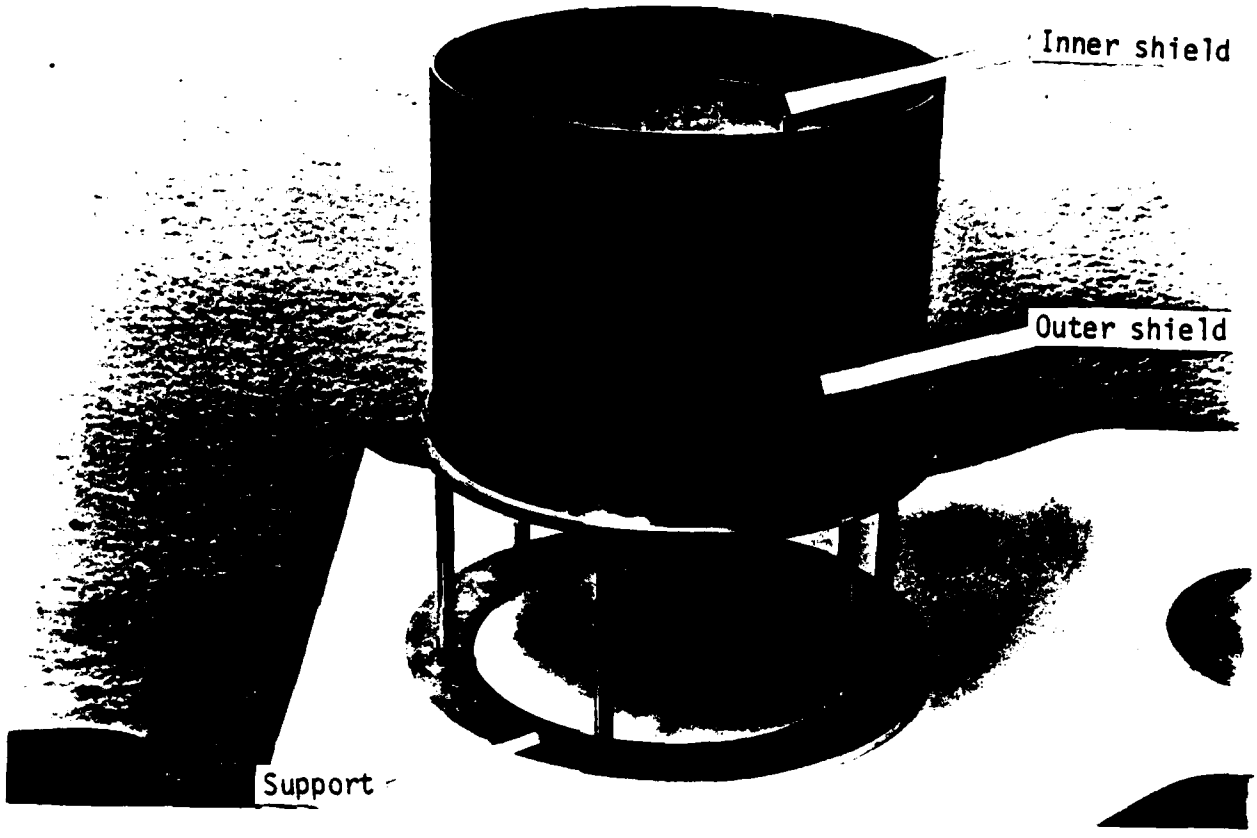

Fig. 7 Detector Assembly Showing Outer Cylinder.

plate.

Figure 8 shows the total detector assembly. In this case the Delrin ring separating the lower electrode and outer cylinder is not shown.

Figure 9 shows the first stage electronics copper enclosure and its Delrin mount. Connection D is the first stage input from the detecting cylinder. Connection C bootstraps the detector cylinder to inner shield capacitance. The black lead is for the single point ground connection, and the two twisted pair cables provide an input to the second stage and power to the first stage op-amp. Although not shown in this photograph, the outer braid of these cables are clamped to the enclosure to ensure shielding continuity.

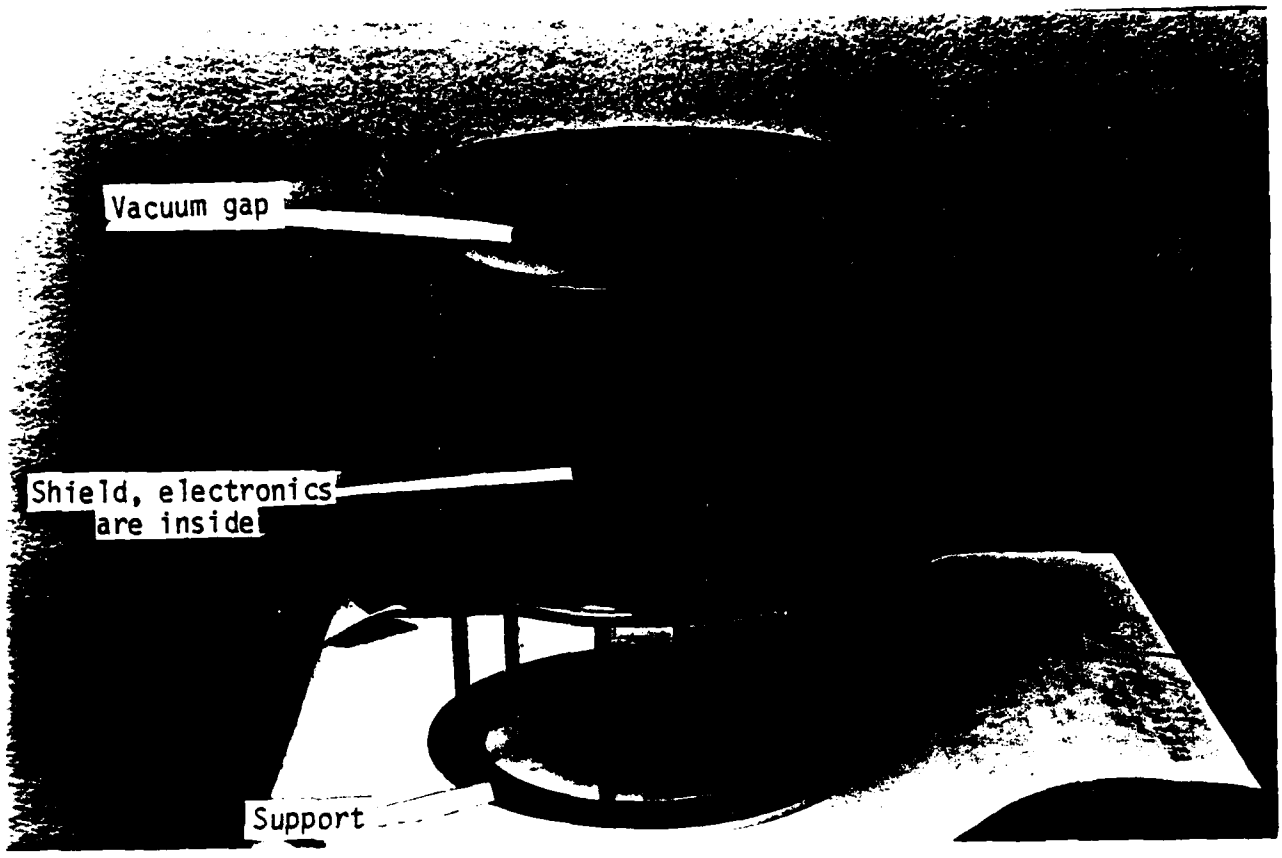

Fig. 8 Total Detector and Vacuum Gap Assembly.

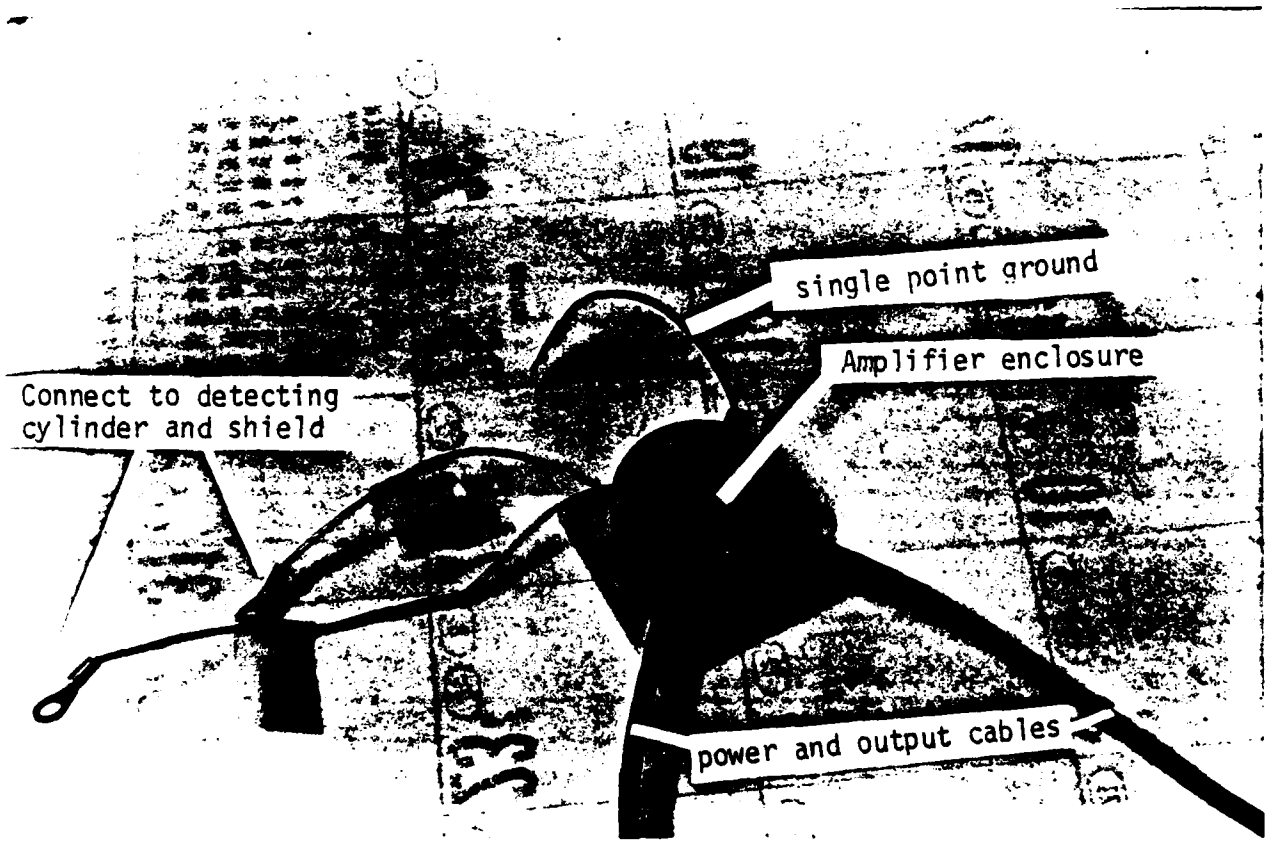

Fig. 9 First Stage Amplifer Enclosure and Electrical Leads.

Appendix C

Analog Risetime Measurements

The effect of grounded or ungrounded guard cylinders on the rise and fall time of the detector response could not be conclusively determined by the charged lead ball or the artificial zinc microparticle data. Analog measurements have therefore been conducted to determine their effect.

Resistive analogs can be used to measure fields arising from various spatial charge distributions. It can be shown that measured currents, in the conductive medium, are analgous to electric fields in dielectric medium. Similarly, the analog for a charge distribution is a current distribution. The fields arising in a dielectric medium due to a given charge distribution can, therefore, be modelled by using a conductive (resistive) medium and a given current source distribution.

The risetime analog of the microparticle system has been constructed using resistive paper. The general layout is shown in Figure 10. The arrangement consists of resistive paper, onto which various electrodes and shields have been painted using conductive paint. The simulating arrangement includes the detector cylinder, two guard cylinders, an inner shield, and an outer shield. All dimensions have been selected such that the relative size and locations of the analog components are the same as in the actual detector system arrangement. All of the componenets shown can be grounded or can float. Wires are used to connect the two detector, guard cylinders, and inner shield sections together to simulate cylindical components.

The analog measurements have been conducted by exciting the arrangement of Figure 10 using a constant current source and a moveable probe. The probe is placed at the desired location and simulates the charged

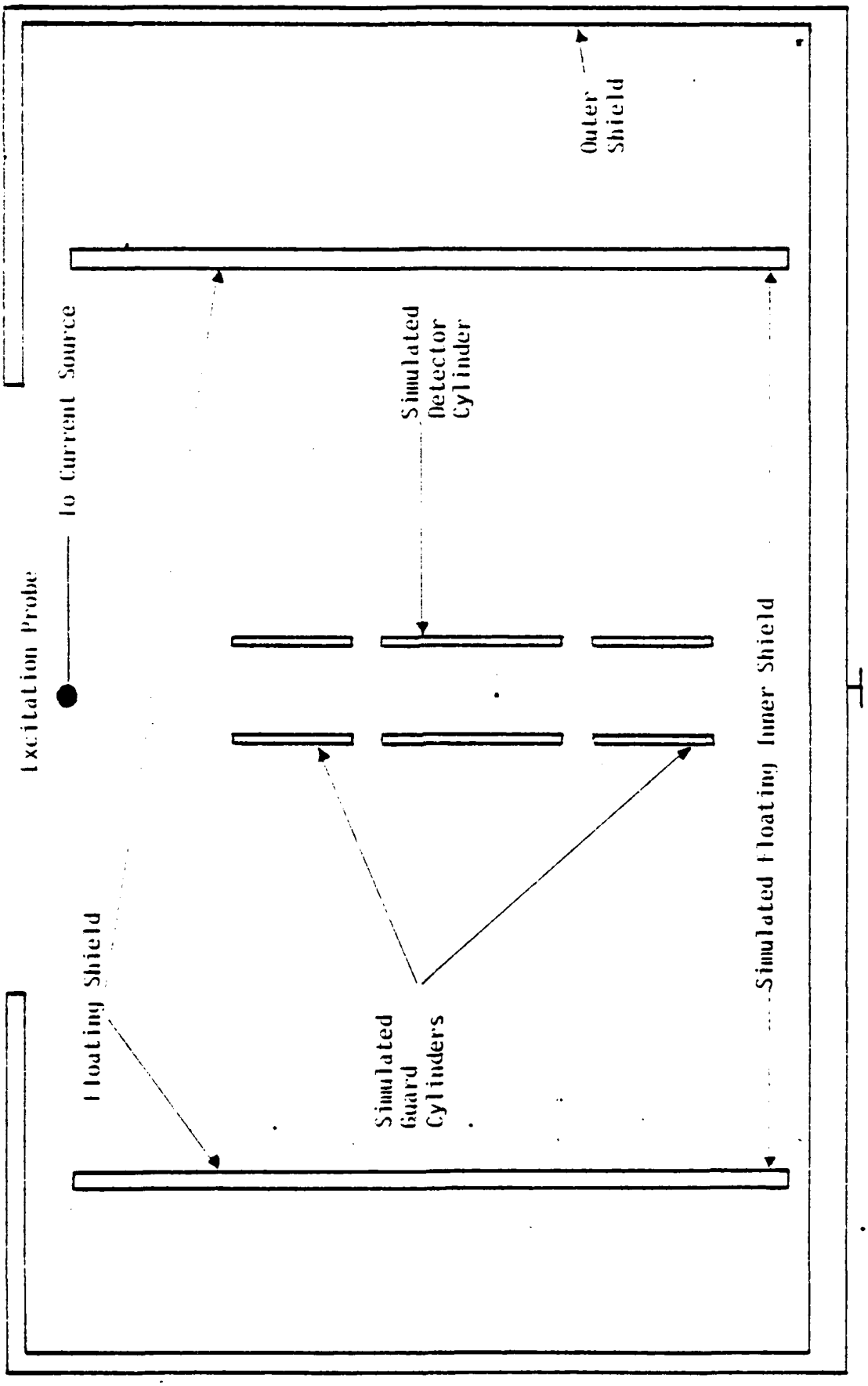

Fig. 10 Resistive Analog Simulation of Detector Assembly.

microparticle. The potential on the detector cylinder is measured using a voltmeter.

The measured detector cylinder potential, as a function of excitation probe location, is shown in Figure 11, in normalized form.

Measurements were made with seven different configurations. The configurations and the resulting seven curves are shown in Figure 11 and are described as follows. Measurements were made with:

(1) grounded outer shield, no guard cylinder, and no inner shield. The results are shown as curve 1. It can be seen that the response increases very slowly as the source probe approaches the detector cylinder.

(2) grounded outer shield, only one floating guard cylinder (on the excitation probe side of the detector cylinder), no floating inner shield. The results are shown by curve 2. This response is also seen to increase slowly.

(3) grounded outer shield, two floating guard cylinders, floating inner shield. These results are shown by curve 3. The response again increases slowly. This configuration is most relevant to simulation of the microparticle detector arrangement with ungrounded guard rings.

(4) grounded outer shield, one guard cylinder only. (The guard cylinder is grounded), no inner shield. The results are shown as curve 4. The response is seen to be small until the excitation probe begins to exit the grounded guard cylinder. The signal response then quickly increases as the probe approaches the detector cylinder.

(5) grounded outer shield, one guard cylinder (grounded), floating

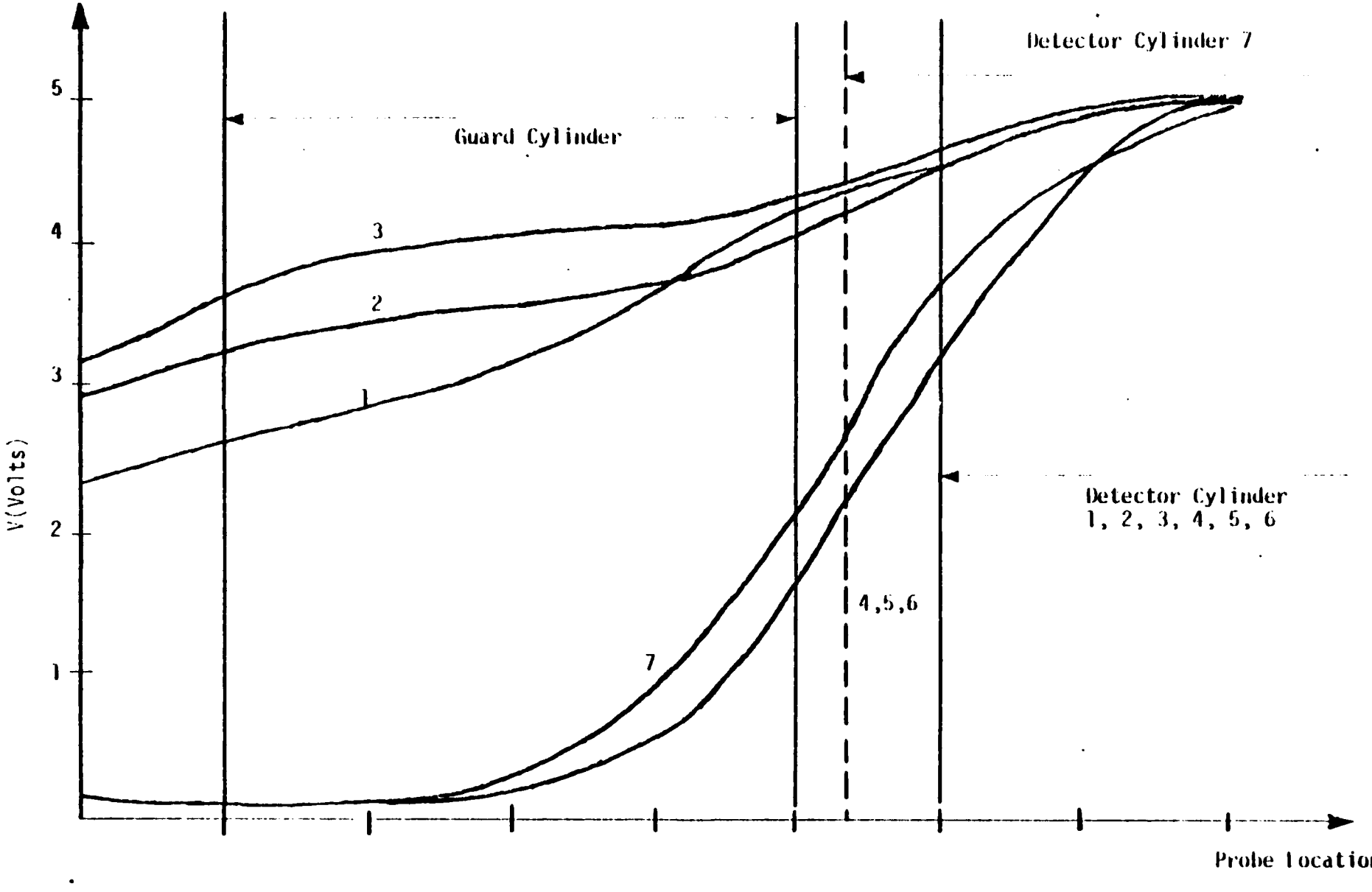

Fig. 11 Relative Detector Output for Excitation Approaching Detector.

inner shield. The results are shown as curve 5 and are essentially the same as obtained in (4).

(6) grounded outer shield, two grounded guard cylinders, floating inner shield. The results are shown as curve 6.

Again the response is small until the probe exits the guard cylinder. The response then quickly increases. This arrangement is most closely analogous to the actual experimental arrangement, which consists of two grounded guard cylinders. Comparison of curves 6 and 3, produced with grounded and ungrounded guard cylinders, shows that the grounded guard cylinders shield the detector cylinder from the probe and effectively "sharpen" the response. This implies that grounded guard cylinders should reduce the risetime and facilitate the production of "square shaped" microparticle signals.

An addition curve, curve 7, is also shown. The conditions for this curve are the same as for 6, with one exception. The data of 1-6 were obtained with a simulated guard cylinder, to detector cylinder, spacing of 5 mm. The data of 7 were obtained with a simulated distance of 1 mm. The results of 6 and 7 are seen to differ very little. This implies that the "squareness" of the microparticle response is not strongly dependent upon this spacing, at least in the range of 1 mm to 5 mm.

It should be noted that the effect of the "virtually" grounded inner shield has not been taken into account. It is presently not known how to resistively model (using analog paper) the "bootstrapped" or actively maintained ground. The inner shield has, therefore, remained floating for the results reported.

REFERENCES

[1] Wood, R.W., "A New Form of Cathode Discharge and the Production of X-rays, Together with Some Notes on Diffraction," Physical Review, Vol. 5, p. 1, (1897).

[2] R. A. Millikan, and R. A. Sawyer, "Extreme Ultra-Violet Spectra of Hot Sparks in High Vacua," Phys. Rev., Vol. 12, p. 167, (1913).

[3] A Maitland, "Spark Conditioning Equation for Plane Electrodes in Vacuum," J. Appl. Phys., Vol. 34, p. 996 (1963).

[4] D. P. Beukena, "Conditioning of a Vacuum Gap by Sparks and Ion Bombardment," Physica, Vol. 61, p. 259, (1972).

[5] H. W.Anderson, "Effect of Total Voltage on Breakdown in Vacuum," Elec. Eng., Vol. 54, p. 1315, (1935).

[6] J. D. Trump and R. J. Van de Graaff, "The Insulation of High Voltage in Vacuum," J. Appl. Phys., Vol. 18, p. 327 (1947).

[7] Van Atta, Van de Graaff and H. A. Barton, "A New Design for a High Voltage Discharge Tube," Phys. Rev. Vol. 43, p. 158 (1933).

[8] A van Ostrom, "Surface Effects in Vacuum Breakdown," Proc. of the IV International Symposium on Discharges and Electrical Insulation in Vacuum, Waterloo, Canada, p. 1, (1970).

[9] H. C. Bourne, "Composition of the Interelectrode Pre-Breakdown Current in High Vacuum," J. Appl. Phys., Vol. 26, p. 625 (1955).

[10] H. Boersch, H. Hamish, and S. Wiesner, "On the Electrical Microdischarges in Vacuum," Z. Agnew., Phys., Vol. 13, p. 450 (1961).

[11] R. Arnal, "On the Initiation of Electrical Discharge in a Vacuum," Completes Rendus, Vol. 238, p. 132 (1954).

[12] G. Steib, and E. Moll, "High-Voltage Conditioning at Large Gaps in Industrial Vacuum," J. Phys. D: Appl. Phys., Vol. 6, P. 243 (1973).

[13] R. Hawley, "Vacuum as an Insulator," Vacuum, p. 310 (1960).

[14] J. G. Trump, "Insulation Strength of High Pressure Gases and of Vacuum," Dielectric Material and their Applications (Wiley),p. 154, (1954).

[15] D. W. Williams and W. T. Williams, "Effect on Electrode Surface Finish on Electrical Breakdown in Vacuum," J. Phys. D: Appl. Phys. Vol. 5, p. 1845 (1972).

[16] Ion Physics Corporation, "High Voltage Breakdown Study, Final Report," TR-ECOM-00394, (1970).

[17] R. J. Hadden, "The Effect of Surface Treatment on Electric Breakdown Between Copper Electrodes at 50 Cycles at Very Low Pressure," A.E.R.E. GlM92 (1951).

[18] D. N. Leader, "Electrical Breakdown in Vacuum," Proc. IEEE (GB), V100, A, p. 138 (1953).

[19] R. V. Latham, "Microparticle Charge Acquisition and Reversal at Impact," J. Phys. D: Appl. Phys. Vol. 5, p. 2044 (1972).

[20] A. K. Vijh and K. Dimoff, "The Effect of Oxide Surface Layers on the Breakdown Voltage in Metal-Vacuum-Metal Sandwiches", J. of Materials Sci., V11, p. 150 (1976).

[21] J. T. Maskrey, and R. A. Dugdale, "The Role of Inclusions and Surface Contamination Arc Initiation at Low Pressures," Brit. J. Appl. Phys., Vol. 17, p. 1025, (1966).

[22] L. Jedynak, "Investigation of Vacuum Breakdown," Ph.D. Thesis, MIT, (1962).

[23] L. Jedynak, "Dielectric Coatings in Vacuum Gaps," Proc. of the I Int. Symp. of Disch. and Elec. Insulation in Vacuum, Boston, Mass., p. 147 (1964).

[24] P. C. Bolin, and J. G. Trump, "Insulating Vacuum Gaps with Dielectric Cathode Surfaces," Proc. of III International Symposium of Disch. and Electrical Insulation in Vacuum, Paris, France, p. 50 (1968).

[25] F. McCoy et al, "Some Effects of Electrode Metallurgy and Field Emission on High Voltage Insulation in Vacuum," Proc. of I International Symposium of Discharge and Electrical Insulation in Vacuum, addendum, Boston, Mass. (1964).

[26] M. Rabinowitz, "Electrical Breakdown in Vacuum," Ph.D. Thesis, Washington State University (1963).

[27] D. J. Simon, and R. Michelier, "Experiments on an Electrostatic New Experimental Observations," Journal Appl. Phys., Vol. 36, p. 1314,(1966).

[28] M. Rabinowitz and E. Donaldson, "Electrical Breakdown in Vacuum: New Experimental Observations", J. Appl. Phys., Vol. 36, p. 1314, (1965).

[29] H. C. Miller, "Influence of Electrode Curvature Upon Electrical Breakdown in Vacuum," J. Appl. Phys., Vol. 37, p. 784, (1966).

[30] D. W. Williams, and W. T. Williams, "Vacuum Breakdown Between Outgassed Molybdenum Eelctrodes," Proc. of the IEEE, Vol. 121., p. 974, (1974).

[31] D. A. Swift, "The Effect of Temperature on the Electrical Characteristics of a Vacuum Gap," J. Phys. D: Appl. Phys., Vol. 5, p. 1588, (1972).

[32] R. N. Allan, and A. J. Salim, "Prebreakdown Currents and Breakdown Voltages in Vacuum at Cryogenic Temperatures," J. Phys. D: Appl. Phys., Vol. 7, p. 1159, (1974).

[33] R. Hackam, and L. Altcheh, "AC(50Hz) and DC Electrical Breakdown of Vacuum Gaps and with Variation of Air Pressure in the Range 10^{-9} -10^{-2}Torr, Using OFHC Copper, Nickel, Aluminum, and Niobium Parallel Planar Electrodes," J. of Appl. Phys., Vol. 46, p. 627 (1975).

[34] R. Hackam, and D. Gavinda Raju, "Electrical Breakdown of a Point-Plane Gap in High Vacuum and with Variation of Pressure in the Range 10^{-7} -10^{2}Torr of Air, Nitrogen, Helium, Sulpher-Hexaflouride and Argon," J. of Appl. Phys., Vol. 45, p. 4784 (1974).

[35] A. Denholm, "The Electrical Breakdown of Small Gaps in Vacuum," Canadian J. Phys., Vol. 36, p. 476 (1958).

[36] J. Halpern et al "Preliminary Studies on the Design of a Microwave Linear Accelerator," Phys.,Rev. Vol. 69, p. 688A (1946).

[37] W. Chump, H. Heard, and E. Lauer, "The Behavior of Electrode Materials Subjected to Energetic High Vacuum R. F. Sparking in the Megavolt Range," Univ. of Calif. Rad. Lab. Report 2099(1954).

[38] H. Doolittle and B. Singer, "Effects of the Impedence of the Power Supply on the Insulation of High Voltages in Vacuum," 1st Intern. Symp. of Discharge and Elect. Insul. in Vacuum, Boston, Mass. p. 247, (1964).

[39] R. Hawley, "The Electrical Properties of High Vacuum," from High Voltage Technology, Harwell Post - Graduate Series, edited by Alston, Oxford Univ. Press, 1968, Chap. 4, p. 59.

[40] R. Hawley, A. Zacky, and Z. Eldine, "The Insulating Properties of High Vacuum," Proc. of IEEE (GB), Vol. 112, p. 1237, (1965).

[41] J. McKibben, and K. Boyer, "Current Loading in Ion Accelerating Tubes,", Phys. Rev., Vol. 82, p. 315 (1951).

[42] W. Mansfield, "Pre-breakdown Conduction in Continuously Pumped Vacuum Systems," Brit. J. Appl. Phys., Vol. 11, p. 454,(1960).

[43] L. Pivovar and U. Gordienko, "Pre-breakdown Conduction Between Electrodes in Ultra-High and High Vacuum," Soviet Physics - Technical Physics, Vol. 7, p. 908, (1963).

[44] A. Bennett, "Electron Multiplication Processes in High Voltage Electrical Discharge in Vacuum," J. Appl. Phys., Vol. 28, p. 1251, (1957).

[45] B. Aarset, R. Cloud, and J. G. Trump, "Electron Emission from Metals under High-Energy Ion Bombardment," J. Appl. Phys. Vol. 25, p. 1365,(1954).

[46] D. Miller, and D. Haneman, "Evidence for Carbon Contamination on Vacuum Heated Surfaces by Electron Paramagnetic Resonance," Surface Science, Vol. 19, p. 45, (1970).

[47] P. Schefer, and P. Chatterton, "Microdischarges and Microdischarge Simulation in Uniform-Field High-Voltage Vacuum Gaps," IEEE Trans. on Electrical Insulation, VEI-11, p. 12, (1976).

[48] B. Singh, and P. Chatterton, "A Model of Microdischarge Current Growth in Vacuum," J. Phys. D: Appl. Phys. Vol. 9, p. 1797,(1976).

[49] R. Fowler, and L. Nordheim, "Electron Emission in Intense Electric Fields," Proc. Roy. Soc. A119, p. 173 (1928)and A121, p. 626, (1928).

[50] M. M. Menon, "The Role of Microparticles in Vacuum Breakdown," Ph.D. Thesis, University of Waterloo, (1973).

[51] R. Good, and E. Muller, "Field Emission, "Handbuck der Physik, Vol. 21, Electron-Emission Gas Discharges I, p. 176, (1956).

[52] P. Chatterton, "A theoretical Study of Field Emission Initiated Vacuum Breakdown," Proc. Roy Soc., Vol. 88, p. 231,(1966).

[53] W. Dyke, and J. Trolan, "Field Emission: Large Current Densities, Space Charge, and the Vacuum Arc," Phys. Rev., Vol. 89, p. 799, (1953).

[54] C. Hill, "30 MHz Radio Frequency Voltage Breakdown of Electrode Gaps Between 1 and 4 mm in a Clean High Vacuum," Proc. IV Sym., p. 137, (1970).

[55] W. Bolye, P. Kisliuk, and L. Germer, "Electric Breakdown in High Vacuum," J. Appl. Phys., Vol. 26, p. 720, (1955).

[56] R. Little, and W. Whitney, "Electron Emission Preceeding Electrical Breakdown in Vacuum," J. Appl. Phys., Vol. 34, p. 2430, (1963).

[57] R. Baker, and A. Webber, "Field Emission Measurements and Electrical Breakdown in Vacuum," J. Vac. Sci., Vol. 9, p. 366, (1971).

[58] G. Fursei and P. Vorobrontsou - Vel'yaminov, "Qualitative Model of Initiation of a Vacuum Arc II, Field-Emission Mechanism of Vacuum Arc Onset," Sov. Phys. Tech. Phys. Vol. 12, p. 1370, (1968).

[59] C. Bennette, L. Swanson, F. Charbonnier "Electrical Breakdown Between Electrodes in High Vacuum. II Experimental," J. Appl. Phys., Vol. 38, p. 634, (1967).

[60] W. Williams, "Vacuum Breakdown Between Superconducting Electrodes," Nature Phys. Sci., Vol. 231, p. 42, (1971).

[61] T. Fabiniak, L. Jedynak, and R. Dodd, "Properties of Vacuum Insulated Single Crystal Tungston Electrodes in High Electric Fields. Part II Nature of Prebreakdown Currents," J. Appl. Phys., Vol. 42, p. 2240, (1971).

[62] B. Cox, "The Nature of Field Emission Sites," J. Phys.,D: Appl. Phys., Vol. 8, p. 2065, (1975).

[63] E. Murphy, and R. Good, "Thermionic Emission, Field Emission, and the Transition Region," Phys., Rev., Vol. 102, p. 1464, (1956)

[64] W. Schottky, "Uber Kalte and Warme Electronenentladungen," Zeitschrift Fur Physik, Vol. 23, p. 63, (1923).

[65] G. Farrall, "Numerical Analysis of Field-Emission and Thermally Ennanced Emission from Broad Area Electrodes in Vacuum," J. Appl., Phys. Vol. 41, p. 563, (1970).

[66] C. Bennette, L. Swanson and F. Charbonnier, "Electrical Breakdown Between Metal Electrodes in High Vacuum I Theory," J. Appl. Phys. Vol. 39, p. 627, (1967).

[67] J. Utsumi, "Cathode and Anode Induced Electrical Breakdown in Vacuum," J. Appl. Phys., Vol. 38, p. 2989, (1967).

[68] I. Brodie, "Studies of Field Emission and Electrical Breakdown Between Extended Nickel Surfaces in Vacuum," J. Appl. Phys., Vol.35 p. 2324,(1969).

[69] D. Alpert et al. "Initiation of Electrical Breakdown in Ultra High Vacuum," J. of Vac. Sci. and Tech., Vol. 1, p. 35, (1964).

[70] G. Vibrans, "Vacuum Voltage Breakdown as a Thermal Instability of the Emitting Protrusion," J. Appl. Phys., Vol. 35, p. 2855, (1964).

[71] W. Nottingham, "Remarks on Energy Losses Attending Thermionic Emission of Electrons from Metals," Phys. Rev., Vol. 59, p. 907, (1971).

[72] D. Williams, and W. Williams, "Field-Emitted Current Necessary for Cathode-Initiated Vacuum Breakdown," J. Phys. D: Appl. Phys. Vol. 5, p. 280, (1972).

[73] D. Davis, and M. Biondi, "The Effect of Electrode Temperature on Vacuum Electrical Breakdown Between Plane, Parallel Copper Electrodes," J. of Appl. Phys., Vol. 39, p. 2979, (1968).

[74] D. Davis, and M. Biondi, "Mechanism of DC Electrical Breakdown Between Extended Electrodes in Vacuum," J. of Appl. Phys. Vol. 42, p. 3089, (1971).

[75] R. Little, and S. Smith, "Field Enhancing Projections Produced by the Application of an Electric Field," J. Appl. Phys. Vol. 36, p. 1502, (1965).

[76] L. Cranberg, "The Initiation of Electrical Breakdown in Vacuum," J. Appl. Phys., Vol. 23, p. 518,(1952).

[77] R. Hawley, and A. Zacky, Progress in Dielectrics, Vol. 7, p. 115, (1967).

[78] R. Hackam, and S. Salman, "Electrical Insulation Properties of Sterling-Silver Electrodes in Ultra High Vacuum," IEEE Trans. on Elec. Insul. Vol. EI-10, p. 9, (1975).

[79] P. Browne, "The Transfer of Metal Between Electrodes in a High Vacuum on Application of a High Electric Field," Proc. Phys. Soc., Vol. 68B, p. 564, (1955).

[80] L. Tarasova, and A. Razin, "Transfer of Electrode Material in the Pre-Breakdown Phase and in Electrical Breakdown in High Vacuum," Soviet Physics-Technical Physics, Vol. 4, p. 879, (1959).

[81] P. Chatterton, and P. Bivadar, "Microparticle Processes Occurring Prior to Vacuum Breakdown," Zeitschrift fur Angewandte Physik, 30, Band 213, Heft, p. 163, (1970).

[82] Chakrabarti, and Chatterton, "Microparticle Trigger Discharges and Impact Damage in a High-Voltage Vacuum Insulated Gap," J. Appl. Phys., Vol. 47, p. 5320, (1976).

[83] Olendzkaya, "Vacuum Breakdown with Transfer of Conducting Particles Between Electrodes," Reported to the 10th Conference on Cathode Electronics, Tashkent, p. 423, (1961).

[84] N. Rozanova, "Breakdown in Vacuum Initiated by Macroparticles," Bull. Acad. Sci., USSR Ser., Vol. 26, p. 1438 (1962).

[85] J. Slattery et al "Vacuum Discharges Initiated by Particle Impact," Appl. Phys. Letters, Vol. 7, p. 23, (1965).

[86] Poshekonov and Pogorelskii, "Initiation of Vacuum Breakdown by Metal Particles," Sov. Phys., Tech. Phys., Vol. 14, p. 811, (1969).

[87] Martynov, "Initiation of Vacuum Discharge by Metal Particles on an Electrode," Sov. Phys. Tech. Phys. Vol. 16, p. 1364, (1972).

[88] Slivkov, "Mechanism for Electrical Discharge in Vacuum," Sov. Phys. Tech. Phys., Vol. 2, p. 1928, (1957).

[89] P. Chatterton, "A Review of Microparicle Phenomena and Theory Relevant to Vacuum Breakdown".

[90] Menon and Srivastava, "Microparticle - Initiated Vacuum Breakdown - Some Possible Mechanisms," J. Appl. Phys., Vol. 45, p. 3832, (1974).

[91] N. Olendzkaya, Radio Engineering and Electronic Physics, Vol. 8, p. 423, (1963).

[92] Martynov and Ivanov, "Microdischarge of Conducting Particles and Breakdown of a Vacuum Gap," Rad. Eng. and Elec. Phys., Vol. 14, p. 1732, (1969).

[93] Martynov, "Microdischarges Caused by Fast Micron-Sized Charged Particles," Sov. Phys., Tech. Phys., Vol. 16, p. 1533, (1971).

[94] Chatterton, Menon and Srivastava, "Processes Involved in the Triggering of Vacuum Breakdown by Low-Velocity Microparticles," J. of Appl. Phys., Vol. 43, p. 4536, (1972).

[95] P. Poshekhonov and I. Solovyev, "Initiation of a Vacuum Breakdown at a Pulsed Voltage with Detachment of a Macroparticle from Electrode Surface," Rad. Eng. and Elec. Phys., Vol. 16, p. 1545, (1971).

[96] F. Rohrback, CERN Report 71-28 (1971).

[97] R. Latham, "Initiation of Electrical Breakdown in Vacuum," Physics Technology, Vol. 9, p. 20, (1978).

[98] R. Latham, and A. Brah, "The Influence of Surface Oxidation on the Electron Tunnelling Mechanism of Microparticle Charge Reversal During a Bouncing Impact on a Charged Conductor," J. Phys. D: Appl. Phys., Vol. 10, p. 151, (1977).

[99] R. Hurley, and T. Parnell, "Field Emission from Metal Particles in a Vacuum Gap," J. Phys. D: Appl. Phys., Vol. 2, p. 881, (1969).

[100] High Velocity Impact Phenomena, edited by R. Kinslow (Academic, New York, 1970).

[101] D. Smith, and N. Adams, "Studies of Plasma Production at Hypervelocity Microparticle Impact," J. Phys. D: Appl. Phys., Vol. 6, p. 700, (1973).

[102] M. A. Cook, The Science of High Explosives (Reinhold, N.Y., 1958).

[103] D. Davis, and M. Biondi, "Detection of Electrode Vapor Between Plane Parallel Copper Electrodes Prior to Current Amplification and Breakdown in Vacuum," J. Appl. Phys., Vol. 41, p. 88, (1970).

[104] G. Parthasarathy, and H. Gopalakrishna, "Prebreakdown Phenomena in Vacuum Gaps Subject to Alternating Voltages," Proc. 4th Symposium of Discharge and Electrical Insulation in Vacuum, Waterloo, Canada, p. 214, (1970).

[105] R. Allan, and P. Sordoloi, "Prebreakdown Phenomena in Vacuum with Direct and Alternating Voltages at Room and Cryogenic Temperatures". J. Phys. D: Appl. Phys., Vol. 8, p. 2170, (1975).

[106] G. Theophilus, van Heeswijk, and K. Srivastava, "Differences Between 60 Hz A.C. and D.C. Breakdown of Vacuum Gaps," 5th International Symposium on Discharge and Electrical Insulation in Vacuum, Poznan - Poland, p. 115, (1972).

[107] R. Huston, "An Experiment to Compare 60 Hz to Radio Frequency Vacuum Breakdown," Proceedings 3rd International Symposium on Discharge and Electrical Insulation in Vacuum, Paris, p. 223, (1968).

[108] T. Lee, "Industrial Application of Vacuum Insulation," Proc. IV Symp., Waterloo, p. 195, (1970).

[109] W. Parkins, "Vacuum Sparking Potentials Under Surge Conditions," U. S. Atomic Energy Commission Report No. MDDC 858, (1946).

[110] N. Rozanova, and V. Granovskii, "On the Initiation of Electrical Breakdown of a High Vacuum Gap," Sov. Phys. Tech. Phys., Vol. 1, p. 471, (1957).

[111] M. Nandagopal, "Impulse Voltage Breakdown Characteristics of Point-Plane Gaps at Low Pressures," IEEE Trans. on Elec. Insul., Vol. EI-11, p. 69, (1976).

[112] G. Kassirov and G. Mesyats, "Breakdown Mechanisms of Short Vacuum Gaps," Sov. Phys.Tech. Phys., Vol. 9, p. 1141, (1965).

[113] G. Kassivov, and B. Koral'chuk, An Investigation of the Time Lag of the Discharge in the Electrical Breakdown of Vacuum Gaps," Sov. Phys. Tech. Phys., Vol. 9, p. 377, (1964).

[114] I. Kalyatskii, G. Kassirov, and G. Smirnov, "Electrical Breakdown of Vacuum Gaps Under Superhigh Voltage Pulses," Sov. Phys. Tech. Phys., Vol. 19, p. 1434, (1975).

[115] I. Kalyatskii, and G. Kassirov, "Effect of Electrode Material on Electrical Pulse Strength of a Vacuum Gap," Sov. Phys. Tech. Phys., Vol. 9, p. 274,(1964).

[116] I. Kalyatskii, et al., "Breakdown Evolution in Centimeter Vacuum Gaps," Sov. Phys. Tech. Phys. Vol. 20, p. 988, (1976).

[117] G. Farrall,"Cranberg Hypothesis of Vacuum Breakdown as Applied to Impulse Voltages," J. Appl. Phys., Vol. 33, p. 96, (1962).

[118] W. Wijker, "The Electrical Breakdown in Vacuum," Appl. Science Research, Vol. B9, p. 1, (1961).

[119] W. Smith and T. Mason, "Preliminary Measurements of Time Lags to Breakdown of Large Gaps," Proc.II Inter. Symp. on Insulation and Elect. Disch.in Vac., p. 97, (1966).

[120] W. Smith et al "Impulse Breakdown and the Pressure Effect," Proc. 3rd Symp., p. 203, (1968).

[121] W. Smith et al "Impusle Breakdown of Large Gaps in Vacuum," Proc. 4th Symp. p. 56, (1970).

[122] F. Rohrbach, "Relationship Between Spark Time-Lag Spectra and the Mechanisms Leading to Breakdown Between Plane Titanium Electrodes in Ultra High Vacuum," Proc. 4th Symp. p. 68, (1970).

[123] D. Milton, "Electrical Breakdown in Cold Cathode Vacuum Oxide," IEEE Trans. on Elec. Insul. VEI-9, p. 68, (1974).

[124] G. Mesyats, "The Role of Fast Processes in Vacuum Breakdown", Proc. 10th Int. Conf. Phenom. of Ionized Gases, p. 333, (1971).

[125] G. Fursei, and V. Zhukov, "Mechanism for Explosive Emission 1. Emission Characteristics of Explosive Emission From Microscopic Metal Points," Soc. Phys. Tech. Phys., Vol. 21, p. 176, (1976).

[126] P. Ravary and M. Goldman, "Study of the Initiation of Breakdown in Vacuum by Analysis of Closing Times," Proc. of 4th Symp., p. 272, (1970).

[127] E. Hantzche et al "Erosion of Metal Cathodes by Arcs and Breakdowns in Vacuum," J. Phys. D.: Appl. Phys. Vol. 9, p. 139, (1976).

[128] R. Hurley, and T. Parnell, "The Capture and Indentification of Particles in a Vacuum Gap," J. Phys. D:, Appl. Phys., Vol. 1, p. 473, (1968).

[129] G. Theophilus, K. Srivastava, and R. van Heeswijk, "In-situ Observation of Microparticles in a Vacuum-Insulated Gap Using a Scanning Electron Microscope," J. of Appl. Phys., Vol. 47, p. 897, (1976).

[130] F. Puiz, "Recherche et Observation de Microparticules Solides Induisant in Claquage Sous Vide," CERN Report 72-8, (1972).

[131] J. Smalley, "Microparticle Detection in an Electrically Stressed Vacuum Gap," J. Phys. D: Appl. Phys., Vol. 9, p. 2397, (1976).

[132] J. Jenkins and P. Chatterton, "The Detection of Microparticles Prior to Vacuum Breakdown Using a Laser Scattering Technique," J. Phys. D: Appl. Phys., Vol. 10, p. L17, (1977).

[133] M. Menon, and K. Srivastava, "Electrostatic Detection of Large Microparticles (>10um) in a High-Voltage Vacuum Insulated Apparatus," IEEE Trans. on Elect. Insul. Vol. EI-9, p. 142, (1974).

[134] C. Texier, "Breakdown Initiation in Vacuum: Electrical Charge of Microparticles Emitted in a Vacuum Gap," J. Phys. D: Appl. Phys., Vol. 10, p. 1693, (1977).

[135] C. Texier, Private Communication in a letter dated October 24, 1979.

[136] C. Texier, "Descharges Electriques Dans le Vide: Impact de Microparticules Spheriques de Fer de la Taille du Micron sur des Electrodes Polies Mecaniquement," Revue de Physique Applique, Vol. 13, p. 165, (1978).

[137] A. Boulloud and C. Texier, "On the Observation of Microparticles Flying Through an Electrically Stressed Vacuum Gap," J. Phys. D: Appl. Phys., Vol. 11, p. L37, (1978).

[138] G. Griffith, D. Eastman, and J. Kivlin, "The Appearance of Microparticles in Accelerator Tubes," Proc. of 8th Symp., Paper F6-1, Albuquerque, N. Mexico, (1978).

[139] "Precision, Low-Power FET-Input Electrometer Op Amp, AD515," Data Acquisition Components and Subsystems Catalog, Analog Devices, p. 1-45, (1980).

[140] "High Accuracy, Low Offset IC FET-Input Op Amps, AD503, AD506," Data Acquisition Components and Subsystem Catalog, Analog Devices, p. 1-21, (1980).

[141] "Low Noise Operational Amplifier - NE/SE5534, NE/SE6634A," Signetics Analog Data Manual, p. 95, (1977).

[142] P. Rogers, "Evaluation of Electric Stress by Means of the Electrolytic Tank," Chapter 12, p. 196, from High Voltage Technology, edited by L. Alston, Oxford University Press, 1968.

END

FEB.

1988

DTIC